

Hughes Research Laboratories  
A Division of Hughes Aircraft Company  
Malibu, California

ION ROCKET ENGINE DEVELOPMENT

Contract NAS 3-6271

Quarterly Report No. 3

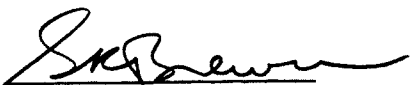
1 April - 30 June 1965

by

S. A. Thompson, H. L. Garvin,  
W. E. McKee, D. E. Zuccaro,  
and A. J. Couvillion

30 December 1965

Prepared for NASA-Lewis Research Center  
Cleveland, Ohio 44135

Approved: 

G. R. Brewer

## TABLE OF CONTENTS

I.	INTRODUCTION . . . . .	1
II.	MULTISTRIP ENGINE DEVELOPMENT . . . . .	5
	A. Engine 42-40-2 IF . . . . .	5
	B. Engine 42-40-3 IF . . . . .	8
	C. Engine 42-40-4 IF . . . . .	14
	D. Conclusion . . . . .	39
III.	OPTICS STUDIES. . . . .	45
	A. Digital Computer Study . . . . .	45
	B. Analog Computer Study . . . . .	45
	C. End Effects Correction . . . . .	48
IV.	FLOW DISTRIBUTION THROUGH IONIZER . . . . .	57
V.	ENGINE MATERIALS . . . . .	65
	A. Low Ion Emission Coatings for Focus Electrodes . . . . .	65
	B. Focus Electrode Sharpening . . . . .	67
VI.	IONIZER MATERIAL EVALUATION . . . . .	71
	A. Introduction . . . . .	71
	B. Analysis of Porous Tungsten . . . . .	72
	C. Coated Porous Ionizer Studies . . . . .	76
	D. Future Work . . . . .	87
VII.	AUTOMATIC CONSOLE . . . . .	89
	A. Introduction . . . . .	89
	B. Console Description . . . . .	89
	C. Summary . . . . .	103
VIII.	PLANS FOR NEXT QUARTER . . . . .	107

## LIST OF ILLUSTRATIONS

Fig. 1.	Thruster life limited by charge exchange ions . . . .	2
Fig. 2.	Engine life limited by ions originated from the tip of a solid tungsten insert for integral focus ion engine . . . . .	3
Fig. 3.	Photograph of the four-strip integral focus thruster with electrodes removed . . . . .	6
Fig. 4.	Accel electrodes with stainless steel insert. Half electrodes are used on the outside ionizer strips. Minimum accel electrode area serves to reduce electron drains both by allowing the accel temperature to increase as well as by reducing the electron emitting area . . . . .	7
Fig. 5.	Neutral fraction versus reciprocal ionizer temperature for HRL 3.8 $\mu_2$ tungsten. Pore count $4.33 \times 10^6$ pore/cm <sup>2</sup> . Engine 42-40-2 IF . . . . .	9
Fig. 6.	Critical temperature data from test of Engine 42-40-2 IF . . . . .	10
Fig. 7.	Perveance data for integral focus engine 42-40-1 2F. The solid line represents computed perveance for the Mod 70 cold focus optics configuration . . . . .	11
Fig. 8.	Isometric sketch of the sloped end correction design as used in engine 42-40-3 IF . . . . .	12
Fig. 9.	Beam current versus test time for engine 42-40-3 IF . . . . .	13
Fig. 10.	Percent accel drain current versus test time for engine 42-40-3 IF . . . . .	15
Fig. 11.	Percent neutral fraction versus test time for engine 42-40-3 IF . . . . .	16
Fig. 12.	Chamber pressure versus test time for engine 42-40-3 IF . . . . .	17
Fig. 13.	Ionizer critical temperature data for engine 42-40-3 IF . . . . .	18

Fig. 14.	Apparent neutral fraction versus reciprocal temperatures for engine 42-40-3 IF . . . . .	19
Fig. 15.	Perveance data for engine 42-40-3 IF . . . . .	20
Fig. 16.	Photomicrograph of a section through the ionizer which shows the sharpened tungsten insert . . . . .	22
Fig. 17.	Life test data of engine 42-40-4 IF . . . . .	23
Fig. 18.	Neutral fraction versus temperature data taken during the 68th and 612th hour of test of engine 42-40-4 IF . . . . .	26
Fig. 19.	Perveance characteristics taken during the first 69 hours and 612th hour of test of engine 42-40-4 IF . . . . .	27
Fig. 20.	Drain current accel-decel ratio characteristics of engine 42-40-4 IF. Measurements made at 14.5 mA/cm <sup>2</sup> . . . . .	28
Fig. 21.	Sketches showing side erosion of accel electrodes . . . . .	30
Fig. 22.	Engine life limited by charge exchange ions (integral focus ion engine) . . . . .	32
Fig. 23.	Multistrip engine accel electrode erosion patterns . . . . .	34
Fig. 24.	Photograph of the base of the accel electrode (x15) showing striated erosion as well as end effect erosion . . . . .	35
Fig. 25.	Composite surface work function versus arrival flux for 27 adsorbate atoms on tungsten . . . . .	37
Fig. 26.	Composite surface work function versus arrival flux for 27 adsorbate atoms on iridium . . . . .	38
Fig. 27.	42-40-4 ionizer and electrode erosion after life test . . . . .	40
Fig. 28.	Post test bubble patterns for engine 42-40-4 IF — High flow rate . . . . .	41
Fig. 29.	Post test bubble patterns for engine 42-40-4 IF — Low flow rate . . . . .	42



Fig. 30.	Influence of accel electrode position on beam profile . . . . .	46
Fig. 31.	Influence of accel electrode centering on beam direction . . . . .	47
Fig. 32.	The influence of accel electrode placement on ion trajectories . . . . .	49
Fig. 33.	The influence of accel electrode placement on ion trajectories . . . . .	50
Fig. 34.	The influence of the edge focusing member on the ion trajectories . . . . .	51
Fig. 35.	End-effect corrections adapted from Model 70 optics . . . . .	53
Fig. 36.	End-effect corrections for integral-focus engine . . .	55
Fig. 37.	Cross section of ionizer with uniform flow . . . . .	58
Fig. 38.	Current density capabilities for integral-focus optics and for Model 70 optics . . . . .	59
Fig. 39.	Standard ionizer cross section with sealed areas to adjust flow for integral-focus optics . . . .	60
Fig. 40.	Ionizer with thickness reduced for electron-beam welding but with flow adjusted for integral-focus optics . . . . .	62
Fig. 41.	Cross section of ionizer which is undercut and shaped to adjust flow for integral-focus optics . . . . .	63
Fig. 42.	Ionizer with flat back and flow adjusted for integral focus optics. Seal surface to A for unwelded lens and to B for welded lens . . . . .	64
Fig. 43.	Critical temperature data for an ionizer strip made from Philips Metalonics Mod E tungsten and evaluated in the UHV ionizer evaluation system (see text for material characteristics) . . .	73
Fig. 44.	Neutral fraction data for an ionizer strip made from Philips Metalonics Mod E tungsten and evaluated in the UHV ionizer evaluation system. (See test for material characteristics) . . . . .	74

Fig. 45.	Current density as a function of ionizer temperature for EOS 1 to 40 $\mu$ porous tungsten . . . . .	77
Fig. 46.	Neutral efflux as a function of ionizer temperature for EOS 1 to 40 $\mu$ porous tungsten . . . .	78
Fig. 47.	Neutral fraction as a function of current density for EOS 1 to 40 porous tungsten . . . . .	79
Fig. 48.	Neutral fraction as a function of temperature of 1.5 $\mu$ thick rhenium sputter coated ionizer . . . . .	81
Fig. 49.	Current density as a function of the temperature of the 1.5 thick rhenium sputter coated ionizer . . . . .	82
Fig. 50.	Critical temperature as a function of the temperature of the 3 $\mu$ thick iridium chemically coated ionizer . . . . .	84
Fig. 51.	Neutral fraction as a function of the temperature of the 3 $\mu$ thick iridium chemically coated ionizer . . . . .	85
Fig. 52.	Neutral fraction as a function of current density for 3 samples . . . . .	86
Fig. 53.	Front view of life test console . . . . .	90
Fig. 54.	Cabinet designation diagram of life test console . .	91
Fig. 55.	+10 kV power supply . . . . .	93
Fig. 56.	HV instrumentation and controller network assembly . . . . .	95
Fig. 57.	Ground level instrumentation . . . . .	100
Fig. 58.	-15 kV power supply . . . . .	104

## I. INTRODUCTION AND SUMMARY

During the period covered by this report a series of three four-strip integral focus ion engines was evaluated. The third engine was tested for 954 hours, until the cesium supply was expended. The theoretical charge exchange limited life for an engine which uses a tungsten ionizer is expected to be two to five times this test period. The drains were less than 1%, and the apparent neutral fraction was 0.6% during the test.

A cesium contact ion engine with a lifetime far greater than that attainable with a tungsten surface appears feasible. Measurements of neutral fraction from both rhenium and iridium coated surfaces show that the neutral fraction can be reduced by 1/20 to 1/50 the value for tungsten. Engine life would increase by the same factor.

The effect of neutral fraction on electrode life is shown graphically in Figs. 1 and 2. For this class of engine (nonporous focus tip), erosion from focus tip originated ions is negligible compared with electrode erosion resulting from charge exchange ions; therefore, Fig. 1 presents the life limiting characteristic of the engine.

A summary of the tungsten as well as rhenium and iridium data is also presented in Figs. 1 and 2. An engine life greater than 30,000 hours at a current density of  $20 \text{ mA/cm}^2$  appears to be attainable with the high work function surface.

Future work will be directed toward optimizing the coating technique as well as the substrate tungsten for over-all stability, critical temperature, and neutral fraction.

The 30 kW automatic console is near completion. This unit will permit unattended operation of either the four-strip or 13-strip engines as well as future larger cesium contact ion engines.

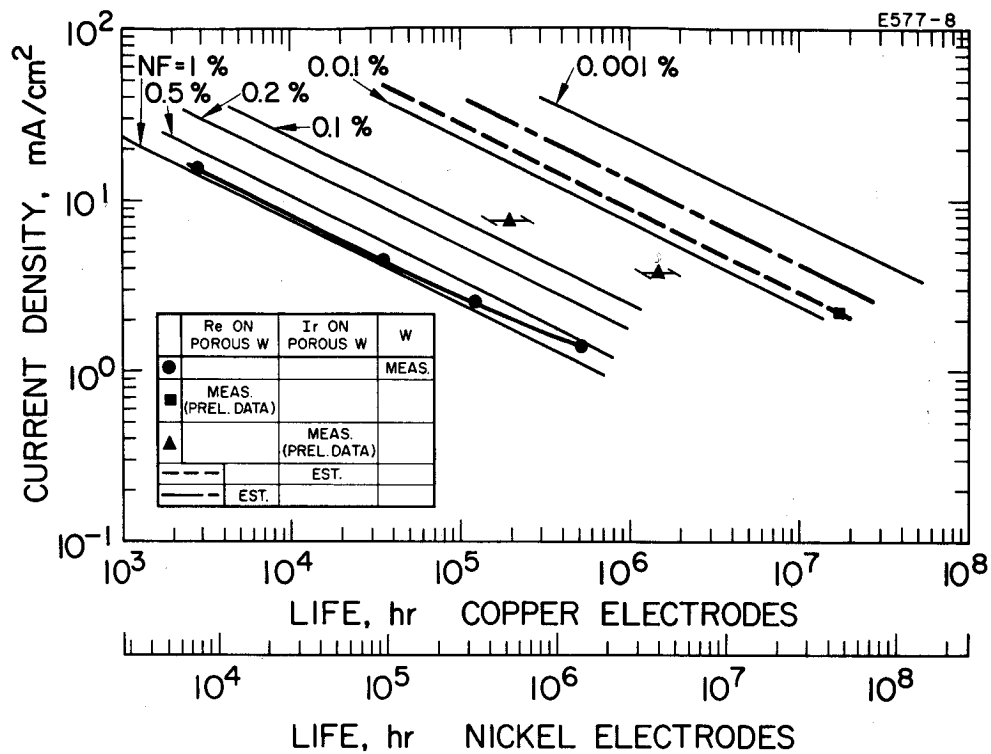


Fig. 1. Thrustor life limited by charge exchange ions.

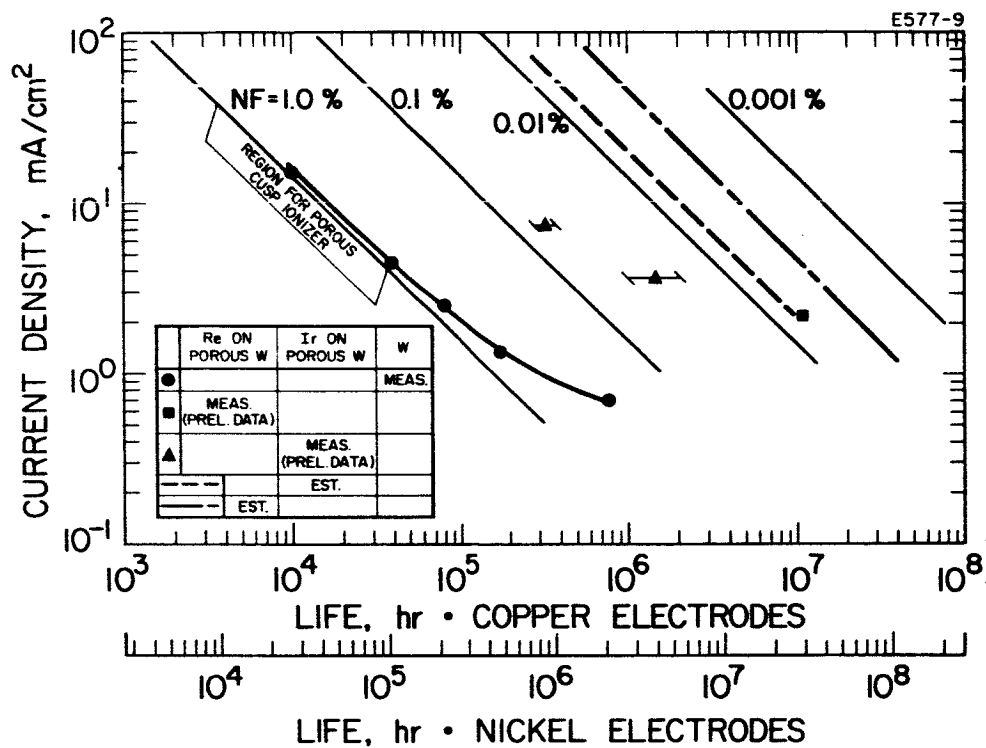


Fig. 2. Engine life limited by ions originated from the tip of a solid tungsten insert for integral focus ion engine.

## II. MULTISTRIP ENGINE DEVELOPMENT

### A. Engine 42-40-2 IF

The second integral focus engine was tested for a planned 30 hours at ionizer current densities to  $20 \text{ mA/cm}^2$ . The purpose of the test was to experimentally evaluate two forms of the end correction to the linear strip optics. The engines used an HRL tungsten ionizer with density of 80 percent of theoretical. The ionizer pore count was  $4.33 \times 10^6$  pores/cm<sup>2</sup>. The particle size was  $3.9 \mu$ . A photograph of the engine assembly less electrodes is shown in Fig. 3. The stainless steel insert copper electrodes are shown in Fig. 4.

The focus electrode end correction shown in Fig. 3 closed the strips with a straight section as well as with a contoured end. The end correction is incorporated in the mask which surrounds the ionizer. The accel electrode end correction spacing used was similar to that used on the cold focus engine (Model 70) design. The ionizer ends were electron beam sealed over a 0.050 in. distance. The engine test showed the shaped correction to be superior to the straight end. Accel erosion was minimal when the shaped configuration was used, and an electrolytic tank-computer analysis, described in Section III, confirms the superiority of the shaped ionizer end. The potential distribution is adjusted so that the accel electrode has a stronger effect on the beam end ions. The effect of the focus electrode at the beam end is suppressed, so that the beam has less tendency to be compressed and spread into the accel electrodes.

The ionizer performed satisfactorily during the 30-hour test. Operation on the clean tungsten line was not achieved, since the surface had a higher work function than that of tungsten ionizers measured previously. The transmission coefficient, computed from boiler temperature, beam current, and ionizer temperature data, was  $9.8 \times 10^{-5}$ . The transmission coefficient for Philips Mod E tungsten is  $4 \times 10^{-4}$ .

During the major portion of the test, the engine operated at  $15 \text{ mA/cm}^2$ , and for 1-1/4 hours at  $20 \text{ mA/cm}^2$ . The accel drain

M 3943

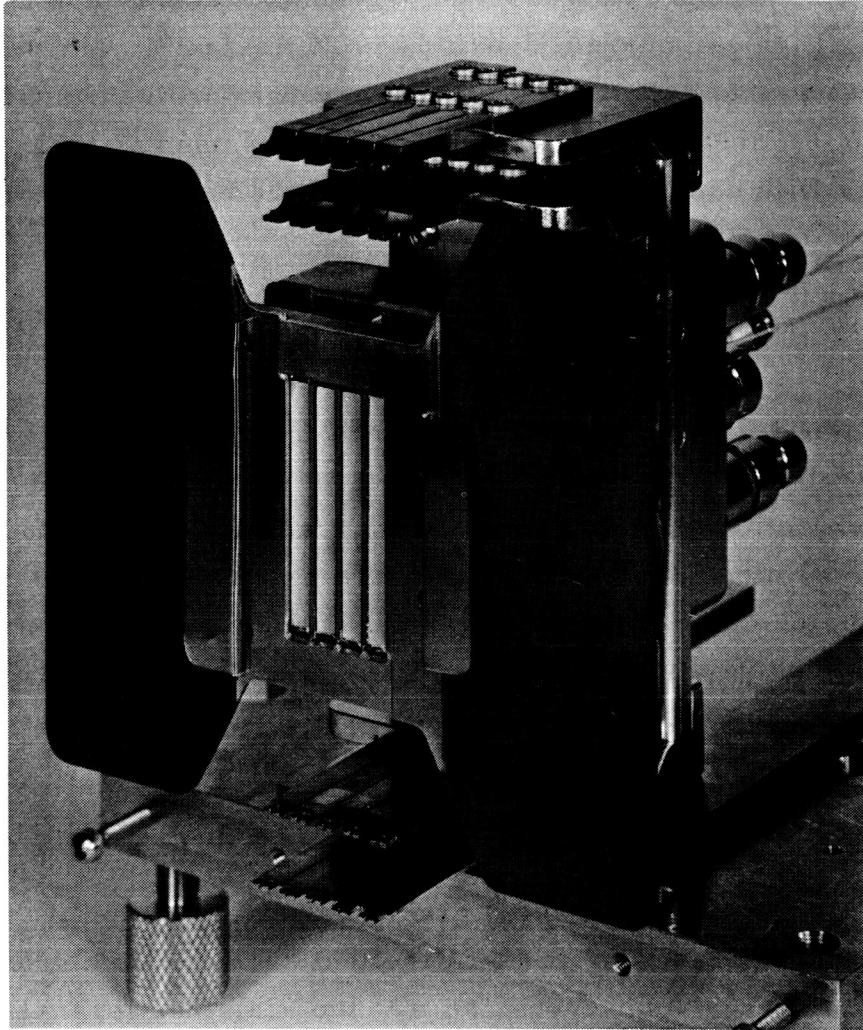


Fig. 3. Photograph of the four-strip integral focus thruster with electrodes removed.

M 3995

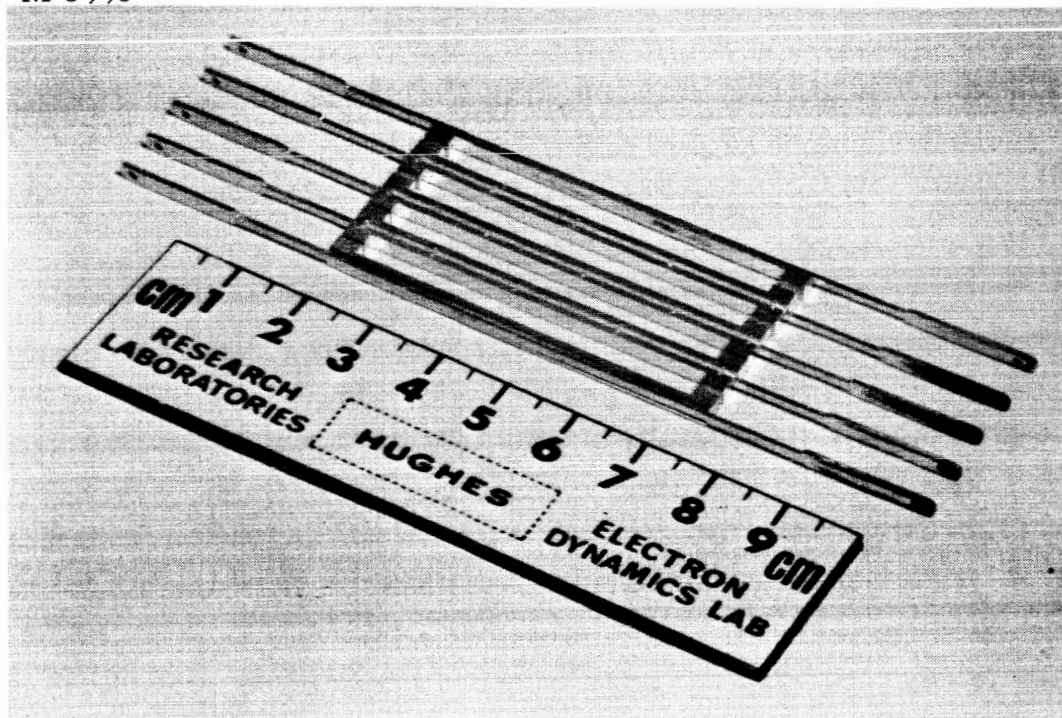


Fig. 4. Accel electrodes with stainless steel insert. Half electrodes are used on the outside ionizer strips. Minimum accel electrode area serves to reduce electron drains both by allowing the accel temperature to increase as well as by reducing the electron emitting area.



current was 4.2%. The high drain current was the result of an ionizer-to-feed system seal leak. The engine operated essentially arc free.

Neutral fraction data for current densities of 15 and 20 mA/cm<sup>2</sup> are shown in Fig. 5. Critical temperature and typical engine performance data are shown in Figs. 6 and 7, respectively. The solid line in Fig. 7 represents theoretical data for Model 70 optics. The points represent integral focus engine experimental results.

#### B. Engine 42-40-3 IF

The third integral focus engine was tested for a period of 65 hours during May 1965. This engine used the HRL 3.9  $\mu$  ionizer used earlier in the test of engine 42-40-2 IF, whose purpose was to evaluate experimentally two types of ionizer end corrections. The 42-40-3 IF engine used the sloped focus end design shown isometrically in Fig. 8.

Examination of the accel electrodes from engine 42-40-2 IF showed erosion of the accel electrode in the region opposite the knife edge insert. The knife edge width was 0.002 to 0.003 in. Ions from the knife edge would have eroded the accel electrode through to the steel insert in 500 hours.

Techniques for sharpening the knife edge were being explored; however, a proven technique applicable to this engine was not available. It was decided to use the 42-40-2 IF ionizer without attempting to reduce the radius of the tungsten insert edge. This engine test served to prove the seal and end correction design as well as to provide a further evaluation of the HRL 3.9  $\mu$  ionizer material. The engine test was accomplished without decel electrodes. The engine performed exceptionally well during the 65-hour test. At the 65th hour the tank was vented to air and the test terminated. A plot of the ion beam current is shown in Fig. 9. The average beam current during the test's last 55 hours was 140 mA. The current density was 12.3 mA/cm<sup>2</sup>. During the first 10 hours, the engine was operated at 15 mA/cm<sup>2</sup>.

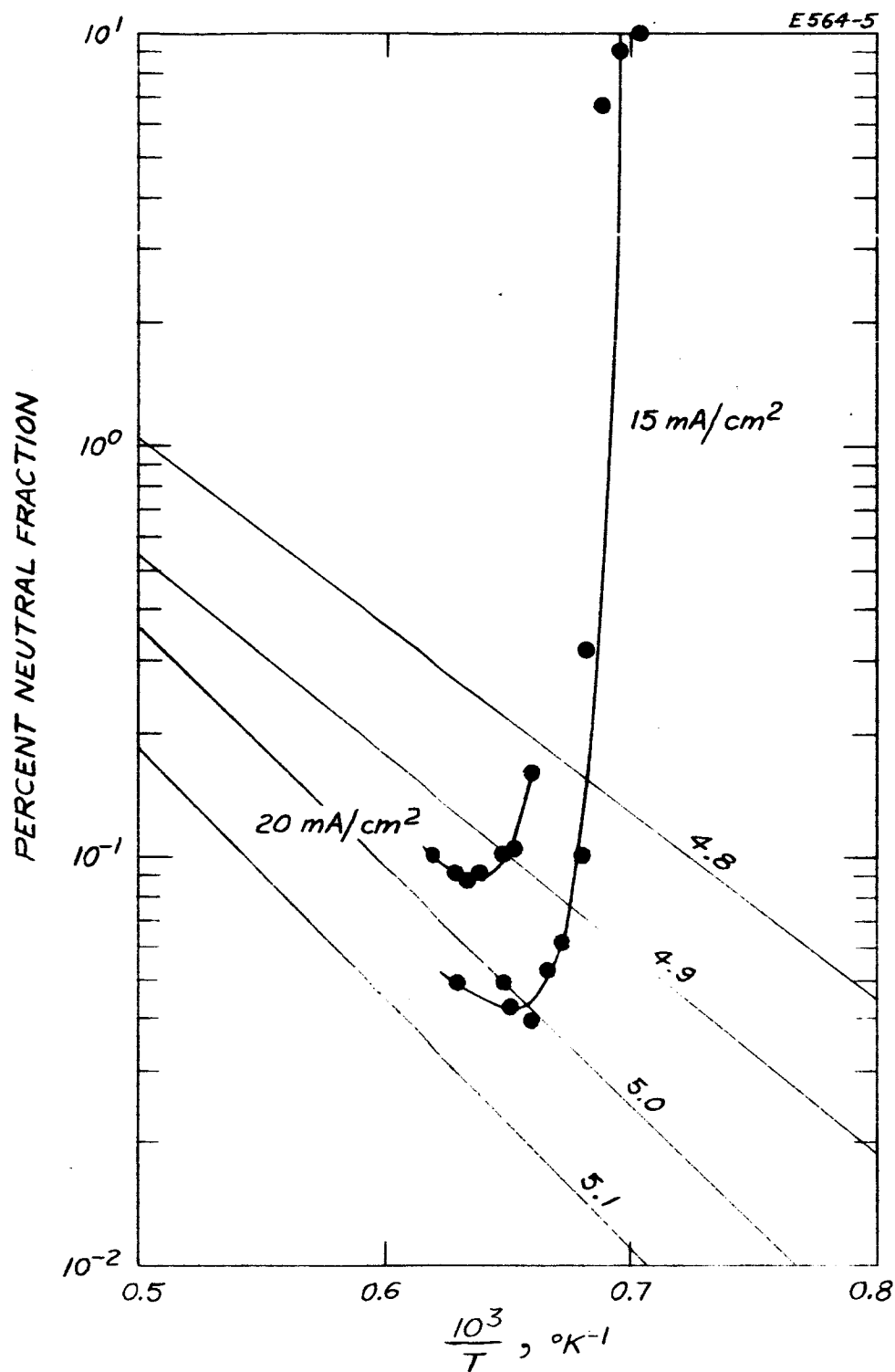


Fig. 5. Neutral fraction versus reciprocal ionizer temperature for HRL  $3.8\mu$  tungsten. Pore count  $4.33 \times 10^6$  pores/cm<sup>2</sup>. Engine 42-40-2 IF.

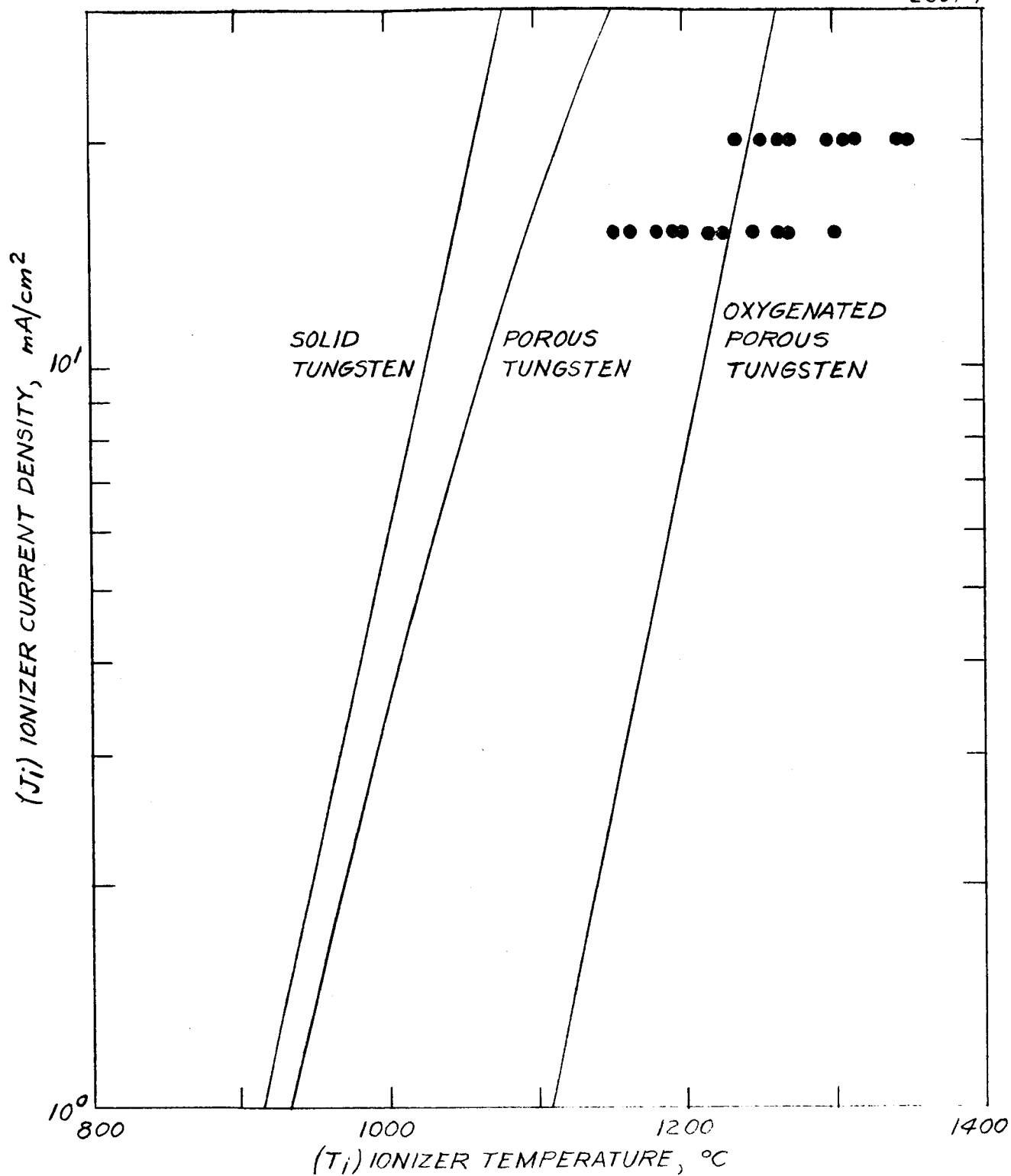


Fig. 6. Critical temperature data from test of Engine 42-40-2 IF.

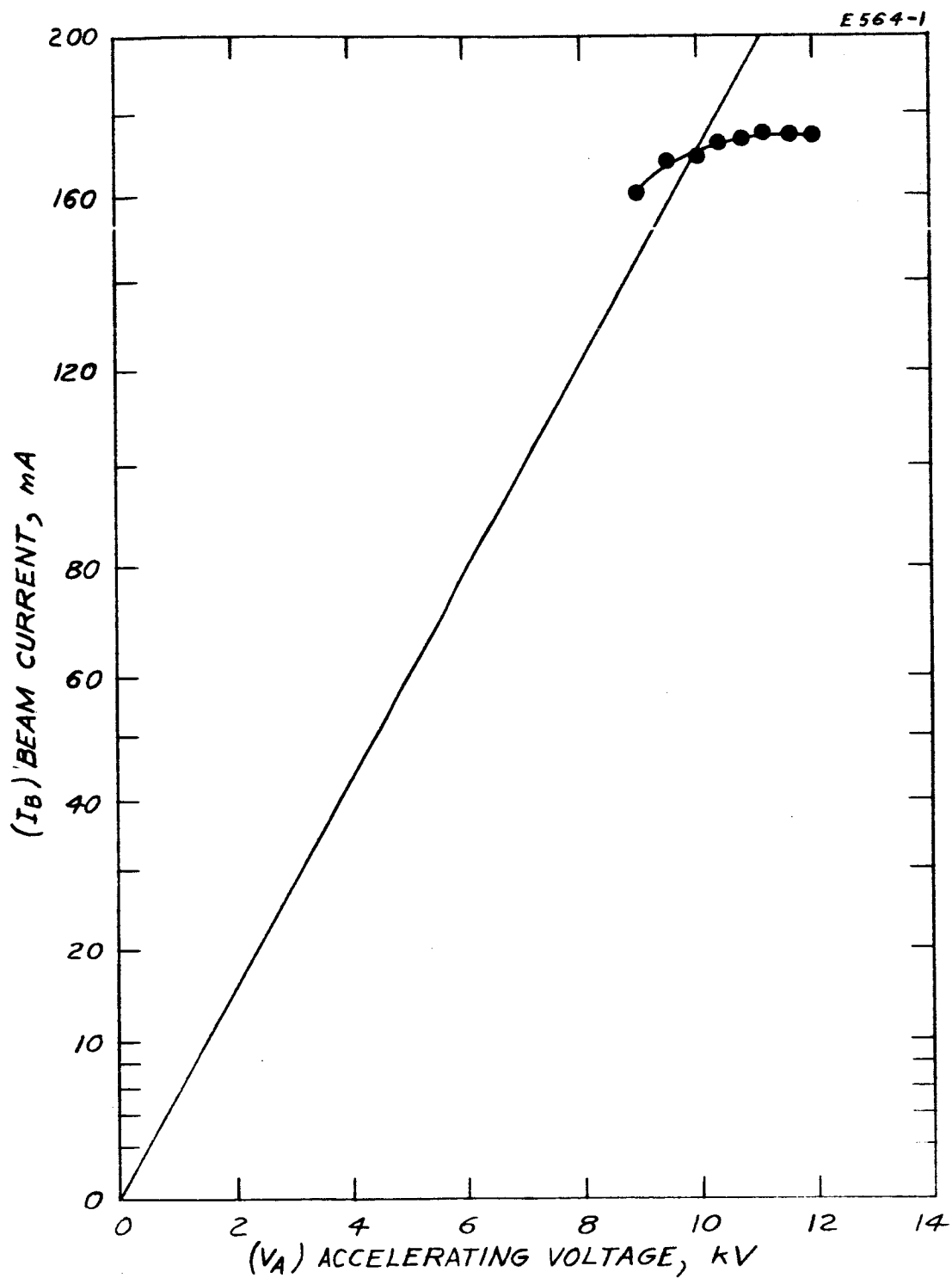


Fig. 7. Perveance data for integral focus engine 42-40-1 IF. The solid line represents computed perveance for the Mod 70 cold focus optics configuration.

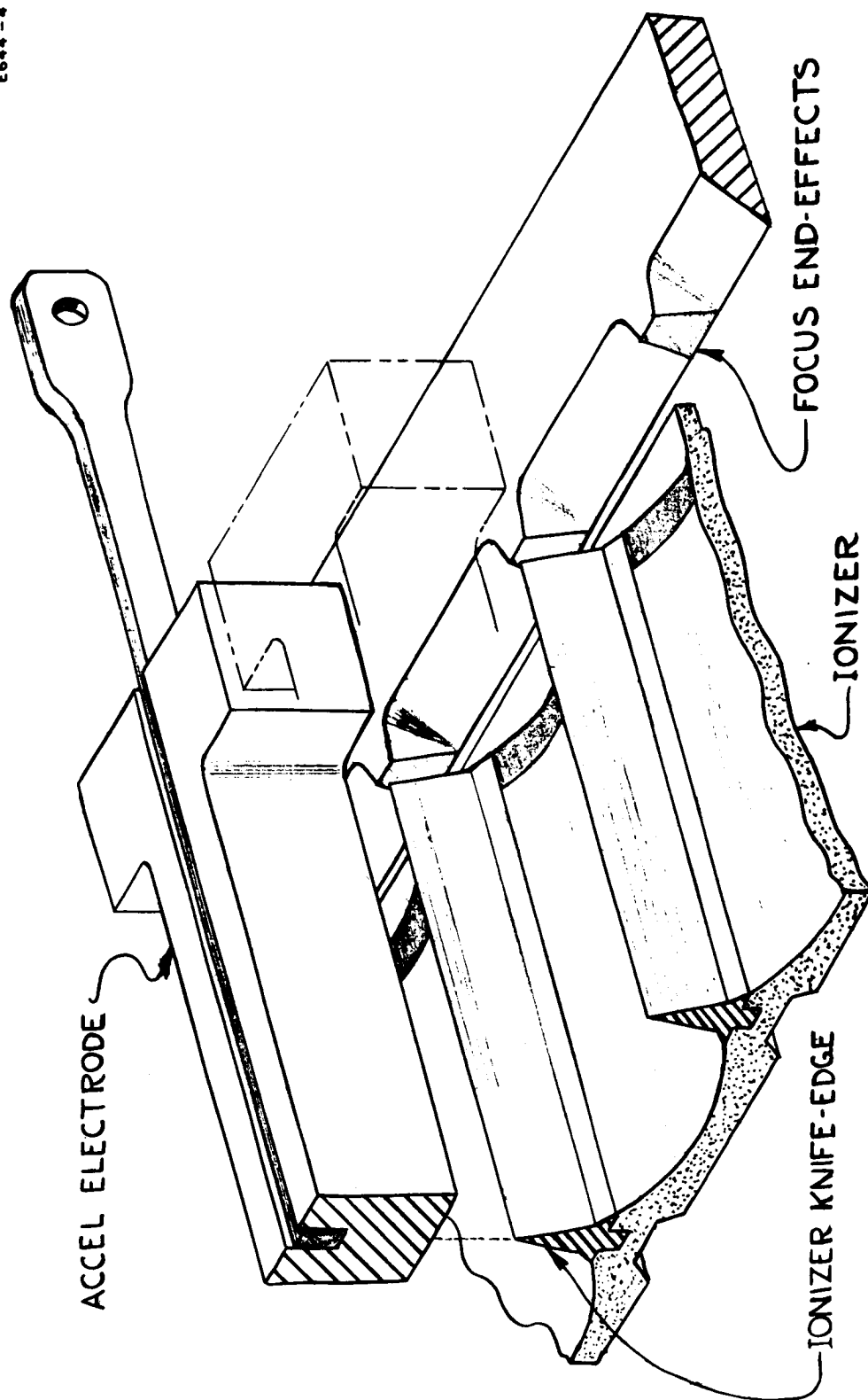


Fig. 8. Isometric sketch of the sloped end correction design as used in engine 42-40-3 IF.

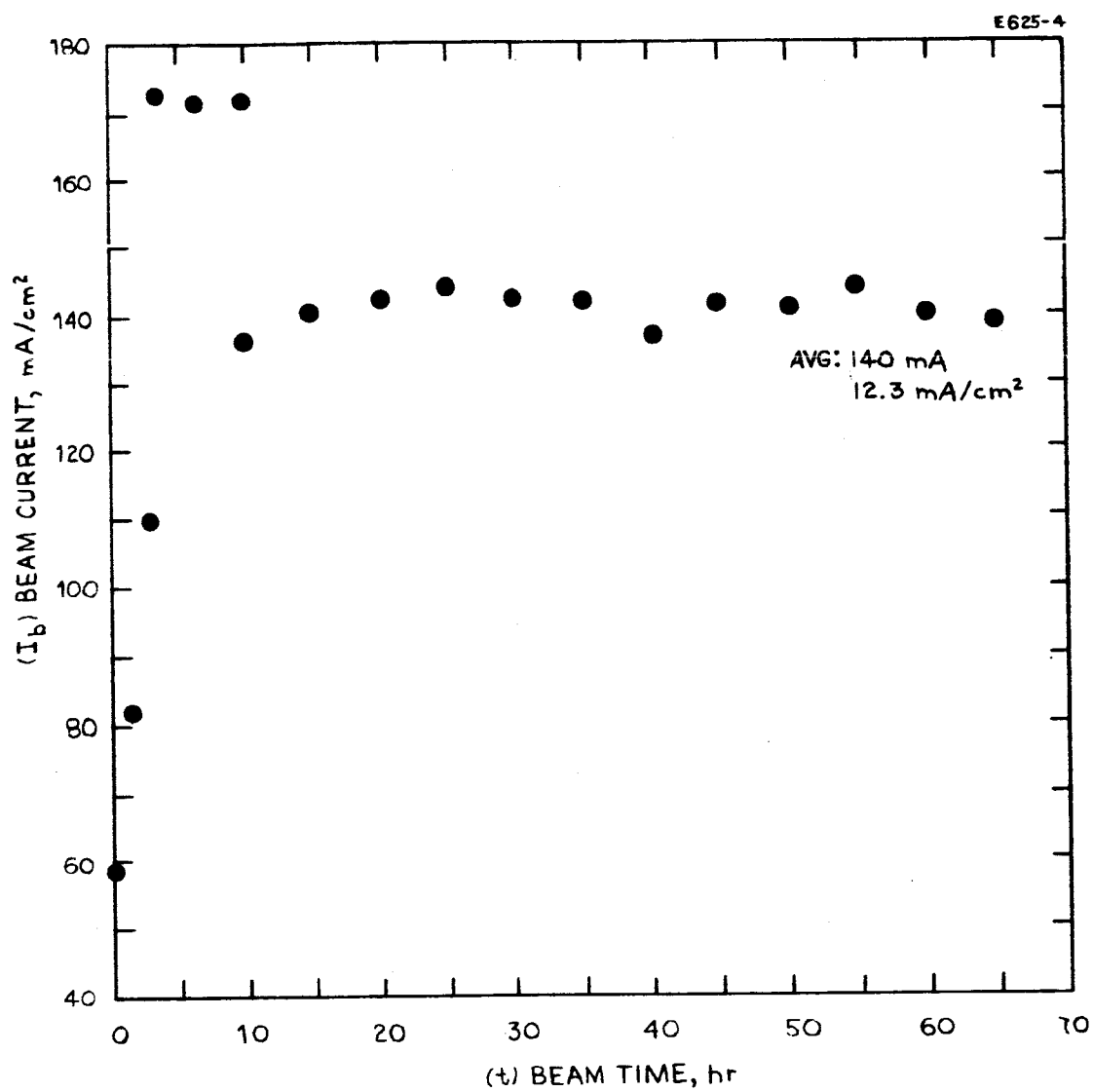


Fig. 9. Beam current versus test time for engine 42-40-3 IF.

The average accel drain current was 0.9%; the peak drain current, 1.2%. A plot of the drain current is shown in Fig. 10. Elimination of a cesium feed tube joint leak resulted in reduced engine drain current (relative to that of engine 42-40-2 IF). The seal had been redesigned for this engine. The ionizer temperature was held constant at 1230°C.

The percent neutrals from the ionizer was also measured. A plot of neutrals versus test time is shown in Fig. 11. The neutral fraction at the end of the test approached 0.05 percent at a beam current density of 12.3 mA/cm<sup>2</sup>. The tank pressure, shown in Fig. 12, started at  $2 \times 10^{-6}$  Torr and slowly decreased to  $9 \times 10^{-8}$  Torr.

A critical temperature plot is shown in Fig. 13. The corresponding neutral-fraction ionizer-temperature data is shown in Fig. 14. The work function for this material is 5 eV. The ionizer surface is either contaminated with fluorine or the surface is oriented such that the average work function is greater than 4.54 eV. It is postulated that the technique used to make this material serendipitously provides a low neutral fraction high work function surface. The neutral fraction for this ionizer did however increase by a factor of three over the previous engine tests. The neutral fraction for engine 42-40-2 IF was 0.05 percent at 15 mA/cm<sup>2</sup> whereas the measured neutral fraction for this engine was 0.15% at the same current density.

The engine perveance data shown in Fig. 15 again confirms that the steel insert in the accel electrode was a design improvement. The perveance remained constant during the test.

#### C. Engine 42-40-4 IF

The fourth integral focus ion engine was tested during the period from June 17, 1965 to July 30, 1965. This engine satisfied the 500-hour life test requirement and in fact was operated continuously, until the cesium supply was expended, for a total time of 954 hours.

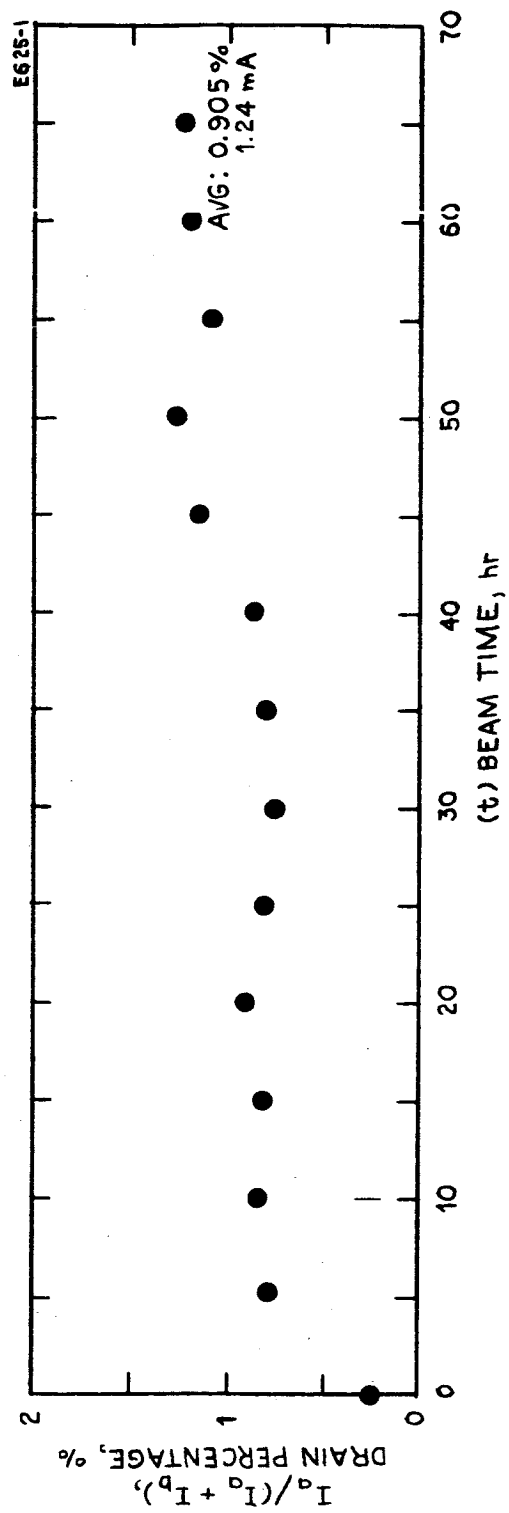


Fig. 10. Percent accel drain current versus test time for engine 42-40-3 IF.



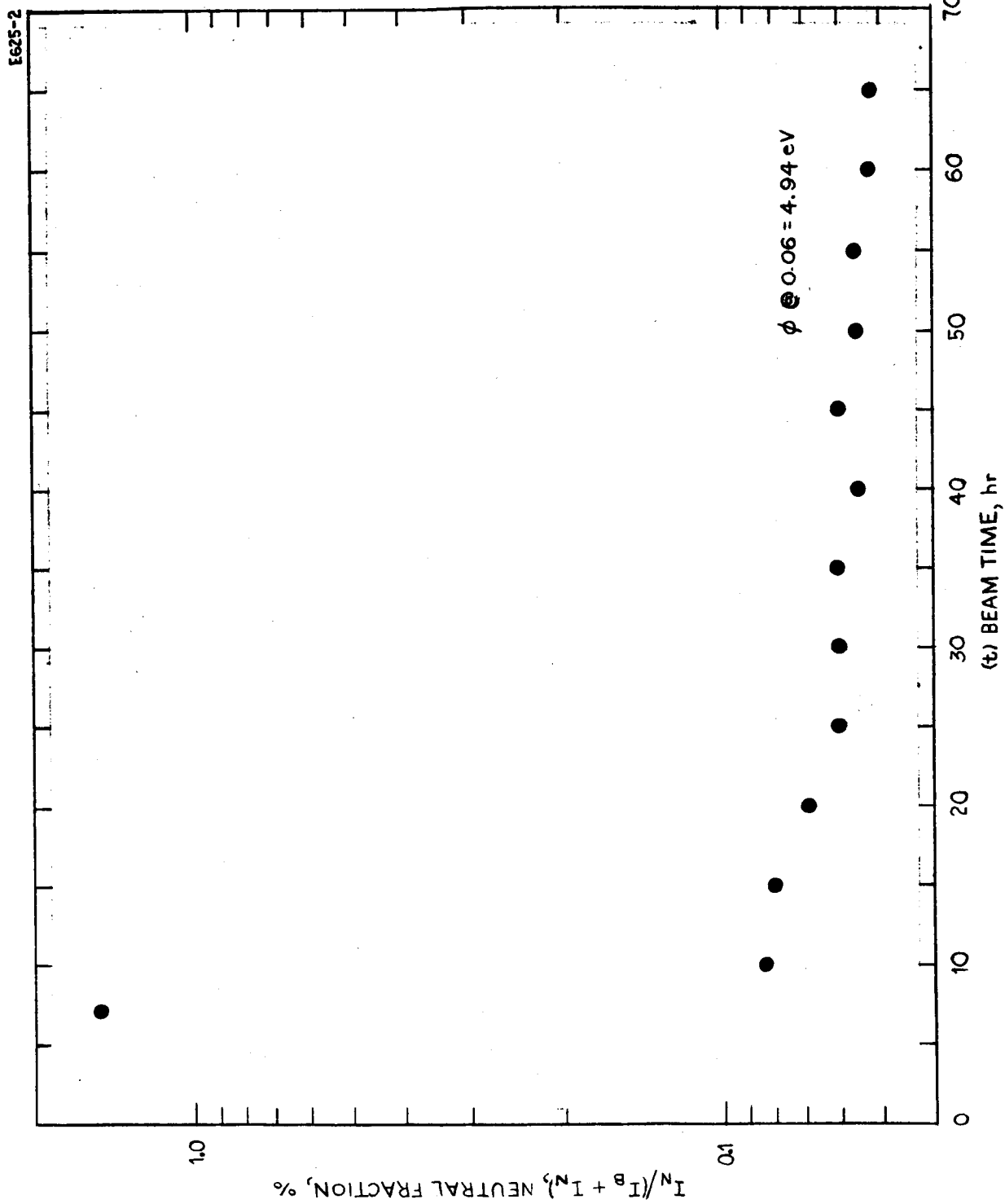


Fig. 11. Percent neutral fraction versus test time for engine 42-40-3 IF.

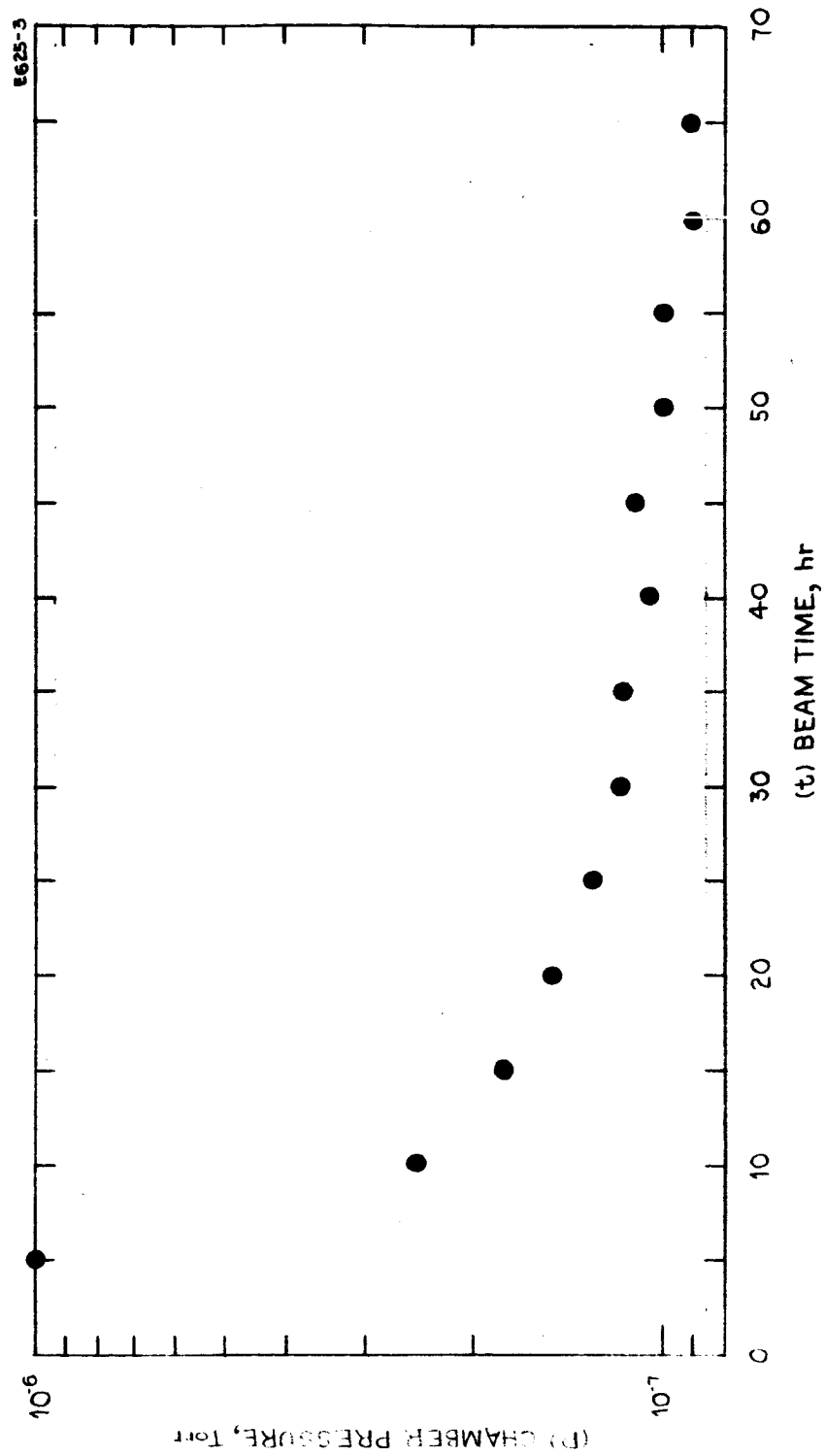


Fig. 12. Chamber pressure versus test time for engine 42-40-3 IF.

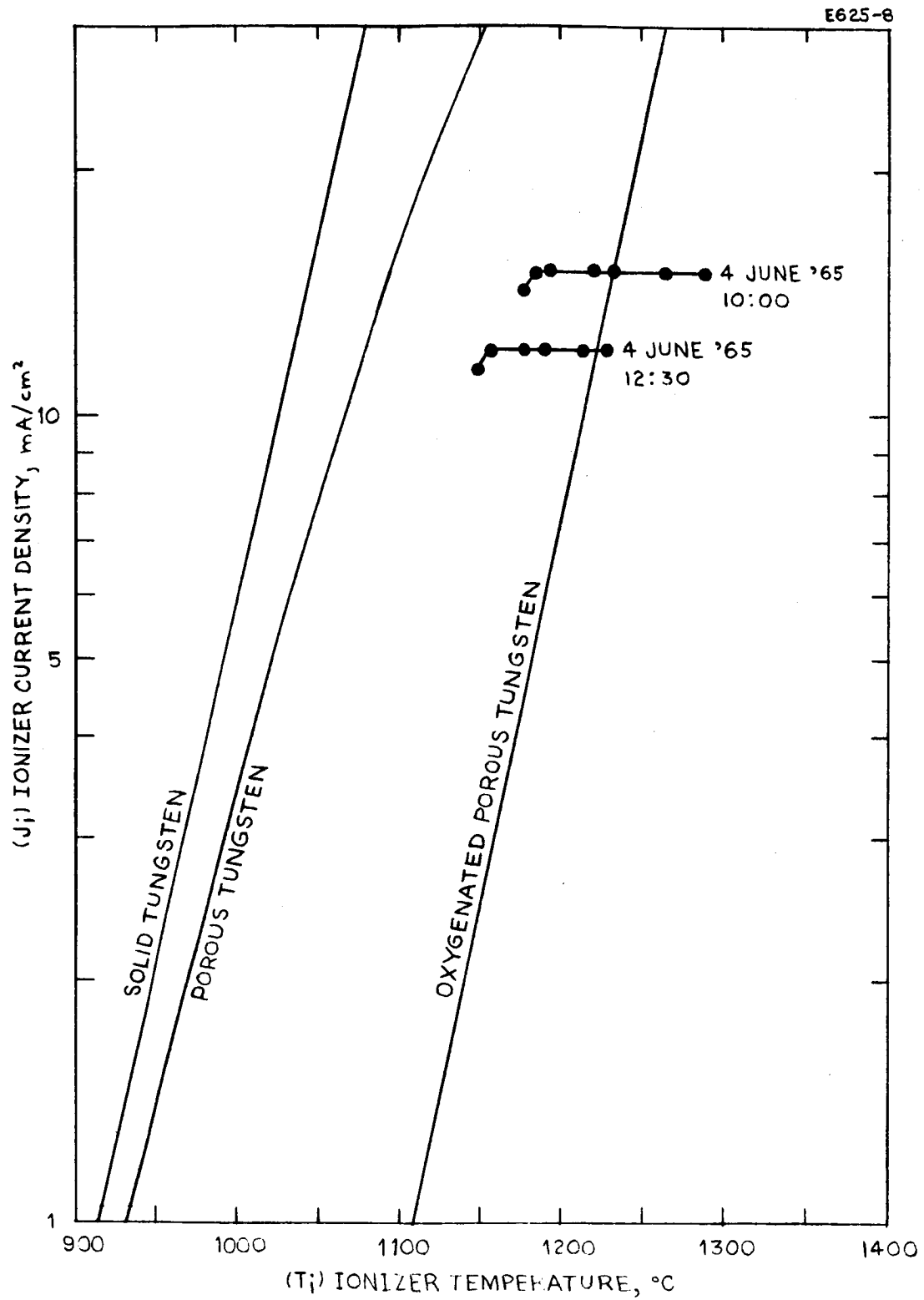


Fig. 13. Ionizer critical temperature data for engine 42-40-3 IF.

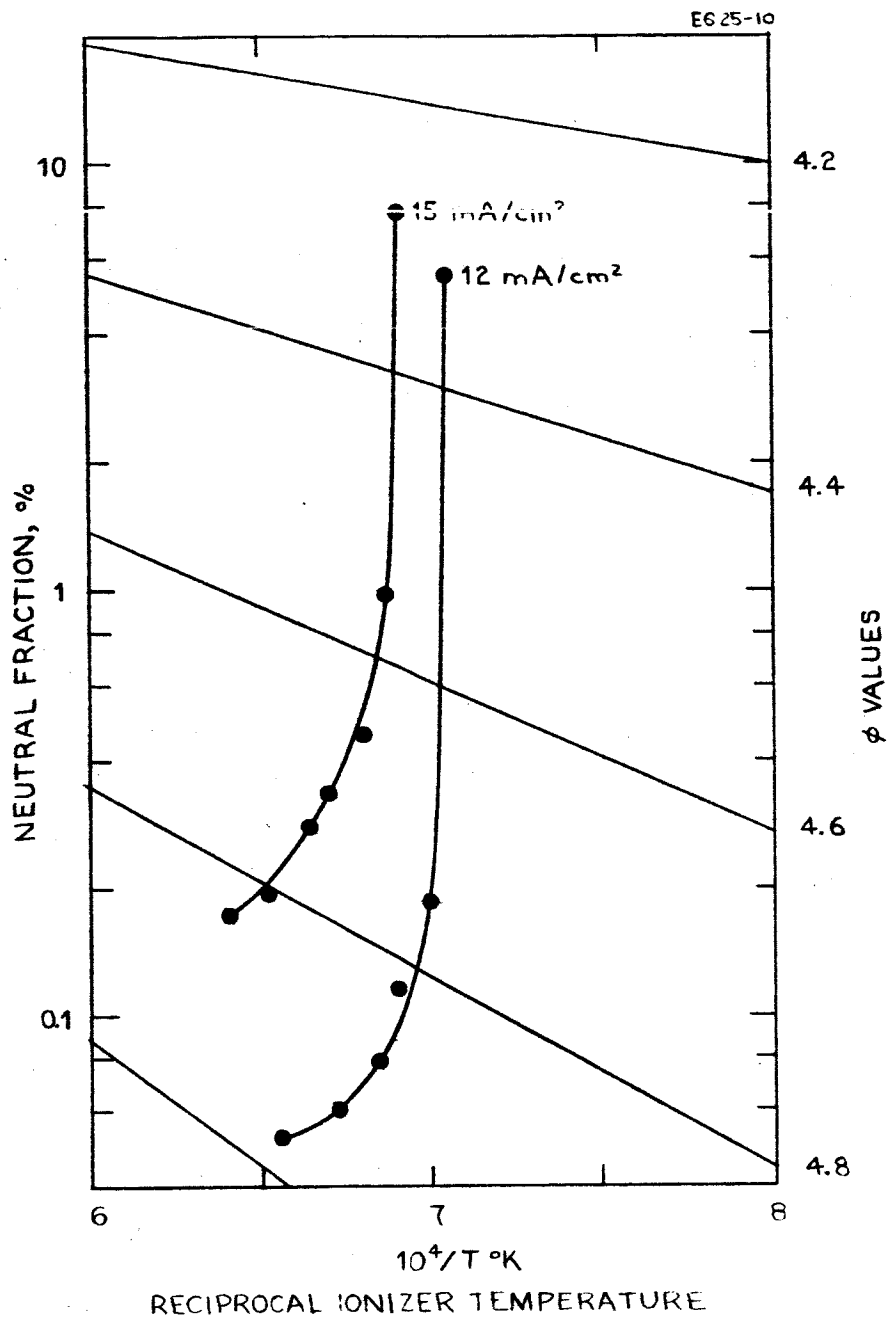


Fig. 14. Apparent neutral fraction versus reciprocal temperatures for engine 42-40-3 IF.

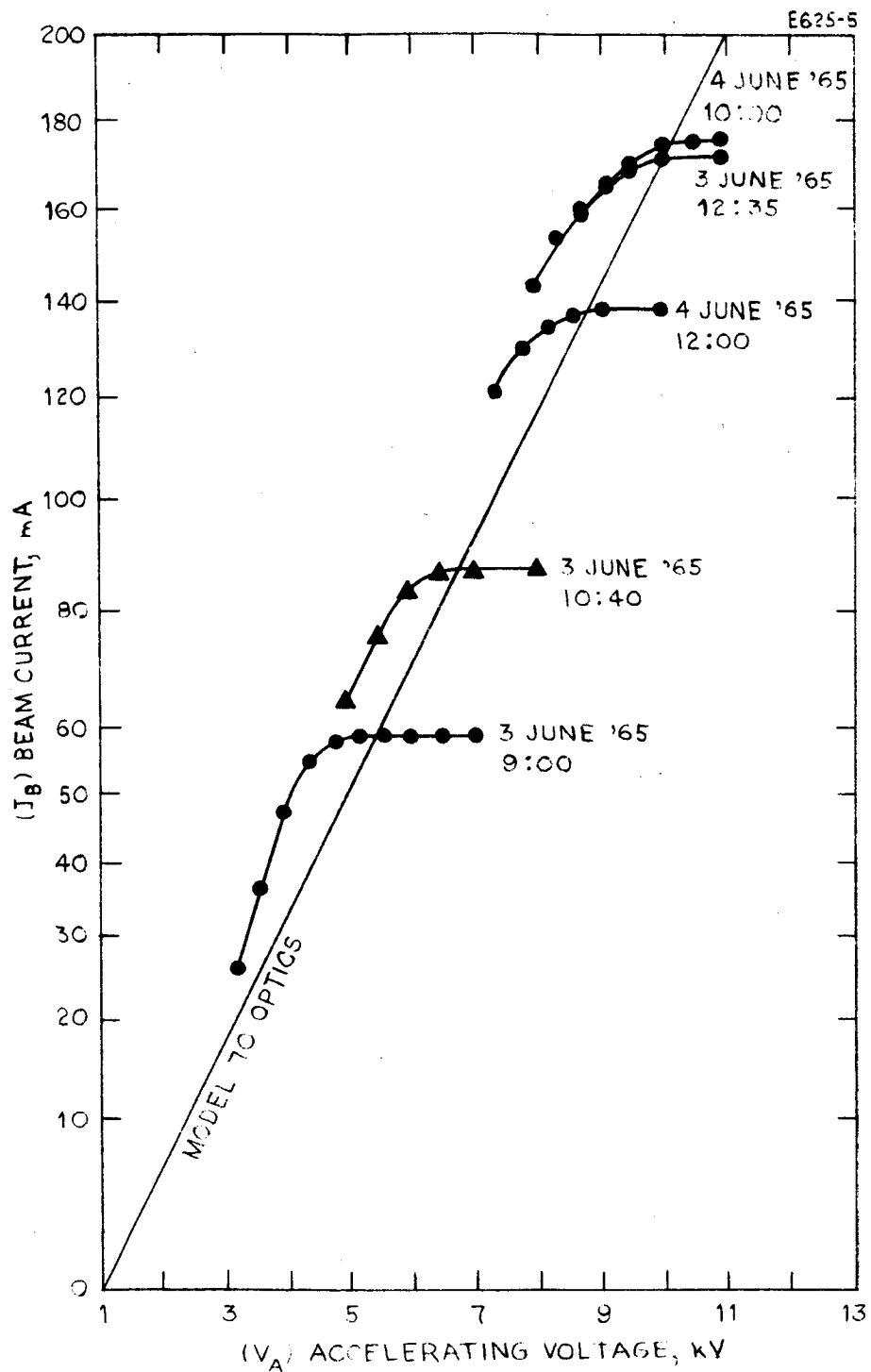


Fig. 15. Perveance data for engine 42-40-3 IF.

The engine used the Philips Mod E ionizer that was first incorporated into engine 42-40-1 IF. However, in contrast to the previous engine, techniques for sharpening the ionizer inserts had been established; therefore, the ionizer integral focus tips were re-worked. The tip radii were reduced from 0.002 inch to 0.0002 inch. Pre-test bubble evaluation of the ionizer indicated a non-uniform distribution of pore sizes. The strip associated with electrode No. 1 was more porous than the adjacent strips.

In addition, the engine used a 0.160-in. thick accel electrode with a stainless steel insert. The previous engine used a 0.100-in. thick accel electrode. The copper thickness below the insert was increased from 0.025 to 0.110 in. Thus, the engine life, as limited by accel erosion resulting from focus tip ions, was increased by a factor of four.

The integral focus end correction was identical to the approach used in engine 42-40-3 IF. The regions within 0.050 in. of the ends of the ionizer strips were sealed with the electron beam welder to permit this ionizer to be used with the end correction design.

The tips of the sharpened integral focus inserts were coated with a sub-micron layer of alumina. A photomicrograph of a typical ionizer section which illustrates the sharpness of the insert tip is shown in Fig. 16.

#### 1. Life Test Data

Life test data for the four-strip integral focus engine 42-40-4 IF are given in Fig. 17. A summary of the test data is presented in Table I. The average current density, as measured on the ionizer surface, was  $12.92 \text{ mA/cm}^2$ . Figure 17 shows that there was no change in engine characteristics over the duration of the test. The accel drain current was consistently under 1%, and the apparent ionizer neutral fraction, which was continuously monitored, was stable at 0.6%. The ionizer critical temperature, measured at the rear of the manifold was stable at  $1375^\circ\text{K}$ . The ionizer surface temperature

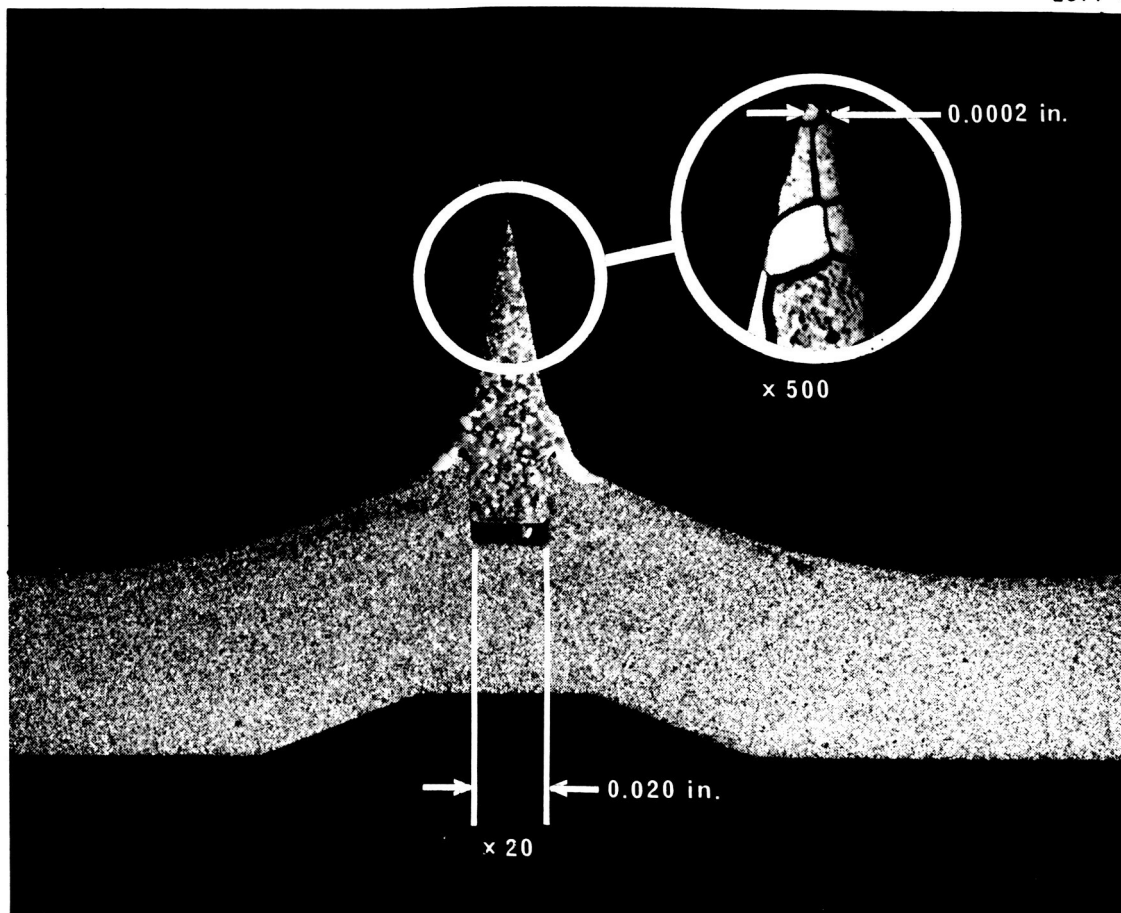


Fig. 16. Photomicrograph of a section through the ionizer which shows the sharpened tungsten insert.

# MULTISTRIP ENGINE LIFE TEST DATA <sup>EST-5</sup>

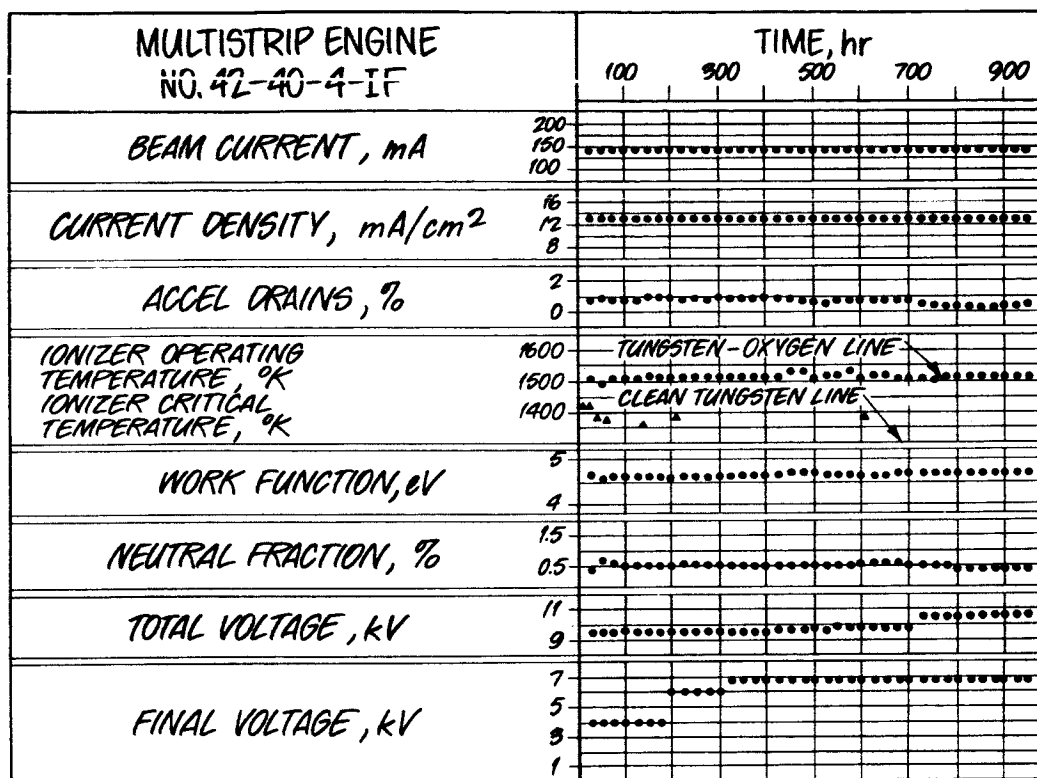


Fig. 17. Life test data of engine 42-40-4 IF.



TABLE I

Summary of Data from 954-Hour Test of  
Engine 42-40-4 IF

Operating time	954 hours
Average beam current	139.43 mA
Ionizer area	10.79 cm <sup>2</sup>
Average ionizer current density	12.92 mA/cm <sup>2</sup>
Average drain current	1.15 mA
Average drain percentage	0.82%
Average neutral current	0.76 mA
Average neutral percentage	0.54%
Average ionizer temperature	1248°C
Average work function	4.67 eV
Ionizer voltage	
0 - 182 hours	4.0 kV
182 - 307 hours	6.0 kV
307 - 954 hours	6.8 kV
Total voltage	
0 - 182 hours	9.6 kV
182 - 307 hours	9.7 kV
307 - 703 hours	9.8 kV
703 - 954 hours	10.6 kV
Specific Impulse	
0 - 182 hours	7,750 sec.
182 - 307 hours	9,500 sec.
307 - 954 hours	10,100 sec.
Chamber Pressure	
0 - 305 hours	1.11 x 10 <sup>-7</sup> Torr
305 - 954 hours	2.65 x 10 <sup>-7</sup> Torr

was approximately  $1350^{\circ}\text{K}$ . The temperature at which the neutral fraction is minimum for this current density is  $1350^{\circ}\text{K}$  and thus the ionizer performed like a clean tungsten surface.

At various times during the test, the neutral-fraction and perveance characteristics were measured. These characteristics are shown in Figs. 18 and 19. There is negligible difference in both characteristics over a 600-hour test period. The effective engine perveance ( $8.55 \times 10^{-9} \text{ A/V}^{3/2}\text{-cm}$ ) was unchanged.

Engine operation was essentially arc free. The arc rate over the 954-hour period was 1.7 arcs/100 hours. The ionizer voltage was varied during the test to reduce the beam spread and minimize the possibility of erosion of the tank cryowall. The accel electrodes were designed to run hot to reduce accel drains, as in the previous two engines, by eliminating the major portion of the electrode which overhangs the ionizer. This decreases the area which rejects heat received from the ionizer, and thus increases the electrode temperature. The reduced electrode end area also helps to reduce accel drain currents to the frame. Power, in the form of accel drain current, is essentially conserved since most of these electrons impinge onto the ionizer. The end area is only 10% of the effective electrode surface area. Electron current density from the accel electrode was approximately  $5 \times 10^{-5} \text{ A/cm}^2$ . The measured accel temperature from separate thermal tests was  $830^{\circ}\text{K}$  for the end electrodes and  $870^{\circ}\text{K}$  for the center electrodes. The accel drain current density agrees well with copper-cesium emission data obtained previously.

The engine drain accel-decel characteristics are shown in Fig. 20. The increase in drain current for accel-decel ratios greater than 5:1 is not understood. Two possibilities exist for this characteristic: (a) either the accel-to-ground leakage current increased or (b) electrons were emitted from the accel to the cage. In either case, the current could be accel voltage dependent. The maximum accel-decel ratio was 6.55:1. This corresponds to a specific impulse of 5000 seconds. The current density was  $14.5 \text{ mA/cm}^2$ .

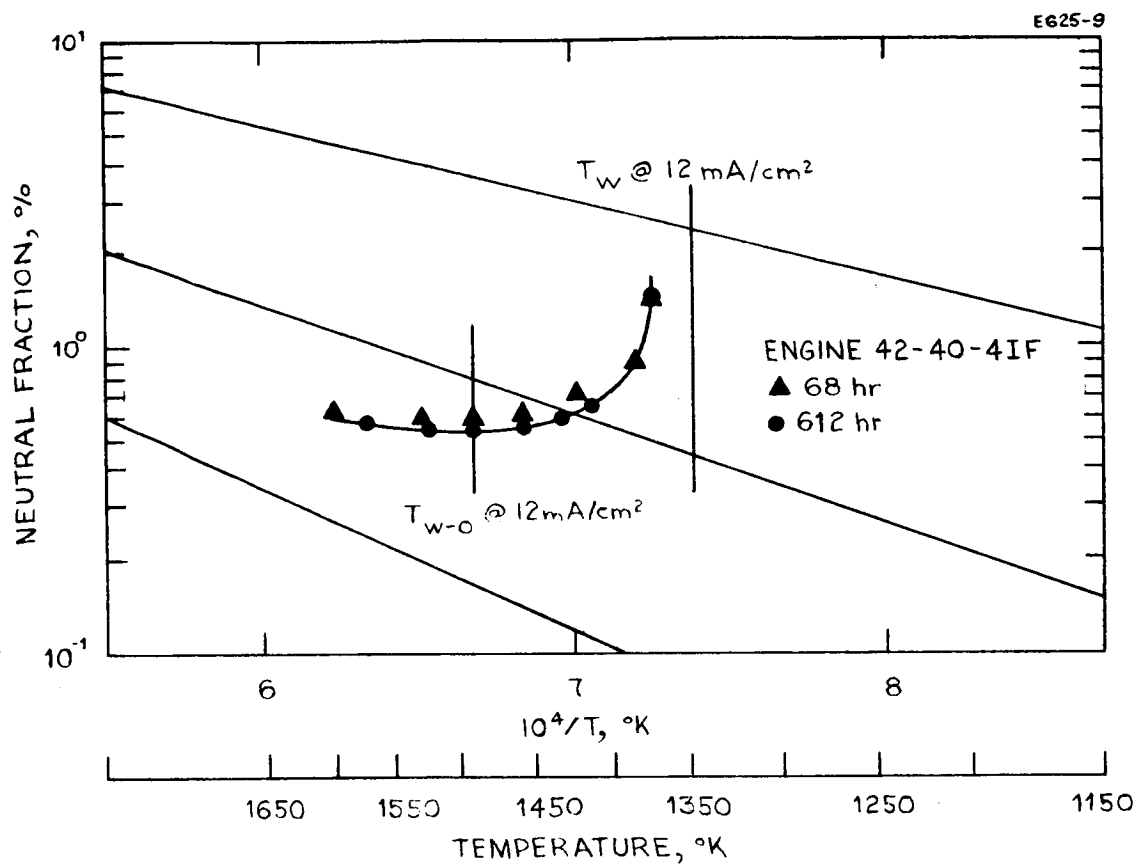


Fig. 18. Neutral fraction versus temperature data taken during the 68th and 612th hour of test of engine 42-40-4 IF.

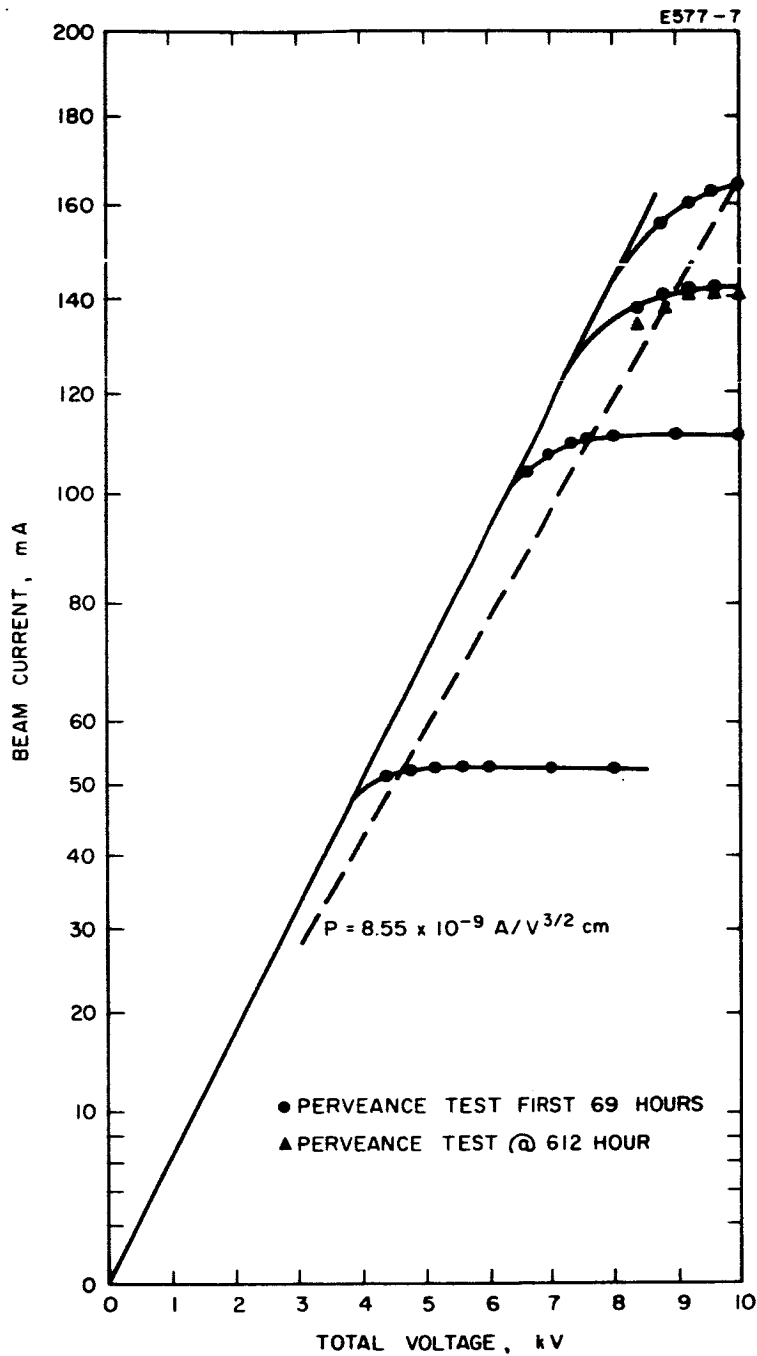


Fig. 19.  
 Perveance characteristics taken during the first 69 hours and 612th hour of test of engine 42-40-4 IF.

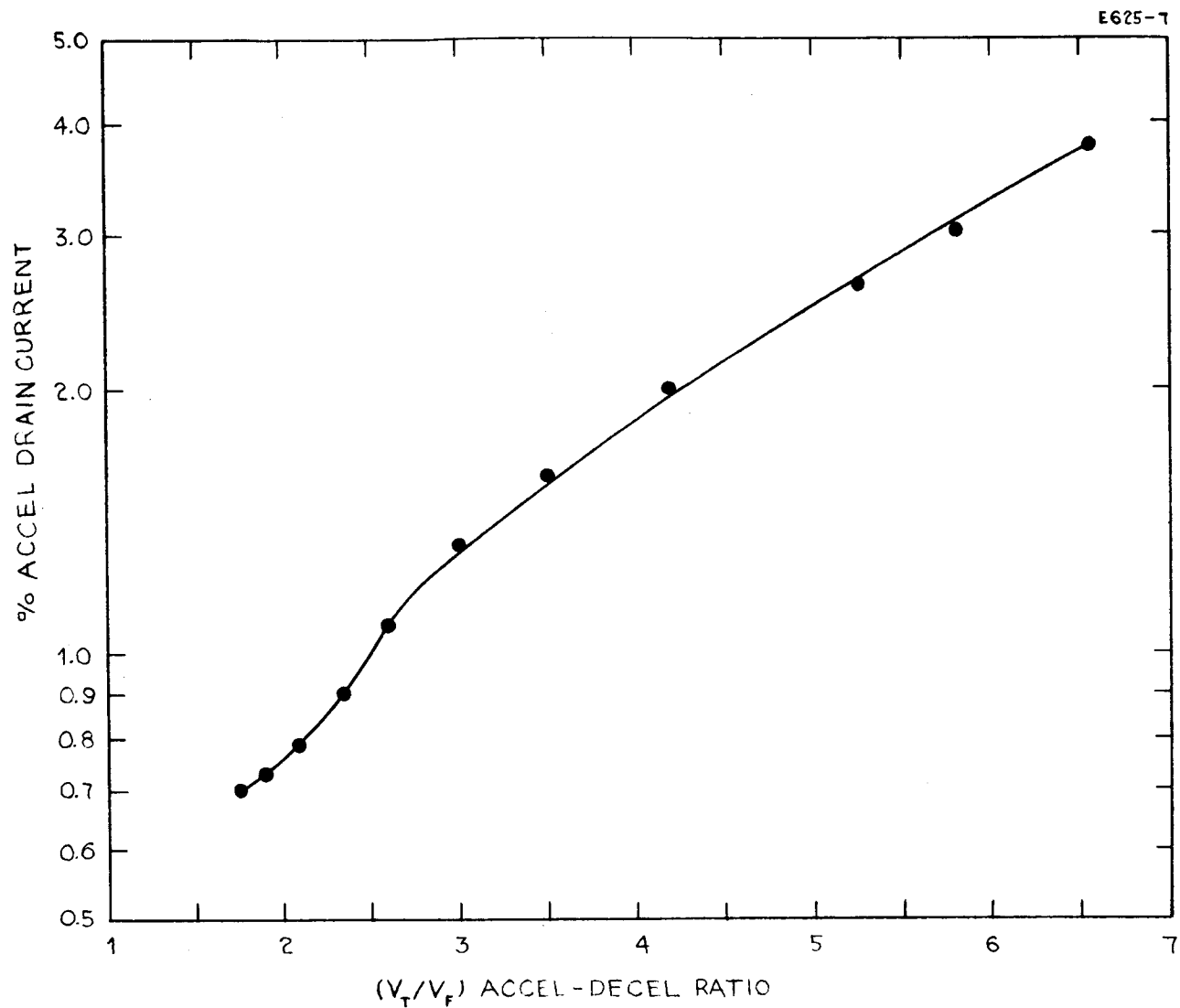


Fig. 20. Drain current accel-decel ratio characteristics of engine 42-40-4 IF. Measurements made at 14.5 mA/cm<sup>2</sup>.

## 2. Post Test Analysis

Examination of the engine after the 954-hour test indicated that the accel electrodes were uniformly eroded along their length. However, the weight loss per electrode was not uniform. A sketch of a section through each electrode is shown in Fig. 21. The erosion pattern of each electrode was similar. The electrode weight data is presented in Table II. The last column is the estimated neutral fraction required to erode 30 percent of the electrode (Fig. 22).

TABLE II

Accel Electrode Data from Test of Engine 43-40-4 IF

Electrode	Initial Weight $W_o$ , g	Final Weight $W_f$ , g	Weight Change, $\Delta W$ , g	Calculated Electrode Life L hours (30% erosion)	Estimated NF (True)
1	4.5362	4.2054	-0.3308	3920	0.8
2	7.0556	6.0704	-0.9852	2040	1.7
3	7.2730	6.8658	-0.4072	5100	0.7
4	7.2677	6.7543	-0.5134	4050	0.8
5	4.555	4.597	+0.042	—	

The electrode life was calculated on the basis of permitting an electrode weight loss of 30%. Therefore,

$$L = 0.3 \frac{W_o \tau}{\Delta W}$$

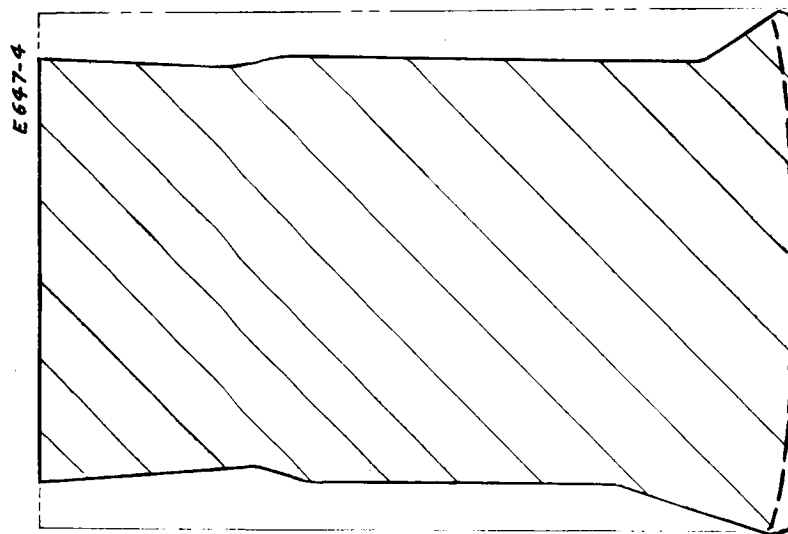
where

- $\tau$   $\equiv$  test time (hours)
- $W_o$   $\equiv$  initial electrode weight, g
- $\Delta W$   $\equiv$  difference weight (+ gained, - lost)
- $L$   $\equiv$  calculated life, hours

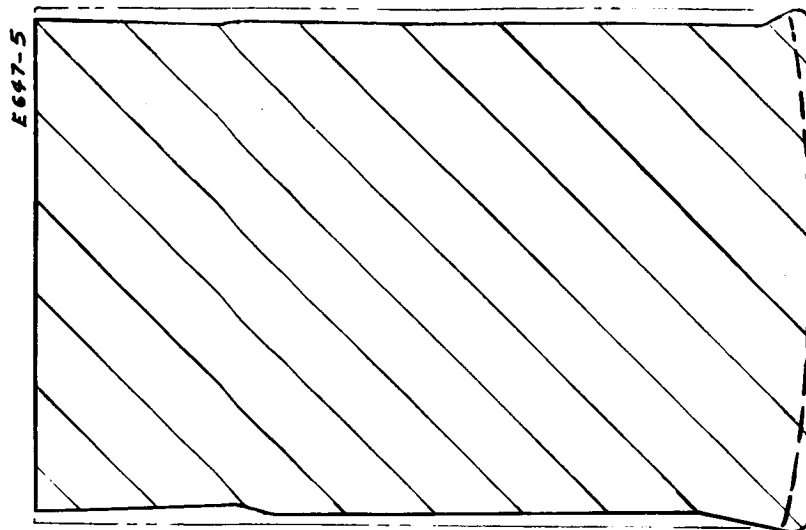
The minimum electrode life is estimated to be 2040 hours. The maximum life is estimated to be 5100 hours. The shorter life corresponds



ELECTRODE NO.1

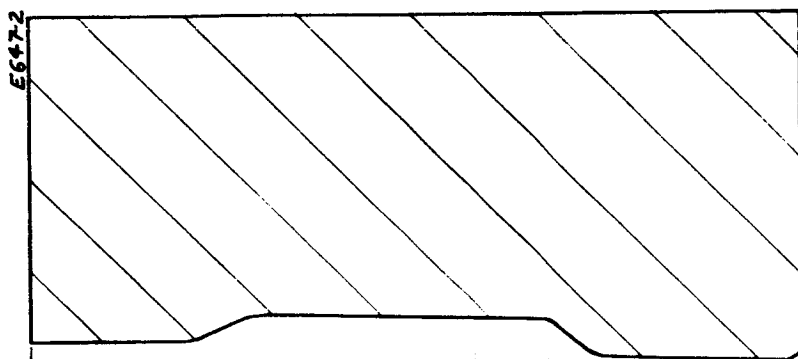


ELECTRODE NO.2

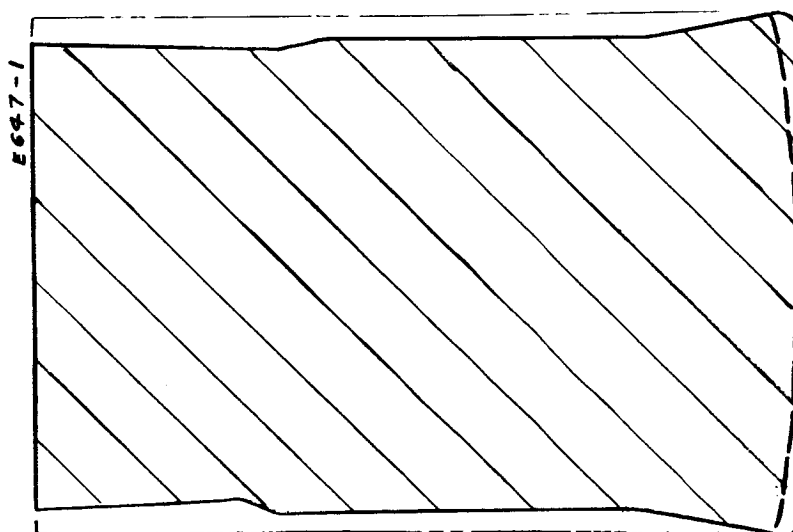


ELECTRODE NO.3

Fig. 21. Sketches showing side erosion of accel electrodes.



ELECTRODE NO. 5



ELECTRODE NO. 4

Fig. 21. Con't.



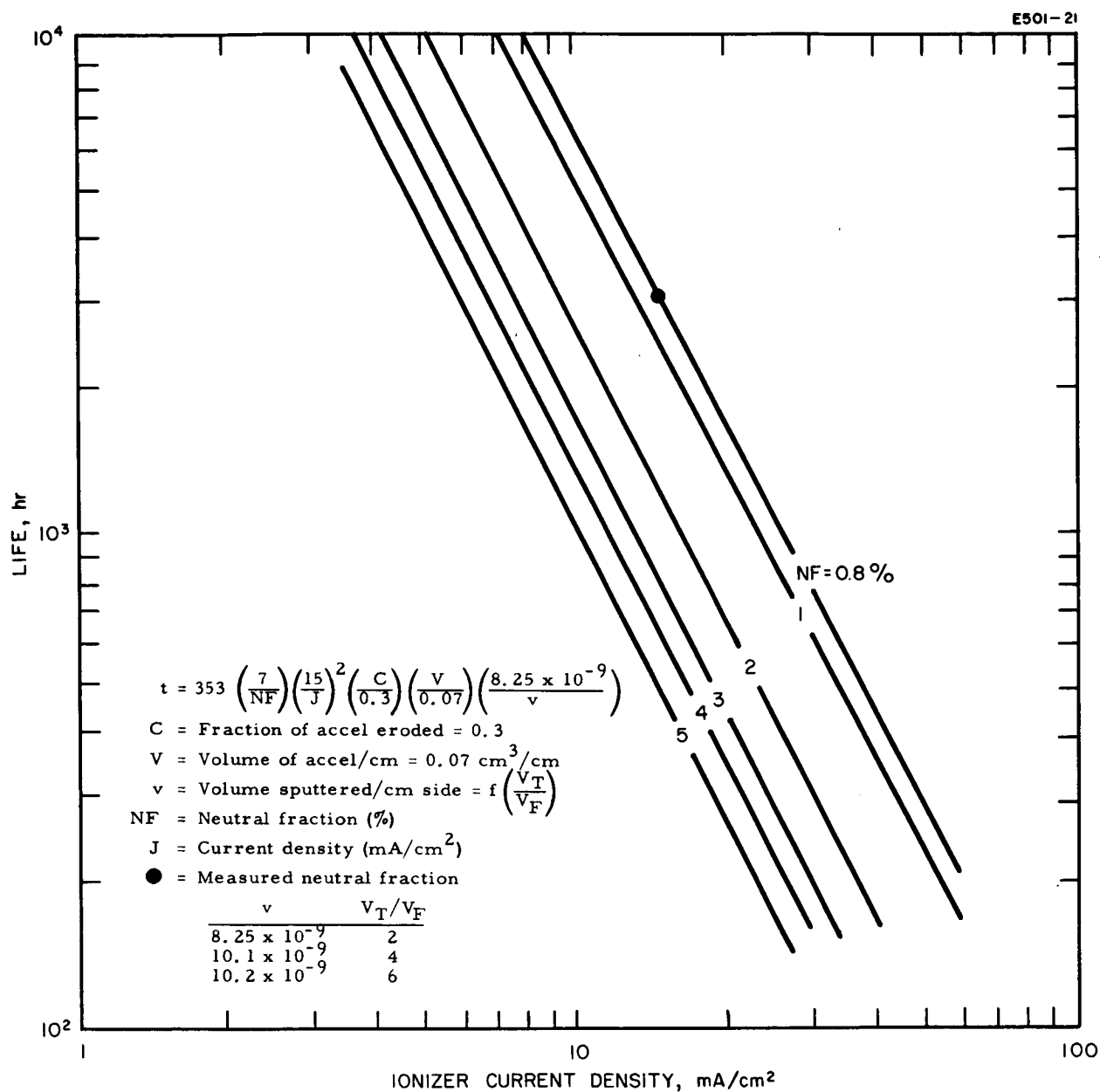


Fig. 22. Engine life limited by charge exchange ions (integral focus ion engine).

to the first and second electrodes which enclose the first ionizer strip. It was observed that the bubble efflux pattern from the first strip was in excess of the other strips. A photograph of a typical electrode is shown in Fig. 23. A 15x photograph of the electrode base is shown in Fig. 24. The striations across the electrode base are approximately 0.005 in. deep. An axial image of the knife edge insert on the accel electrode was not apparent. The maximum penetration appears at the electrode side. Erosion was not apparent at the base of the outer accel electrodes. Thus, the erosion is originating from the hot tungsten inserts and not from the cold outer focus electrodes. The semicircular erosion pattern at the electrode end is due to ions emitted from the gap between the tungsten knife edge insert and the end effect mask. A design modification in process should eliminate this erosion. The measured neutral fraction was 0.54%. In accordance with the Space Technology Research Laboratories analysis relating to apparent and true neutral fraction, the true neutral fraction was approximately 1%.

The arrival rate of copper from the beam collector to the ionizer was measured after the life test. This factor is of concern for three reasons: (a) the copper arrival rate can depress the ionizer work function, (b) the copper can build up on the electrodes and subsequently peel and cause an electrode short, and (c) the copper can build up on the electrode and alter the engine optics.

Engines 42-40-1, 2, 3, and 4 were designed to use three integral focus insert electrodes (electrodes 2, 3 and 4). The outside electrodes on the first and fourth strip were incorporated into the end correction mask. During engine operation, the mask is "cold" (approximately 470°C) and therefore returning copper sticks to these outer focus electrodes whereas it evaporates from the 1200°C insert electrodes. The copper buildup adjacent to electrode 1 varied between  $7.5 \times 10^{-3}$  and  $8.8 \times 10^{-3}$  inch. The copper buildup adjacent to electrode 5 was  $4.5 \times 10^{-3}$  inch. These thicknesses correspond to a copper arrival rate varying between  $2.8 \times 10^{14}$  and  $5.5 \times 10^{14}$  atoms/cm<sup>2</sup>-sec,

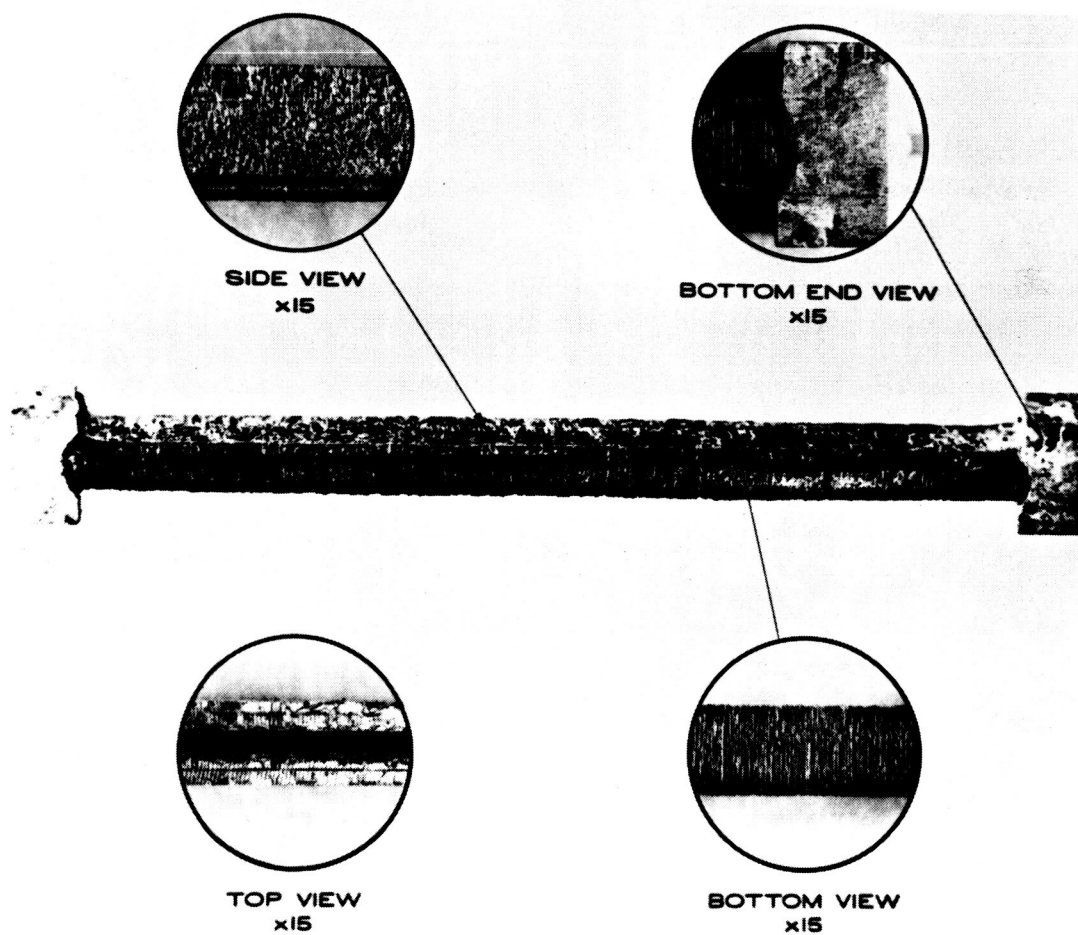


Fig. 23. Multistrip engine accel electrode erosion patterns. Test time — 953 hours, current density —  $12.9 \text{ mA/cm}^2$ .

M 1653

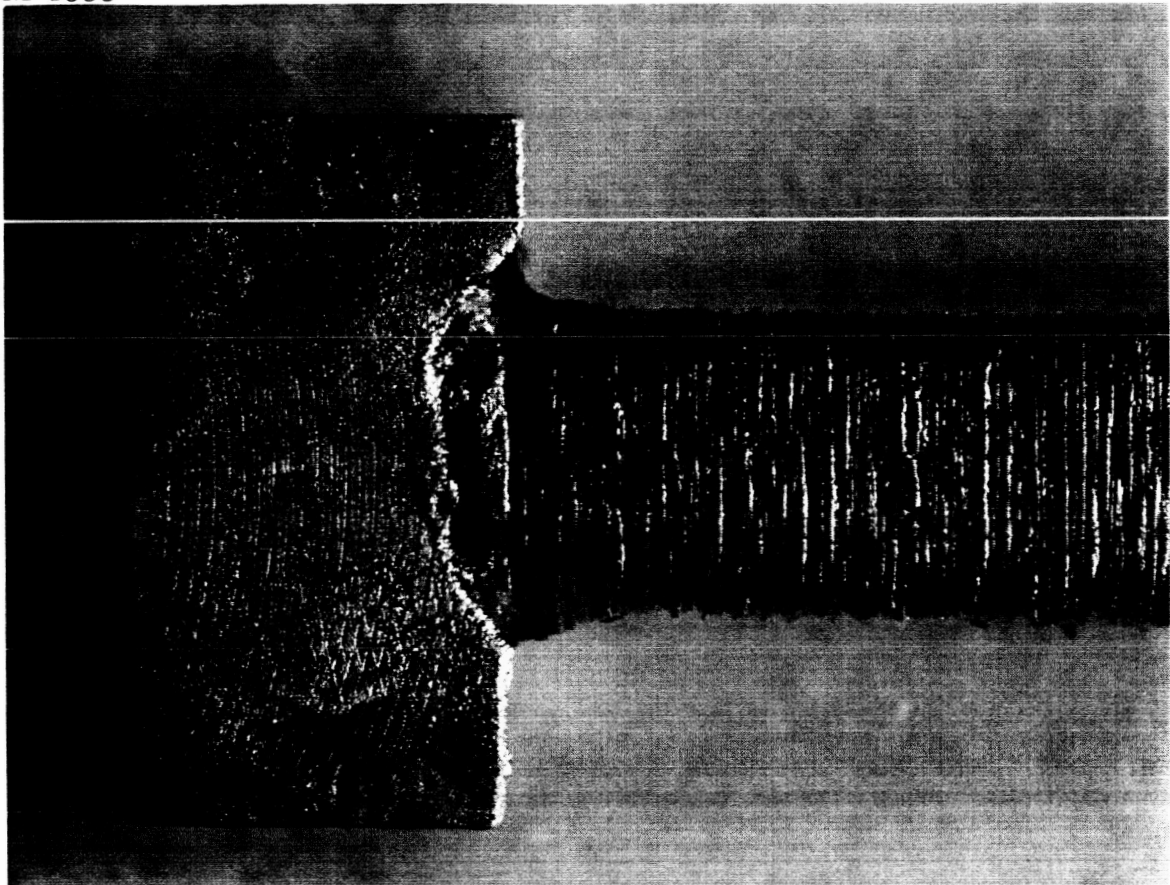


Fig. 24. Photograph of the base of the accel electrode (x15) showing striated erosion as well as end effect erosion.

where: 
$$\mu = \frac{t \rho A}{M \tau} = 0.59 \times 10^{20} \frac{t'}{\tau'}$$

- $\mu$  = arrival rate (atoms/cm<sup>2</sup> - sec)
- $t$  = thickness cm [  $t'$  (inches) ]
- $\rho$  = density copper (gms/cc)
- $A$  = Avogadros number (particles/mole)
- $M$  = molecular weight
- $\tau$  = test time (sec) [  $\tau'$  (hours) ]

The departure rate of cesium ions from the ionizer surface at 12.9 mA/cm<sup>2</sup> is  $8.1 \times 10^{16}$  ions/cm<sup>2</sup>-sec. The ratio of the average atom to cesium ion rates is therefore  $0.5 \times 10^{-2}$  or, one copper atom arrives for every 200 cesium particles which leave the ionizer. Five 0.75 square inch tabs were located on the front face of the engine. These tabs were also used to measure the copper arrival rate. The average weight change for these tabs was 0.216 grams.

The arrival rate was computed from

$$\mu = \frac{\Delta W A}{M \tau a}$$

where:

- $\Delta W$  = the weight change (grams)
- $a$  = tab area (cm<sup>2</sup>)

The average arrival rate was  $1.36 \times 10^{14}$  atoms/cm<sup>2</sup>-sec. The ratio of copper to ion rates is thus  $1.68 \times 10^{-3}$  or, one copper atom arrives for every 600 cesium particles which leave the ionizer.

According to the work-function arrival-rate data of Wilson, an arrival rate of  $5 \times 10^{14}$  atoms/cm<sup>2</sup>-sec can reduce the work function of tungsten by 0.05 volts (Fig. 25). Similarly, the same arrival rate on an iridium surface can reduce the effective work function by 0.2 volts (Fig. 26).

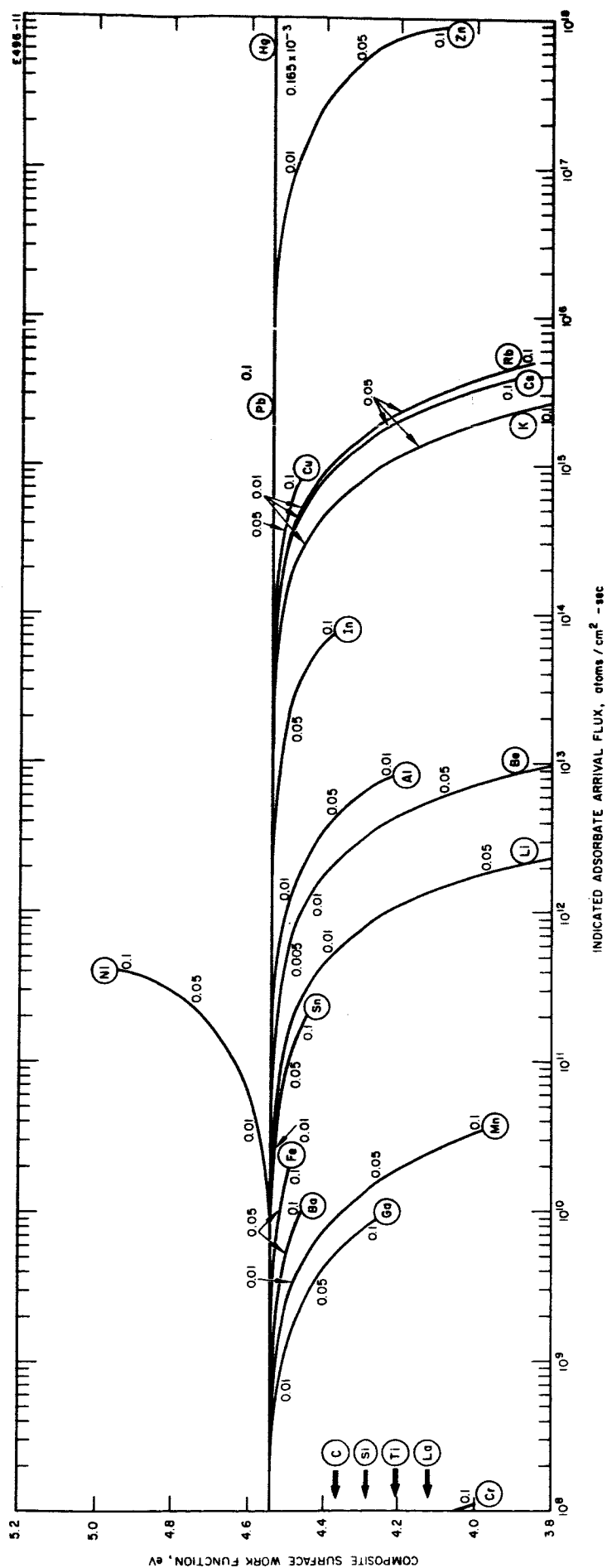


Fig. 25. Composite surface work function versus arrival flux for 27 adsorbate atoms on tungsten.

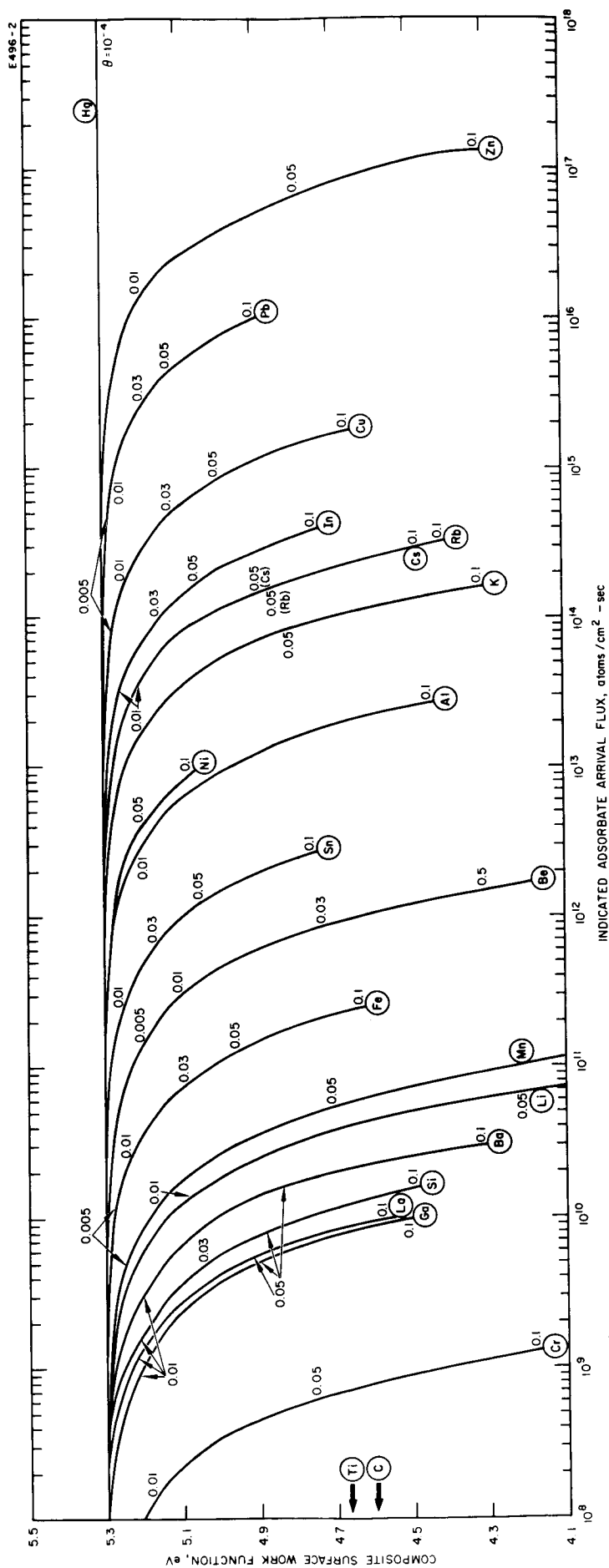


Fig. 26. Composite surface work function versus arrival flux for 27 adsorbate atoms on iridium.

### 3. Post Test Ionizer Examination

A microscopic examination of the ionizer indicated slight erosion patterns. The strip enclosed by electrodes 1 and 2 exhibited the maximum erosion estimated to be between 5 and 6 mils deep. A sketch of the estimated erosion is shown in Fig. 27.

The results of a post test bubble evaluation of the ionizer are shown in Figs. 28 and 29. The higher pressure pattern (Fig. 28) accentuates the nonuniformity of the ionizer. The bubble patterns show excess flow in the vicinity of strip number 1. This correlates with the electrode erosion patterns.

A detailed surface examination of the ionizer was not performed prior to the life test. The ionizer was previously used in engine 42-40-1 IF which had a cesium leak.

It is possible that the ionizer erosion is attributable to negative ion bombardment of the ionizer surface. This phenomenon is neutral fraction dependent. The erosion could have occurred during the test of engine 42-40-1 IF (high background cesium pressure resulting from a leak) or during this life test. Subsequent engine tests should provide additional data on the erosion of the ionizer as it relates to neutral fraction.

### D. Conclusion

The integral focus cesium contact engine described herein performed in a completely satisfactory manner during this life test. All parameters indicated that the fundamental problems associated with this class of engine were essentially solved.

Erosion, drains, critical temperature, neutral fraction, etc., were at their expected levels. The test showed that the engine life with a tungsten ionizer would be as prescribed by theory. The present engine has an estimated electrode life between 2000 and 5000 hours. The HRL 3.9  $\mu$  ionizer material, if available for this engine test, would have easily permitted the minimum life to be 5000 hours.



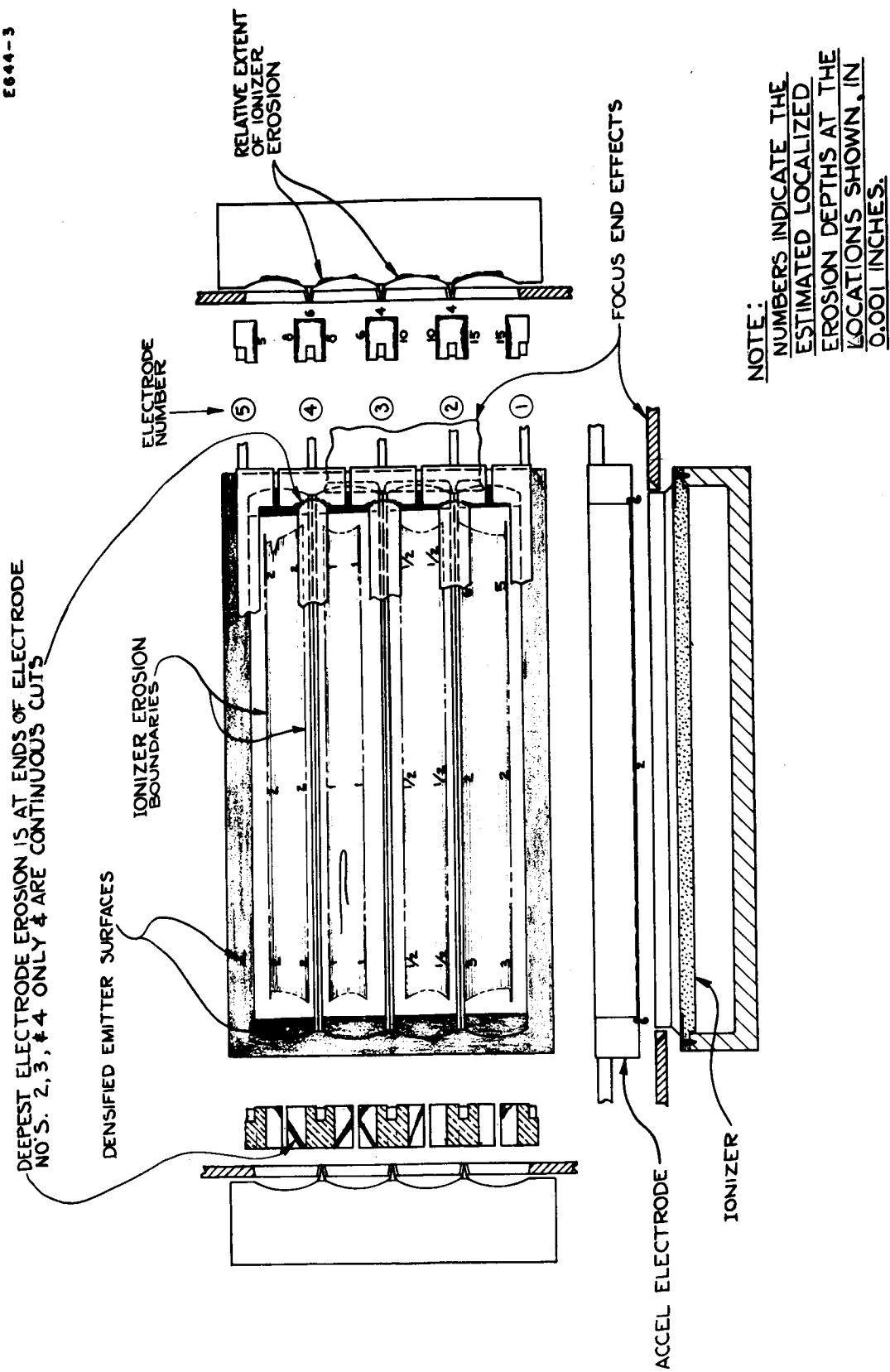


Fig. 27. 42-40-4 ionizer and electrode erosion after life test.

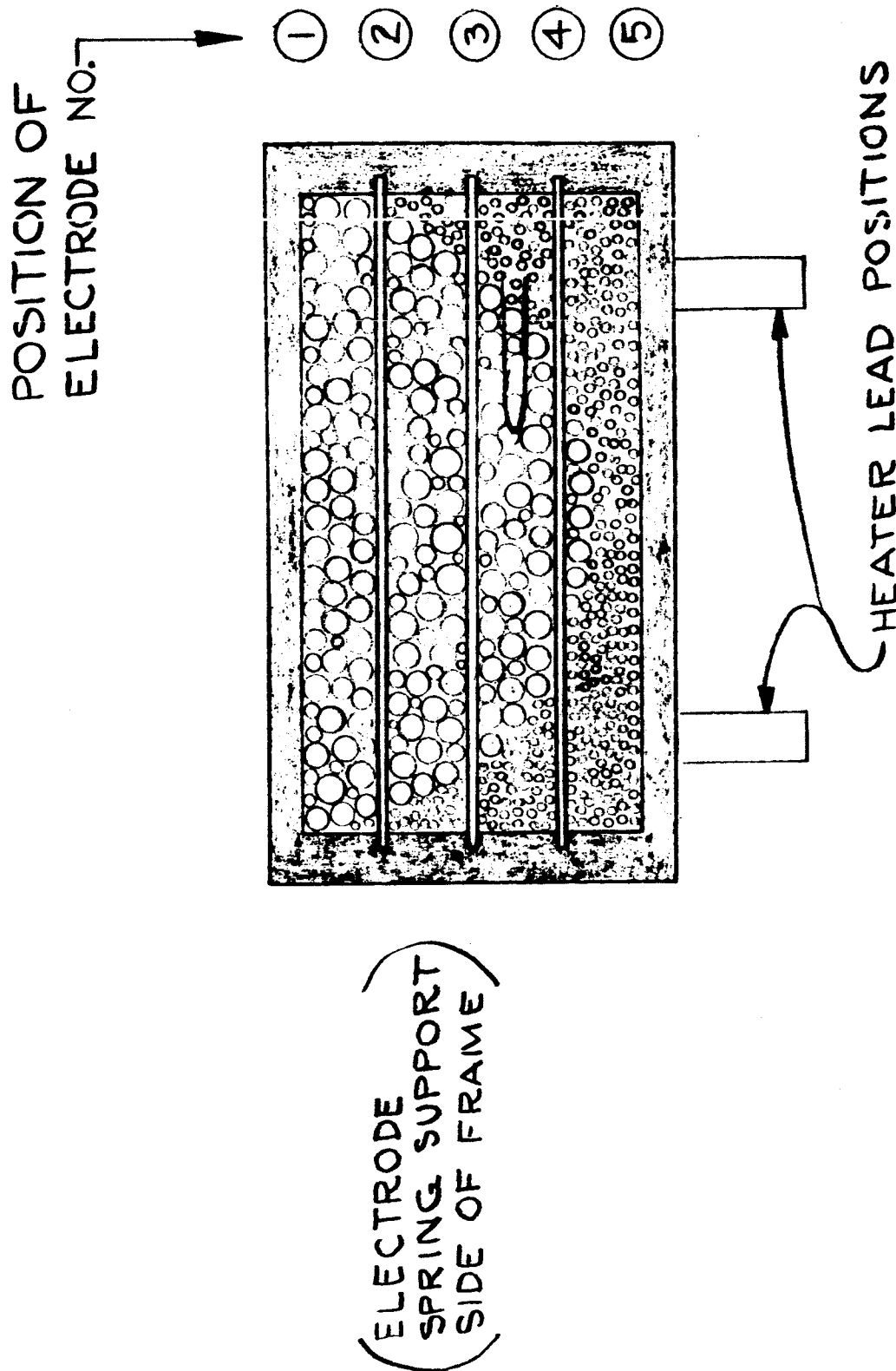
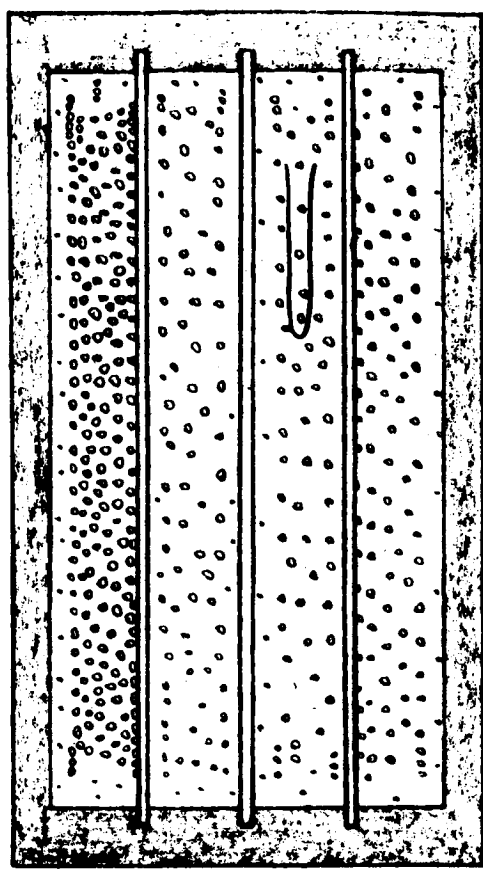


Fig. 28. Post test bubble patterns for engine 42-40-4 IF - high flow rate.

POSITION OF  
ELECTRODE NO. 7

- ①
- ②
- ③
- ④
- ⑤



(ELECTRODE  
SPRING SUPPORT  
SIDE OF FRAME)

HEATER LEAD POSITIONS

Fig. 29. Post test bubble patterns for engine 42-40-4 IF - low flow rate.

The data presented herein is only the stepping stone for the potential capability for this engine. Our recent successes with high work function surfaces, also reported herein, show that the expected life for the cesium contact engine can approach 100x the life attainable with a tungsten ionizer.

### III. OPTICS STUDIES

#### A. Digital Computer Study

A recalculation has been carried out of the ion trajectories and space charge limitations for the knife-edge insert configuration of integral-focus engine. The results confirm the previous calculations which show that ion trajectories are focused clear of the accelerating electrodes and the current capability is higher than that of the Model 70 optics. In full space charge operation, a total voltage of 10 kV would accelerate a cesium ion current of  $17.5 \text{ mA/cm}^2$  at the center line of a linear strip lens and an ion current of  $24.5 \text{ mA/cm}^2$  near the edges.

A study in which the inner sides of the accel electrodes were indented to one-half of the electrode width to simulate charge exchange erosion showed no detrimental effects on the trajectories or current capability. When the total accel width was reduced to one-half its normal value the current capability at the center of the lens dropped to  $12.5 \text{ mA/cm}^2$  at 10 kV total voltage.

#### B. Analog Computer Studies

The analog trajectory tracer has been used to study the sensitivity of the beam trajectories to displacement of the accel electrodes in the knife-edge type of integral focus optics. In the standard position, with the accel electrodes centered over the knife edges, the beam is centered through the accel opening and has a typical  $1/2$ -angle spread of approximately  $5^\circ$ . Moving the accel electrodes away from the ionizer by .020 in. decreases the typical  $1/2$ -angle spread to  $1-1/2^\circ$ , whereas moving the electrodes toward the ionizer by .020 in. increases the  $1/2$ -angle spread to  $12^\circ$  (see Fig. 30).

The lateral displacement of the accel electrodes by .009 in. with respect to the center of the knife-edges causes a deflection of the beam centerline by  $4^\circ$  toward the closest accel (see Fig. 31). Displacing the accel electrodes .020 in. from the centered position deflects the beam by  $10^\circ$  toward the closest accel electrode.

E558-1

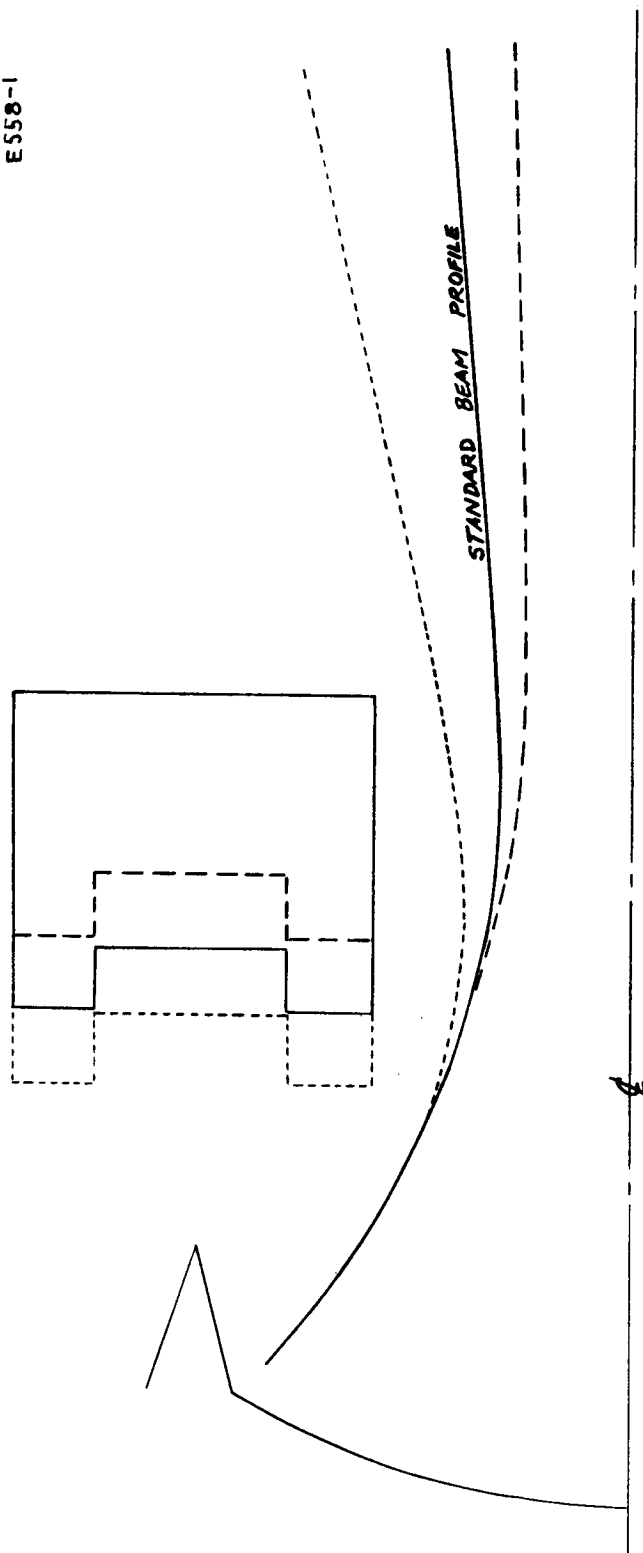


Fig. 30. Influence of accel electrode position on beam profile.

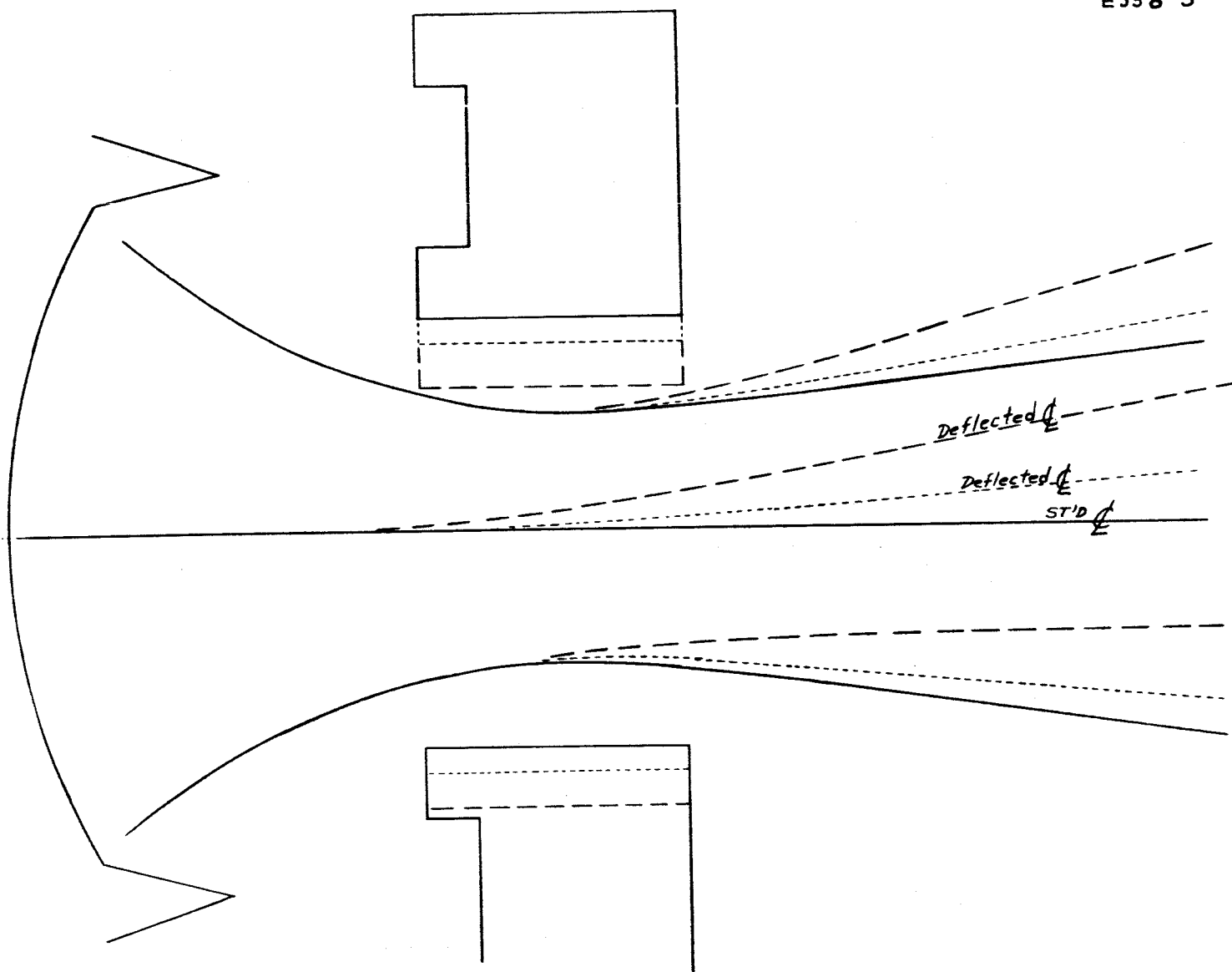


Fig. 31. Influence of accel electrode centering on beam direction.

In addition, we have also investigated the effect of moving the electrode on only one side of the lens while the other electrode remained in position. In Fig. 32, we see that when the No. 1 accel electrode is moved .010 in. and .020 in. toward the beam center, the beam is deflected  $4\frac{1}{2}^\circ$  and  $7^\circ$  toward the No. 1 accel. This results in ion interception with the accel electrode for displacements greater than 0.010 in.

When the No. 1 accel electrode is moved 0.010 in. and 0.020 in. away from the beam (see Fig. 33), the beam center is deflected  $6^\circ$  and  $8^\circ$ , respectively, toward the opposite side and ion interception on the decel becomes more pronounced.

The displacement of the accel electrode away from the center of the beam has the additional disadvantage that it reduces the field strength and therefore reduces the current capability at the centerline of the ionizer lens. Thus, it is important that lateral displacement of an accel electrode be kept below 0.010 in.

In the 42-40-1, -2, -3, and -4 IF engines, a cooled picture frame, enclosing the front of the ionizer, contained the focus end correction and also the focusing edge on the outer two ionizer strips. A study of the influence of moving this side element toward the beam by .020 in. shows that the beam centerline (see Fig. 34) is deflected by  $5^\circ$  and that very little effect is seen on the trajectories on the far side of the beam. Thus, decel erosion appears to be a more sensitive function of accel electrode displacement than of focus electrode placement.

### C. End Effects Correction

The Model 70 ion optics studies developed the optimum arrangement of electrodes in a linear strip thruster utilizing a "cold" focus electrode. Both the digital and analog computer studies of this thruster analyzed the flow of ion current through a representative cross section of the ion beam. The linear strip of ionizer and electrodes were assumed to be infinite in each direction from this cross section. In actual practice, the strips do terminate at the ends of the ionizer lens surface and thus consideration must be given to the influence of this termination on the ion trajectories.



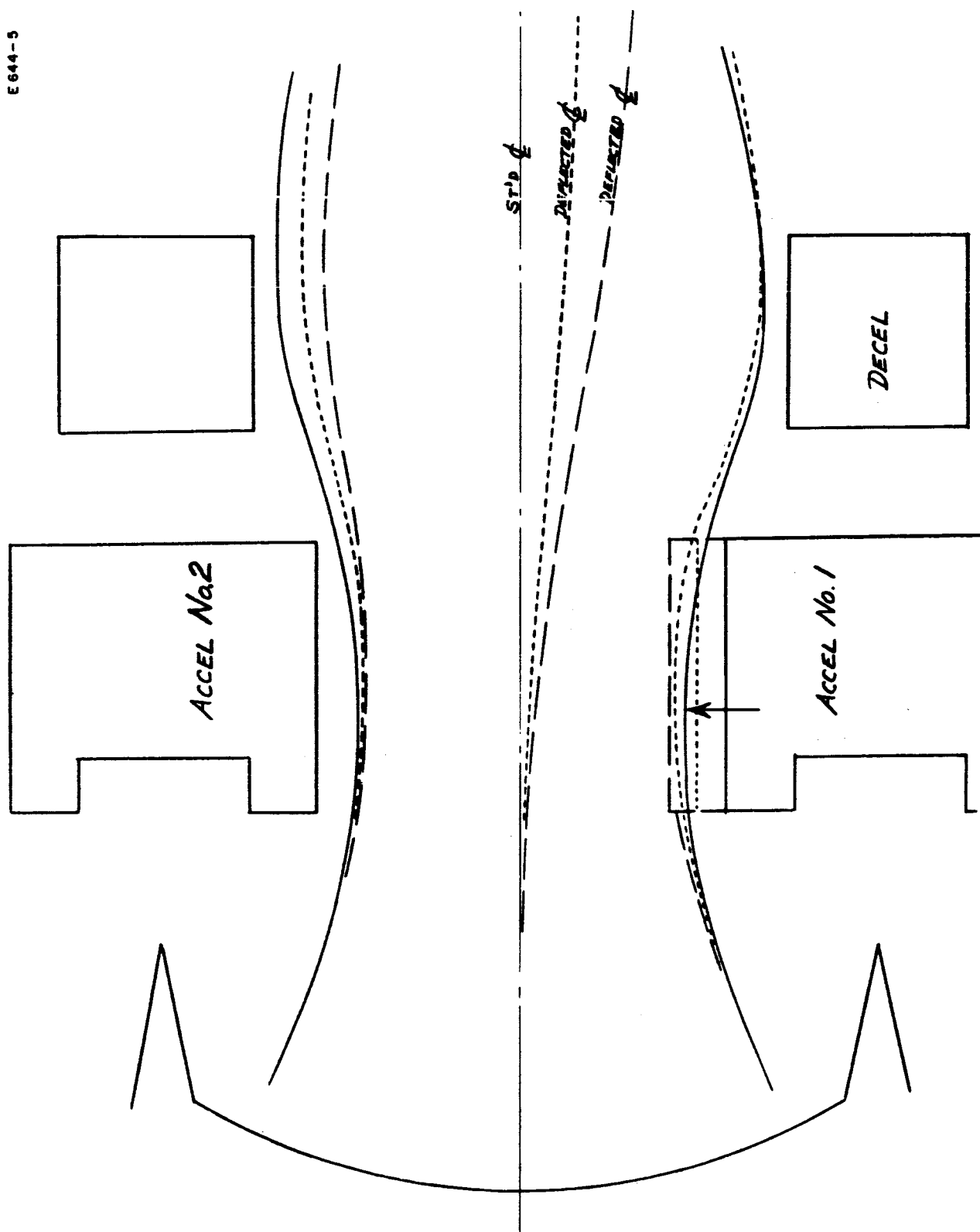


Fig. 32. The influence of accel electrode placement on ion trajectories.

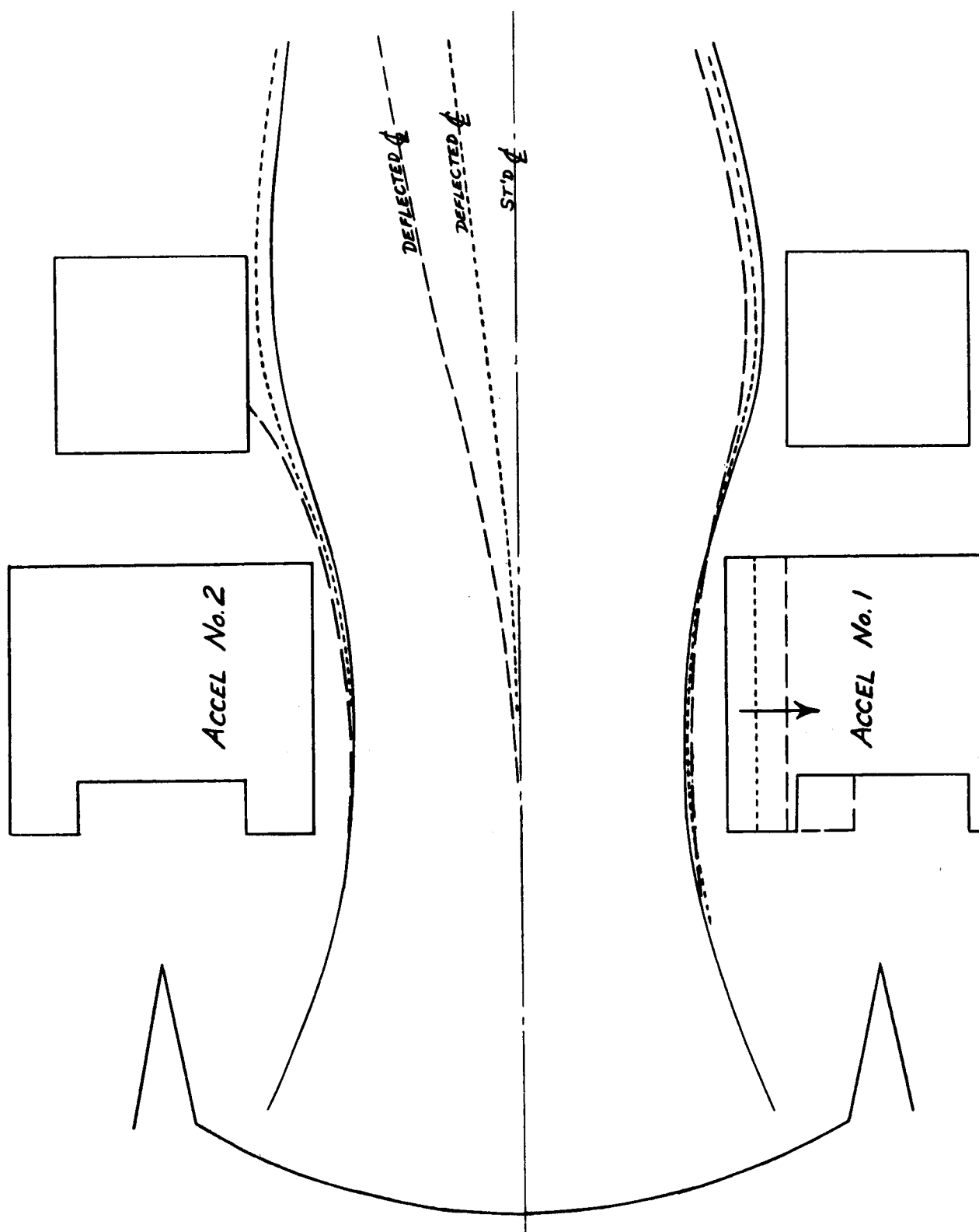


Fig. 33. The influence of accel electrode placement on ion trajectories.

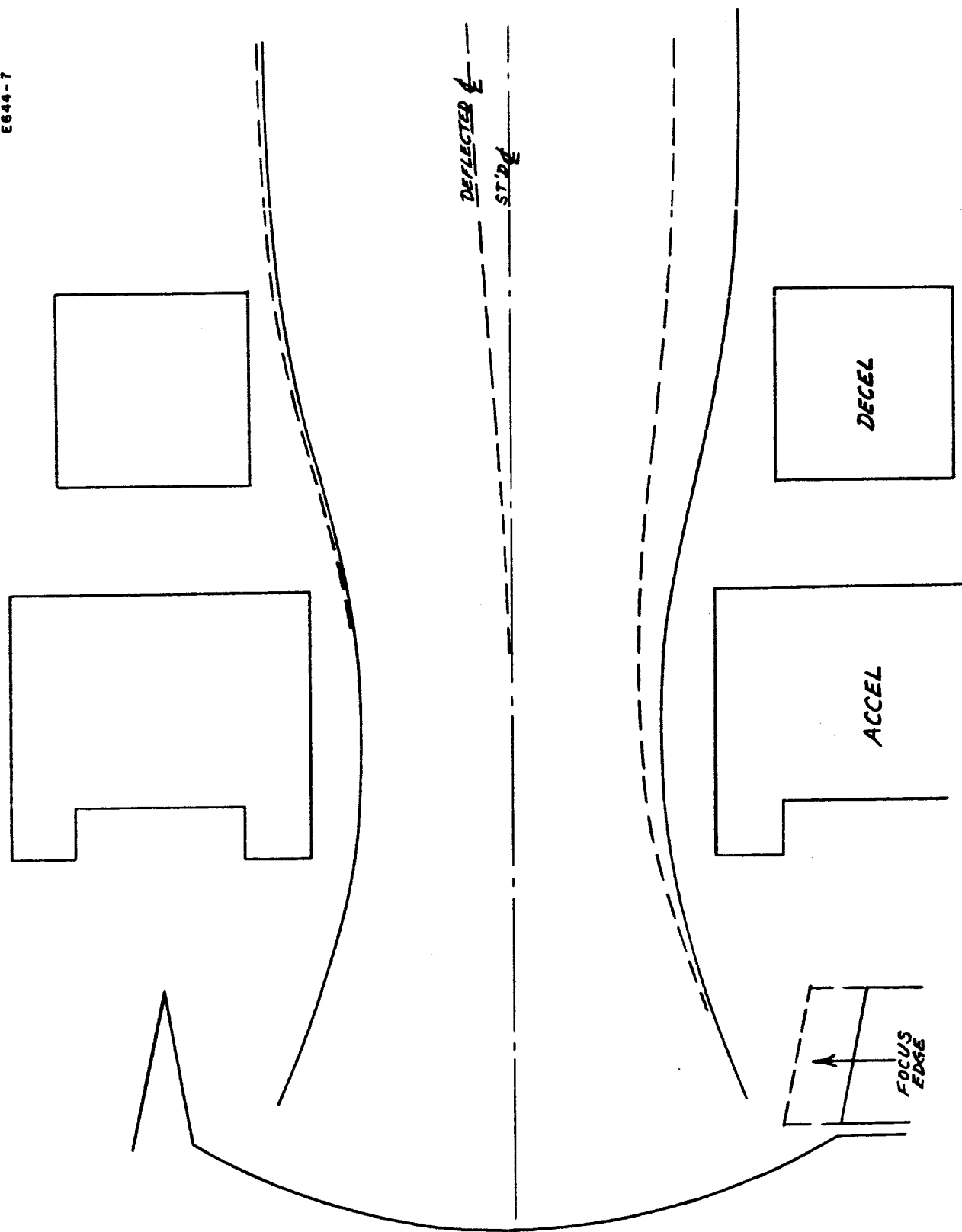


Fig. 34. The influence of the edge focusing member on the ion trajectories.

By the method described in the Phase III Summary Report of Contract NAS 5-517, the first solution at controlling the ion trajectories at the ends of the ionizer lenses is to provide end effects correction to the accel and focus electrodes which produce the same potentials as the beam would see at an internal cross section. The electrolytic tank solves basically a two-dimensional representation of the problem (except for rotational symmetry simulated by the slanted-bottom tank). The potential match of the end electrode shapes is generally made to the centerline of the ion beam; the potential is assumed to be independent of angle when examining the optics through the center of the strip. The solutions of trajectories near the end corners of the lens would be difficult to simulate with any accuracy.

The optimum end-effects extensions to the accel and focus electrodes for the Model 70 optics were used in the 2018-150-1 engine, and it was noted that little or no erosion occurred as a result of interception by improperly focused ions from the ends of the ionizer strips.

The integral-focus optics is similar to the Model 70 optics as far as ionizer curvature and accel spacing; thus, in the operation of the first integral focus engine, 42-40-1 IF, the standard Model 70 end effects corrections were used. Heavy erosion patterns on the accel and decel electrodes indicated that the corrections were not performing as they should. Thus, the electrolytic tank trajectory tracer was used to solve for the best solution to this problem. The first electrode arrangement (see Fig. 35a) was of the corrections as they existed in the 42-40-1 engine. Two types of end corrections were employed in the 42-40-2 IF engine and these are depicted in Figs. 35b and 35c. (Note that the sealing of the ends of the lens surfaces in the 42-40-2 IF configuration makes the relative placement of the end effects with respect to the emitting lens very nearly the same in Figs. 35a and 35b.) The end effect shown in Fig. 35c was accomplished in the engine by shaping the cooled picture frame in the regions between the knife edge focusing inserts. The potential distribution along the centerline for each of the arrangements in Fig. 35 indicated that the ions at the end of the beam would be deflected inward, giving a compression to the

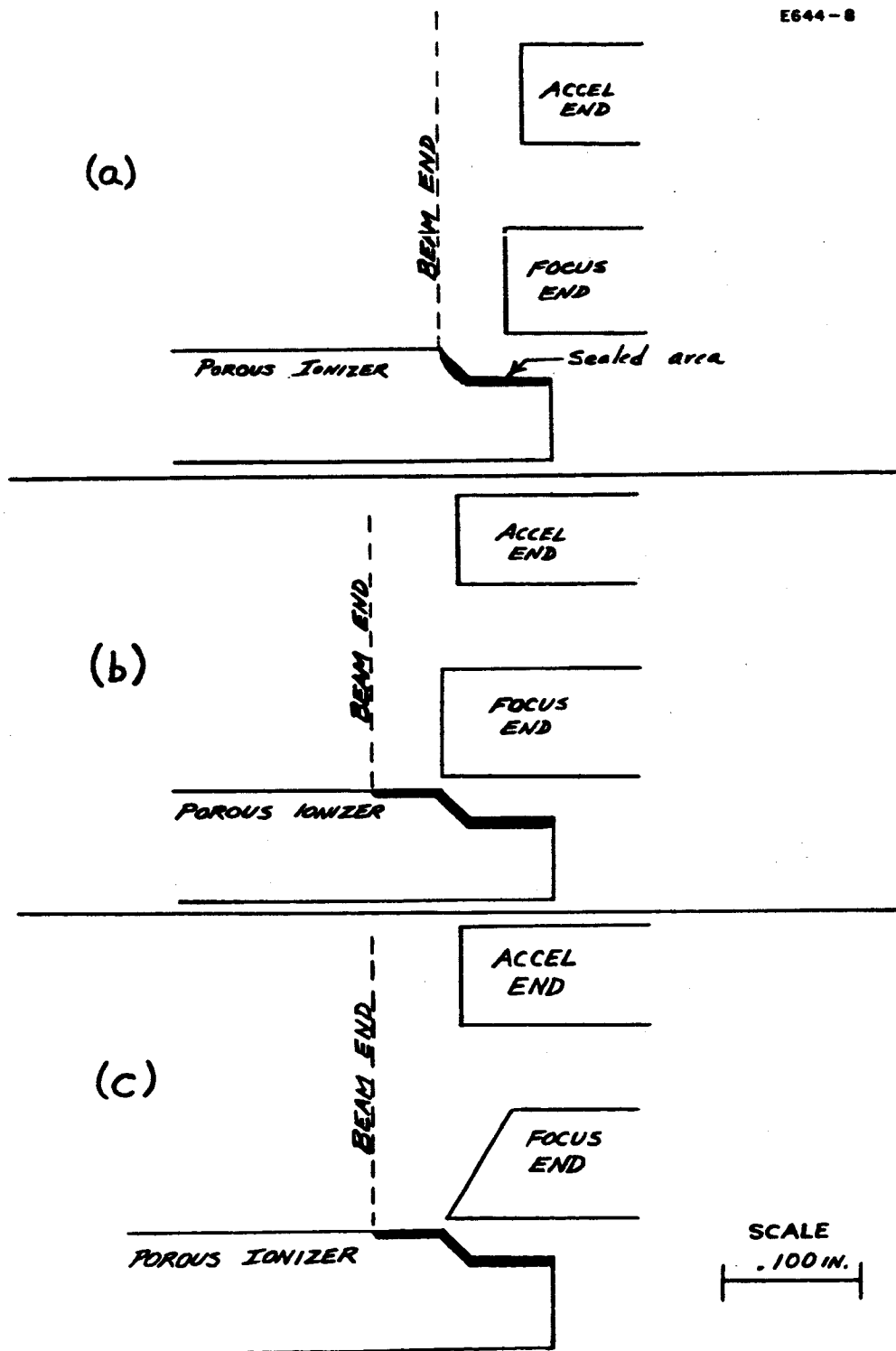


Fig. 35. End-effect corrections adapted from Model 70 optics.

beam. This increased compression would cause an expansion perpendicular to the beam flow and would result in the interception erosion patterns seen on the ends of the accel and decel electrodes. To reduce this compression the potential on the centerline above the end of the lens should be reduced by moving the focus end effect back or slanting its surface away from the lens and by placing the accel electrode correction closer to the ion beam. The combination of these two changes (see Fig. 36a) results in a close match to the internal beam potentials so that excessive compression and resultant beam spread should be eliminated.

Scattered neutrals which arrive in the wash area at the ionizer end in Fig. 36a have the possibility of being ionized and accelerated toward the accel electrodes. This is especially true since the surfaces at the ends are not well defined lens surfaces to start the ions out with controlled directions. To reduce the effect, it is desirable to seal the end positions of the ionizer lens by a light electron beam weld. Then the placement of the electrode end-effects corrections is as shown in Fig. 36b and the sealed area of the ionizer is of the proper radius of curvature to eject stray ions which may be formed. This configuration was incorporated in engine 42-40-3 IF and improvement was observed.

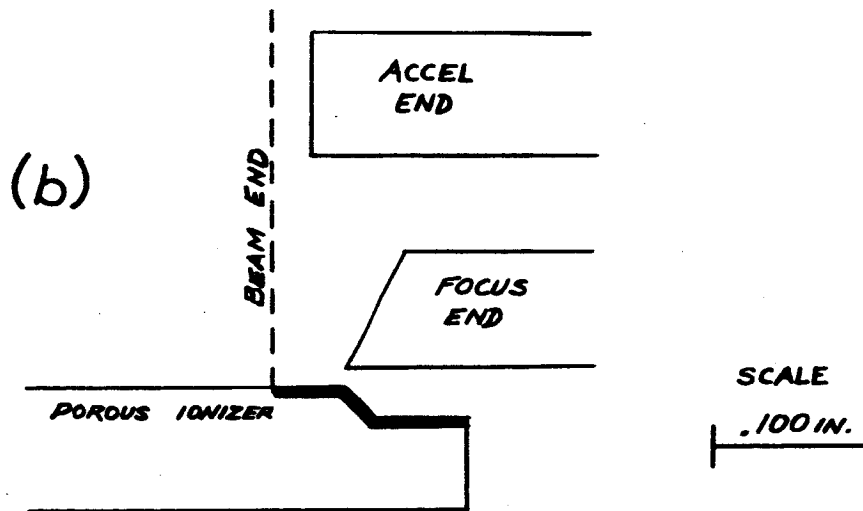
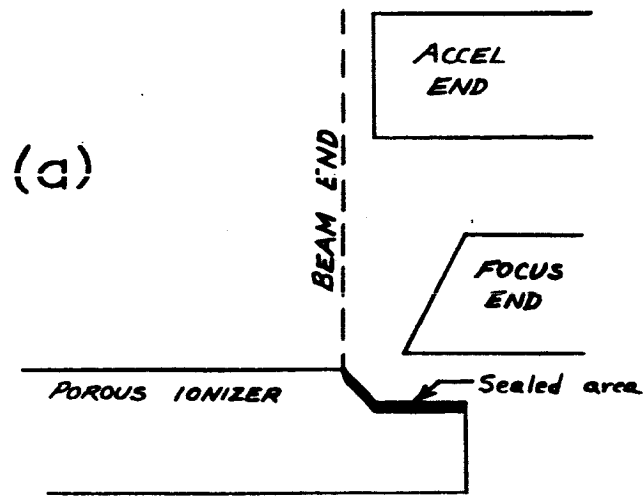


Fig. 36. End-effects corrections for integral-focus engine.

#### IV. FLOW DISTRIBUTION THROUGH IONIZER

Analysis of the Model 70 ion optics has shown that the current capability is essentially uniform from the center to the edges of the porous ionizer lens surface. Thus, an ionizer cross section as shown in Fig. 37 was developed which has been studied on the analog trajectory tracer and is seen to produce the uniform flow which matches the current capability.

The development of the integral focus ionizer with the knife-edge insert produced optics with a nonuniform current capability as shown in Fig. 38. The fields are able to accelerate a higher current density of ions from the edges than from the center of the ionizer lens. In order to achieve maximum perveance from this structure, it is desirable to adjust the flow rate of cesium vapor through the ionizer to match the current capability. The current capability of the lens will then increase from an average of  $17 \text{ mA/cm}^2$  to an average of  $20 \text{ mA/cm}^2$  for the same 10 kV total voltage. Several cases have been studied. They include:

Case(a): a standard ionizer cross section with areas of the rear surface sealed to prevent the flow of cesium into those areas.

Case(b): rear surface sealing of a standard ionizer cross section for the lens in which electron beam welding to the manifold is required for lens attachment or for better thermal conduction.

Case(c): a flow-controlled ionizer where undercutting and section thickness is used to control the cesium flow.

Case(d): a flow-controlled-ionizer section where undercutting and area sealing is used for the open lens and the electron-beam-welded lens surface.

The study designated case(a) was carried out with the possibility in mind that ionizers with the standard cross section which are on hand might be modified by sealing selected areas on the back surface to accomplish the flow adjustment required to utilize the full current capability. The results indicate (see Fig. 39) that a large portion of the back area of the ionizer would need to be sealed. Also, the area which would remain open is critical as to size and location.



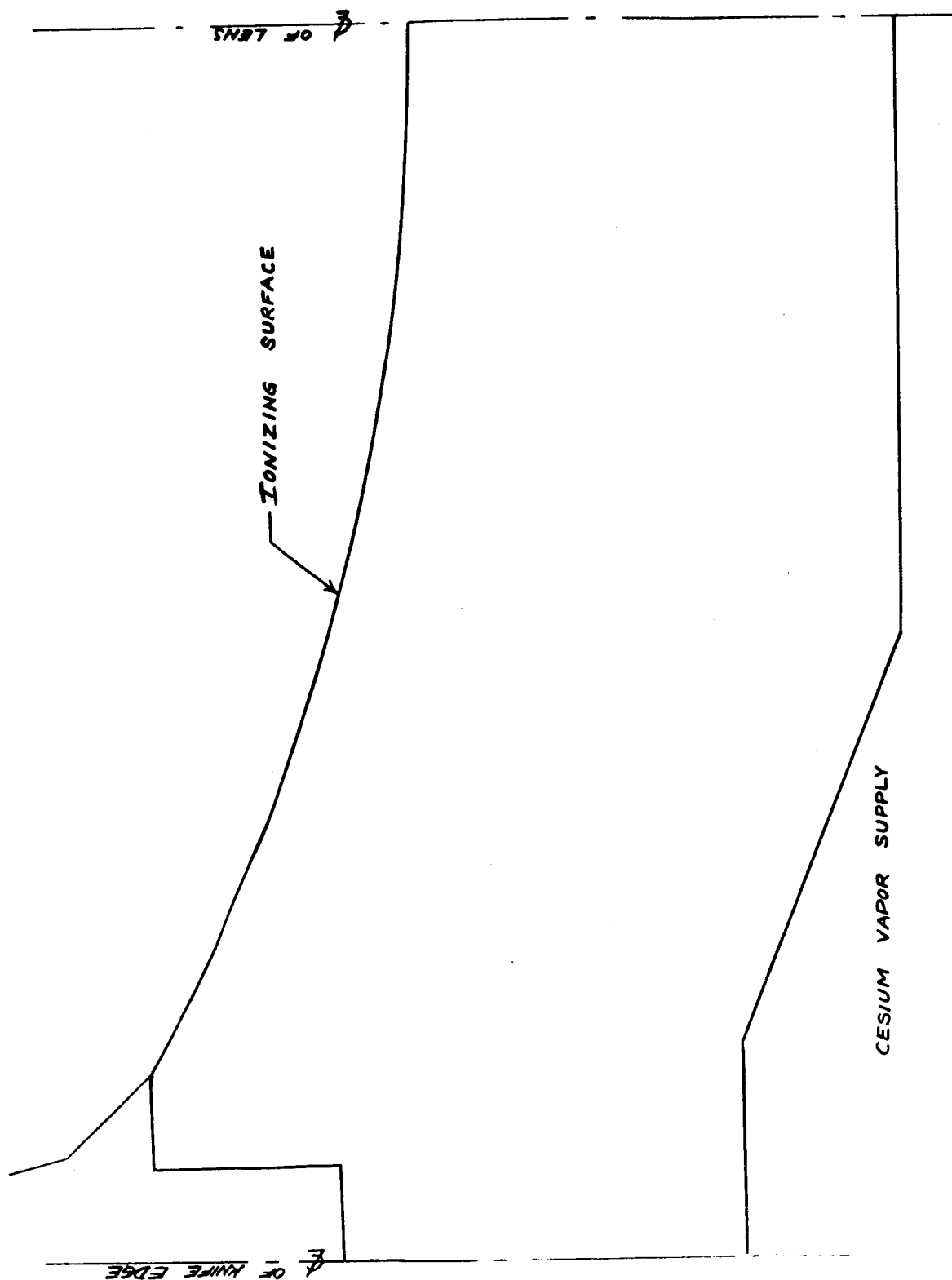


Fig. 37. Cross section of ionizer with uniform flow.

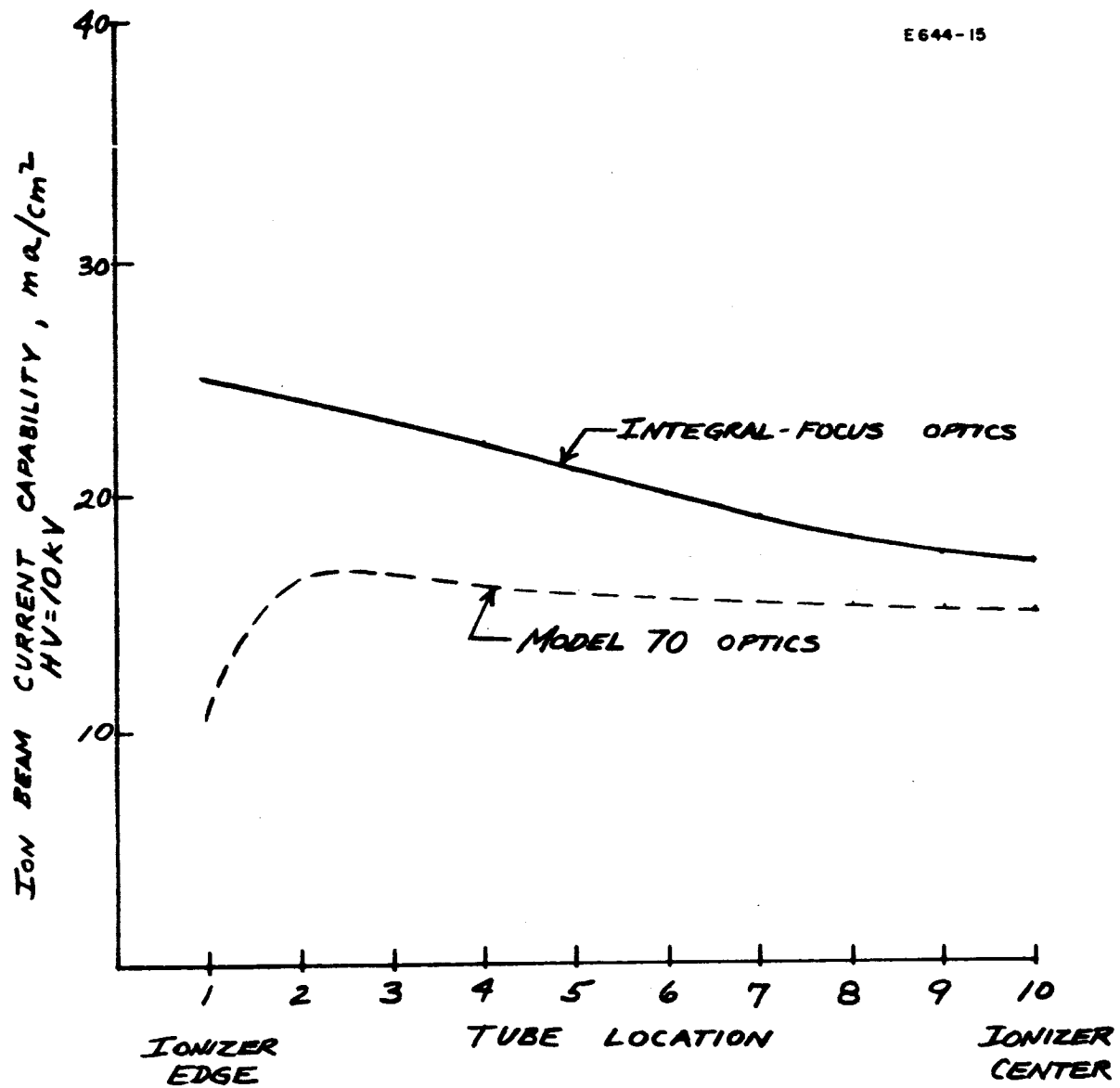


Fig. 38. Current density capabilities for integral-focus optics and for Model 70 optics.

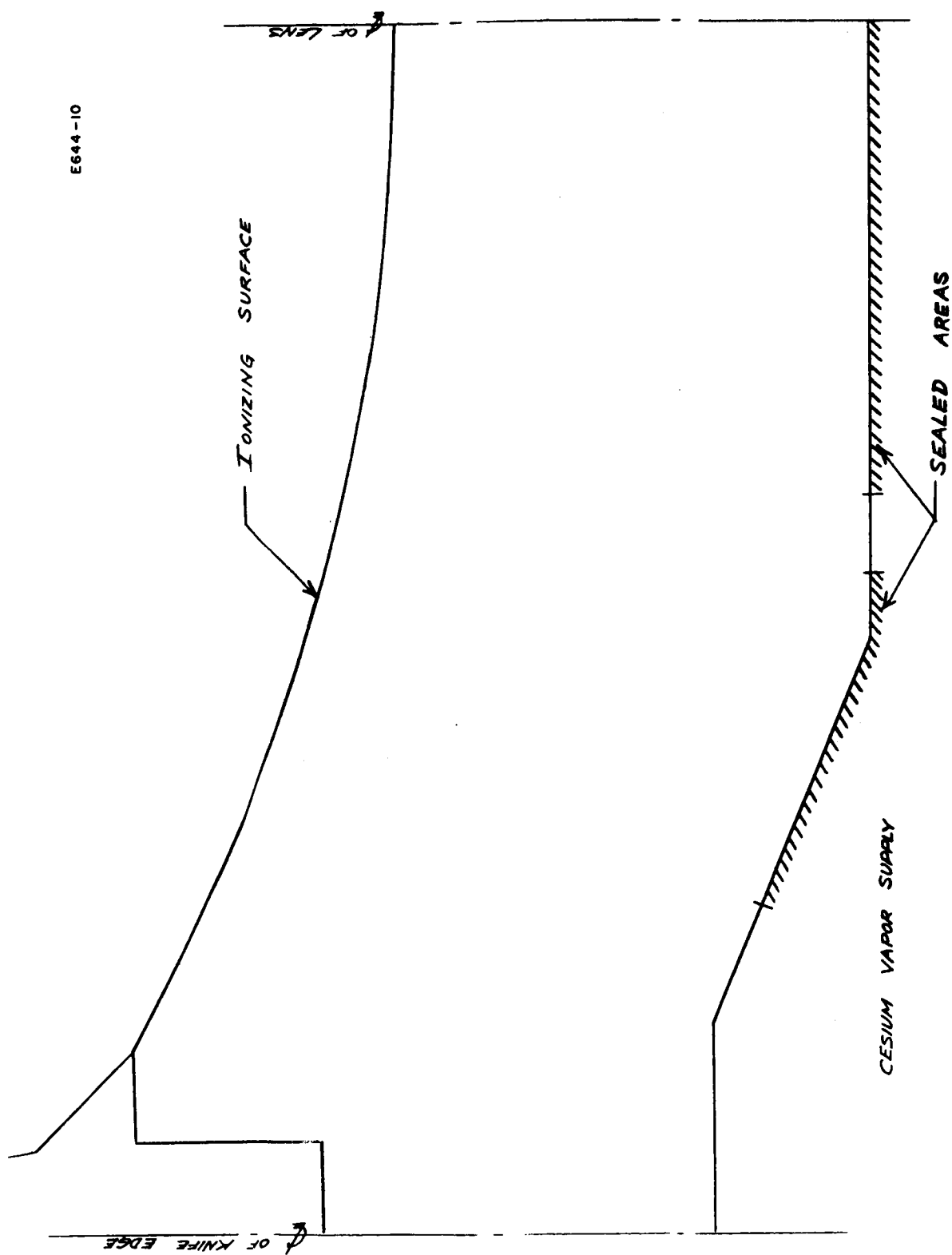


Fig. 39. Standard ionizer cross section with sealed areas to adjust flow for integral-focus optics.

Case(b) (shown in Fig. 40) was also studied on the basis that existing ionizers with the standard cross section might be modified to give the adjusted flow pattern. In this case, the lens surface involved is the one through which an electron beam weld is made to seal the ionizer to the manifold. In this case the open (unsealed) area of the back of the ionizer is even more critical because the flow is required to be impeded in the center region where the cross section is made thin to facilitate electron beam penetration. Therefore, a conflict of requirements must be evaluated. It should be remarked at this time that adjusting the flow by maintaining the standard thickness at the lens edge and thickening the center position is not satisfactory because cesium vapor will be fed from the edges and provide excessive flow at the ionizer center.

If it is determined before manufacture that the ionizer is to be purposely shaped to control the flow then the control is most easily accomplished by undercutting the back of the ionizer to increase the flow at the edges with respect to the centerline flow. In this case [case(c), shown in Fig. 41], the flow may be accurately matched by ionizer cross-section design. If it is desired to simplify the design of the rear surface of the ionizer by machining only the undercut position and leaving the flat areas (see Fig. 42) for attachment to the manifold, then case(d) represents the best solution. It combines the increase in flow at the lens edge with some impedance to flow by sealing a region in the rear of the ionizer near its centerline. The same cross section may be used for the welded and unwelded lens and the only difference will be the extent of sealed areas in these two cases.

The techniques considered for sealing the ionizer areas include electron beam welding, mechanical burnishing to close the pores, and sputtering or vapor depositing refractory material onto the surface. These techniques are still under experimentation and the most satisfactory is yet to be determined.

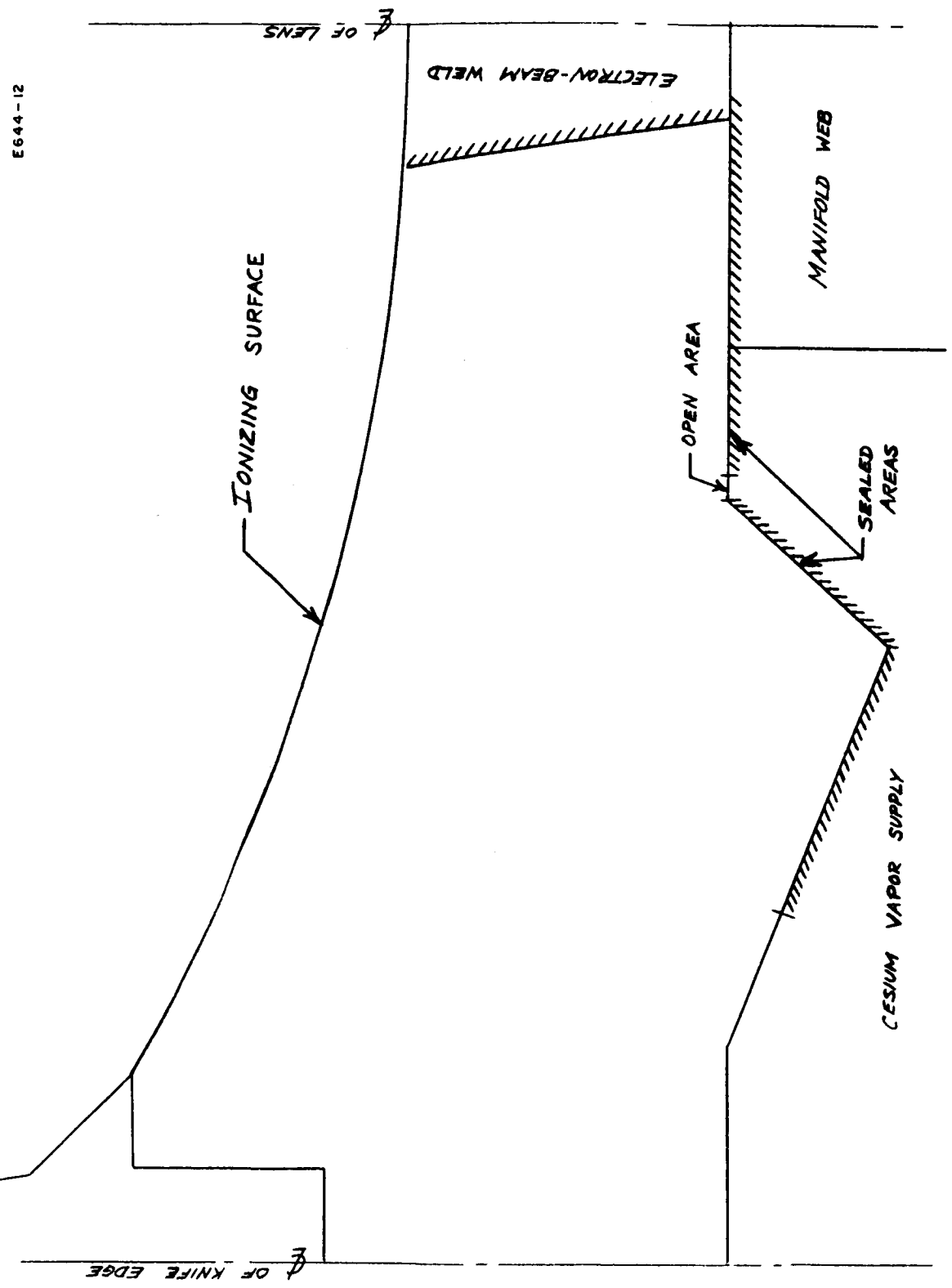


Fig. 40. Ionizer with thickness reduced for electron-beam welding but with flow adjusted for integral-focus optics.

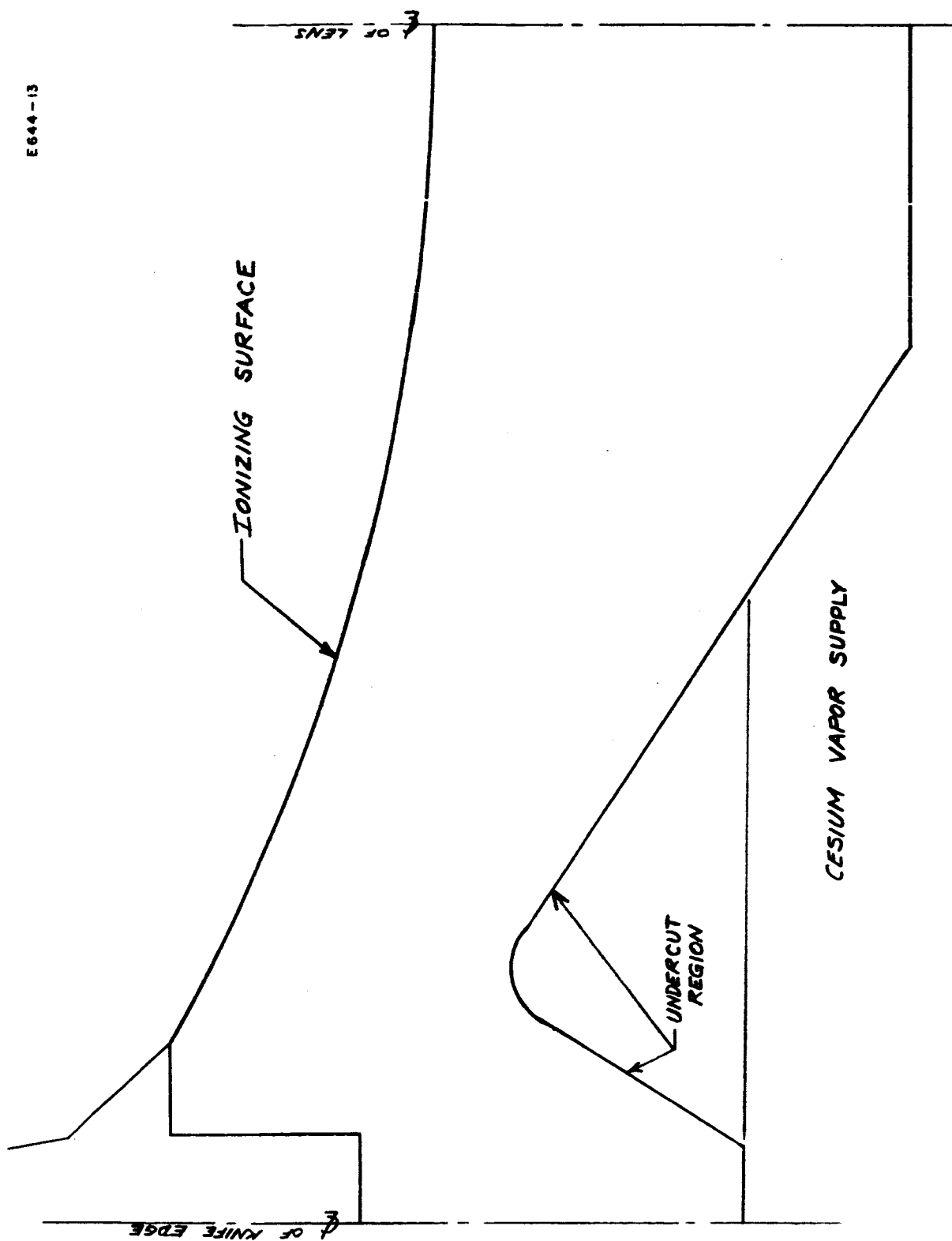


Fig. 41. Cross section of ionizer which is undercut and shaped to adjust flow for integral-focus optics.

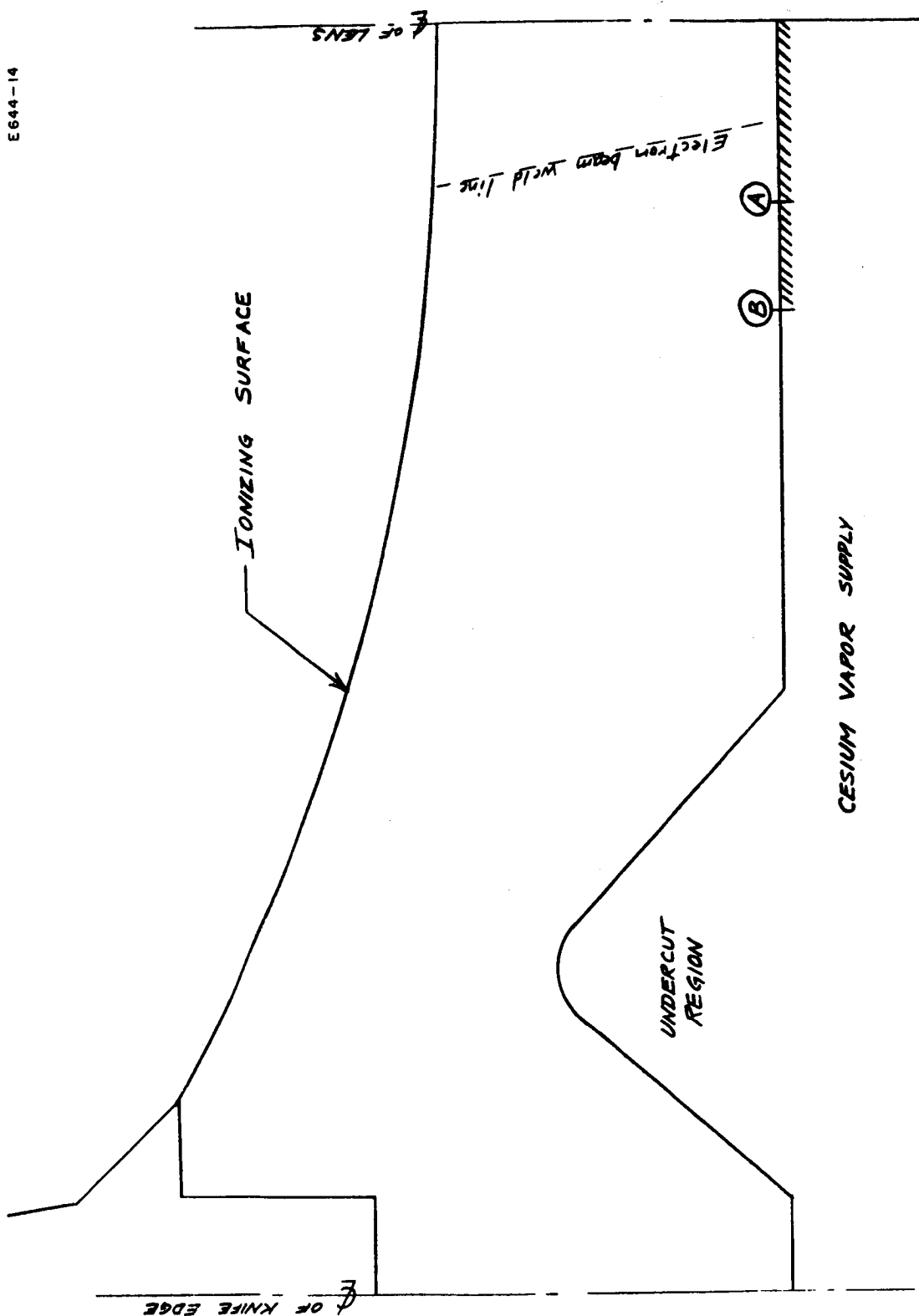


Fig. 42. Ionizer with flat back and flow adjusted for integral focus optics. Seal surface to A for unwelded lens and to B for welded lens.

## V. ENGINE MATERIALS

### A. Low Ion Emission Coatings for Focus Electrodes

In an attempt to minimize erosion of accel electrodes due to ions formed on the tips of solid tungsten integral focus electrodes, efforts were made to coat the tungsten tips with alumina. Previous studies had shown that solid alumina could be used as a focus electrode material and that it had desirably low cesium ionization tendencies. On electrodes which were already installed, the most promising method appeared to be that of simply painting on a slurry or suspension of alumina. A commercial product "Baymal" by DuPont is a submicroscopic water suspension of boehmite alumina ( $\text{Al OOH}$ ) which has excellent adhesion and coating characteristics. Upon heating to  $1000-1100^{\circ}\text{C}$ , it is converted to  $\alpha$  alumina, the high temperature stable form. Suspensions of this material in water at concentrations less than 5% by weight are quite fluid and can be readily painted or sprayed on a surface. Due to its thixotropic nature, these films will stay in place with very little running. This is ideal for painting on an already installed electrode. X-ray diffraction patterns of very thin coats of this material showed the presence of  $\alpha$  alumina after  $1000^{\circ}\text{C}$  wet hydrogen firing.

A thin coating of a suspension of 3% "Baymal" in a 2.5% by weight  $\text{Al}(\text{NO}_3)_3 \cdot 9\text{H}_2\text{O}$  solution was painted on about 1 square inch of sheet tungsten. The amount of alumina remaining after firing was too small to detect by weighing on an ordinary analytical balance (less than 0.1 mg weight change), but it could be detected by light interference patterns. An x-ray diffraction pattern showed definite peaks of  $\alpha$  alumina. The coating was therefore a few tenths of a micron thick.

The coating deposited by this mixture tended to flake if more than one layer was applied, but one layer adhered to a test piece of a tungsten integral focus insert. Pure "Baymal" suspension was more adherent in thicker coatings.



The focus electrodes on engine 42-40-3 IF had undesirably wide tips because of the inability of mechanical grinding techniques to consistently produce radii (of less than about 2 mils) at the tips. These wide points had previously shown evidence of causing erosion of the accel electrodes.

The 3% "Baymal" 2.5% aluminum nitrate solution described above was painted on the tips and ends of the electrodes by means of a small artist's paint brush. The solution was also painted carefully on the washed areas at the edges of the engine. Extreme care was exercised to prevent getting the solution on the ionizer face. The engine was assembled, installed in the chamber, and after being pumped to a satisfactory vacuum, it was heated slowly to 250 - 400°C for a few minutes. The temperature was then raised to 1000 - 1100°C for conversion of the coating to  $\alpha$  alumina. After five hours of operation, the engine was removed for inspection. Some evidence of erosion of accel electrodes was noted due to ions from the focus electrode tips, but the erosion was less than on previous tests with uncoated electrodes. Another coating of alumina suspension was applied. This time, a thicker suspension consisting of 5% "Baymal" and 1% aluminum nitrate was used to paint on the electrode tips. The engine was reassembled and heated as before. After approximately 60 hours of operation, the engine was removed, because of accidental vacuum loss, and inspected. The accel electrodes showed very minor evidence of erosion. It was estimated to be less than that caused by five hours of operation with the thinner coating of alumina. Of particular interest was the fact that there was no significantly larger amount of erosion caused by a large chip in one focus electrode which presented a flat surface about 80 mils long by 5 - 10 mils wide. It was therefore assumed that the presence of alumina on the electrode tip strongly inhibited the formation of cesium ions.

## B. Focus Electrode Sharpening

Computer studies indicate that the smaller the radius of the focus electrode tip, the less will be the erosion on the accel electrode from ions formed on the tip. Mechanical grinding did not produce less than about a 2-mil radius because of the tendency of the brittle tungsten to chip off. Electropolishing techniques were investigated as a means of overcoming this problem. Hopefully, metal could be removed from the sides of the wedge shape electrode faster than the tip, thus sharpening the point. In this technique, the part to be polished is made the anode and an inert metal is used for the cathode. Metal from the anode is thus oxidized and will dissolve away in an appropriate electrolyte. For tungsten, an alkaline electrolyte is used as it forms soluble tungstates. An alkaline tartrate solution (150 grams NaOH and 150 grams sodium tartrate per liter of water) was found to electropolish tungsten rapidly and to smooth and sharpen ground edges markedly. If the entire piece was to be immersed in the electrolyte, the areas not requiring etching could be masked with bituminous or acrylic paints. Application of 4-8 volts across a suitable masked tungsten anode and a stainless cathode immersed in the electrolyte worked efficiently but was too fast and hard to control. The immersion procedure also could not be used on an ionizer which already had the electrodes welded in place. This electrolyte was also risky to use near porous tungsten because of the chance of carbonaceous contamination.

Another approach was to hold the electrolyte in a porous medium between the anode and cathode and then rub the cathode over the surface of the anode (in this case the focus electrode surface). Various filter papers, porous alumina and cotton cloths were tried but the most satisfactory electrolyte support was 9 oz. per yard Dynel cloth.

A polishing electrode was fabricated out of 3/16" stainless tubing. One end of a 5" length was flattened to a 1/4" width, so that it still had a 3-mil opening across the tip. A syringe needle hub was brazed to the outer end. A strip of Dynel cloth 1-1/2" long x 3/8" wide was folded over this flat tip and held in place with a small

stainless spring clamp. A syringe could be inserted into the needle hub, so that electrolyte could be forced through the Dynel cloth to saturate it and replenish the electrolyte as needed. It was found that the electrolyte had to be flushed away regularly as it became saturated with tungstate and too concentrated because of evaporation.

For use near porous tungsten, an alkaline electrolyte which would be completely volatile when heated in vacuum was required. Ammonium formate in dilute ammonia was reasonably satisfactory but a solution of cesium hydroxide (25 gms cesium hydroxide dissolved in 65 cc  $H_2O$ ) gave better results because of a higher conductivity and greater alkalinity. Any traces of cesium compounds left on the porous tungsten should be volatile.

Electrodes which are to be polished before welding can be held in a plexiglass clamp. If the electrodes are already in an ionizer, the porous tungsten must first be saturated with distilled water to minimize absorption of cesium hydroxide. The porous area near the electrode is covered with thin tungsten and flushed frequently with water.

Controlled tungsten removal from the sides of the electrodes in a manner which would reduce the radius of the tip was accomplished at a current of 0.1 - 0.3 amps through the polishing electrode at 16 - 20 volts. Because it is not possible to measure the area of tungsten in contact with the electrode, it is difficult to calculate the actual current density.

During polishing, the cloth is rubbed back and forth across the length of the side of the tungsten electrode. The electrolyte content in the cloth is maintained such that the current stays between the above mentioned values. If the current gets too high, the electrolyte foams and the cloth may have holes burned through it. The sides of the focus electrode are polished and visually inspected at intervals until the desired tip is obtained. Some individual nicks a few mils long were rounded out using a cathode of 30-mil stainless wire which had Dynel thread wrapped around the end as an electrolyte pad. Current passage in this case is only a few mils.

It has been found possible to produce a mirror-like finish on the electrodes and reduce the tip radius from an estimated 2 - 3 mils to a few tenths of a mil. Before polishing, the wide tip also has some flat surfaces which are not desirable. Even if these are not completely removed, they are at least rounded, so that there are essentially no flat areas facing the accel electrode. Exact measurement of the final tip dimensions will be made by metallographic techniques at a later date when spare electrodes are available.

## VI. IONIZER MATERIAL EVALUATION

### A. Introduction

The most important accomplishment of this report period was the evaluation of an iridium coated porous tungsten ionizer and of a rhenium coated porous tungsten ionizer. The iridium coated sample exhibited a surface work function of 5.0 to 5.1 eV.<sup>1</sup> The neutral fraction was approximately 5% of that of the porous tungsten. The critical temperature<sup>2</sup> was found to be approximately 180° higher than the porous tungsten value. Only a limited amount of data could be obtained from the sample of rhenium coated porous tungsten because of a cracked electron beam weld in the feed line. At a current density of 2.2 mA/cm<sup>2</sup>, the surface work function was 5.2 eV, the neutral fraction was about 2% of that of porous tungsten and the critical temperature was approximately 150° higher than for porous tungsten.

Prior to the study of the coated ionizers, samples of porous tungsten were studied extensively to evaluate the apparatus, verify the operating conditions and to establish the basic porous tungsten ionization parameters. The porous tungsten exhibited critical temperatures about 60° greater than the Langmuir-Taylor value for solid tungsten and a surface work function of 4.6 eV.

During the next report period, more coated samples will be analyzed to determine if the method of coating or the thickness of the coating has any effect on the basic ionization parameters as well as determining if these coatings are stable.

---

<sup>1</sup> All work functions presented in this section are computed from the Saha-Langmuir equation using the observed values for the atoms and ions evolved from the surface.

<sup>2</sup> In all but one case, the critical temperature refers to the value associated with the minimum neutral efflux—this value is approximately 25° higher than the temperature associated with the break in the ion current.

## B. Analysis of Porous Tungsten

Samples of porous tungsten were selected to be the first analyzed in the apparatus which was described in the second quarterly report. The Mod E sample provided an immediate and necessary correlation of data obtained in this UHV system with that obtained from tungsten operating in conventional vacuum systems. In addition, this provided a means of checking out the apparatus and developing confidence in its operation.

The material used in run 1 was Philips Metalonics Mod E porous tungsten and that in run 2 was EOS 1 to 40  $\mu$  (unclassified) powder porous tungsten. Only Philips Mod E and the HRL 3.9  $\mu$  material, to date, have been used in the multistrip engine. The metallurgical data is presented in Table III. After machining, the copper was boiled out of the sample, and the porous ionizer was electron beam welded into a tungsten manifold. The unit was nitrogen gas flow checked and bubble tested for leaks. The unit was wet hydrogen fired and then had a molybdenum feed tube and support tabs EB welded to it. The ionizer assembly was completed and after a final leak test of the feed line, the assembly was mounted in the chamber. The neutral detector was optically aligned to the ionizer. The system was evacuated under a 350°C bakeout of 30 to 50 hours total duration. The system pressure was typically  $3 \times 10^{-9}$  after bakeout. The composition of the residual gas is discussed in a following section.

The Mod E material exhibited a critical temperature of about 70°K higher than the Langmuir-Taylor value for solid tungsten (see Fig. 43). A limited number of neutral fraction measurements were made at temperatures up to 200° higher than the critical temperature (see Fig. 44) when a leak occurred in the cesium feed line. The crack was a result of metal fatigue of a thin section of the line which was caused by vibrations in the system. This was corrected and the system was reevacuated under bakeout. Although the ionizer exhibited a work function of 4.6 eV and a critical temperature about

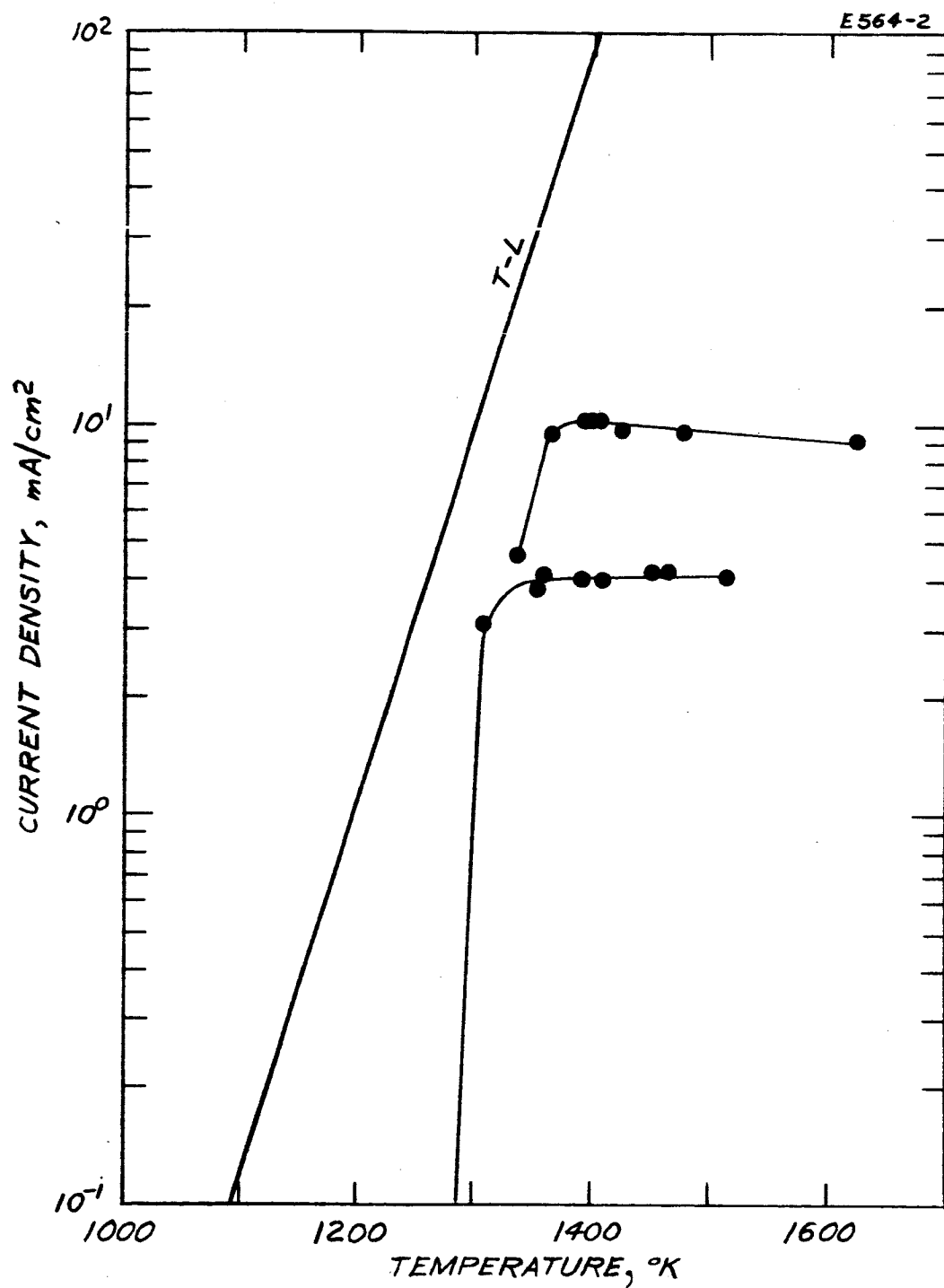


Fig. 43. Critical temperature data for an ionizer strip made from Philips Metalonics Mod E tungsten and evaluated in the UHV ionizer evaluation system (see text for material characteristics).

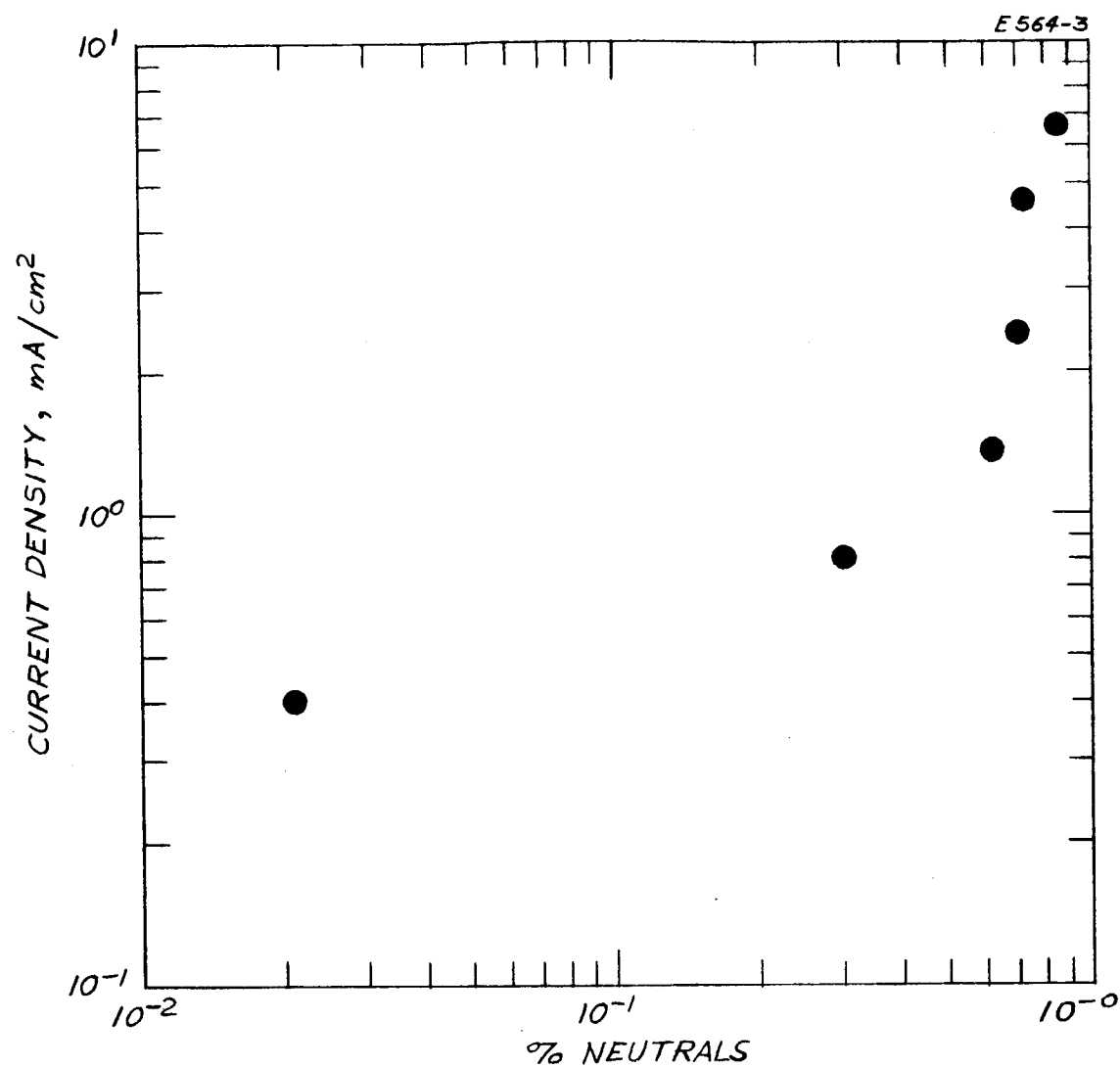


Fig. 44. Neutral fraction data for an ionizer strip made from Philips Metalonics Mod E tungsten and evaluated in the UHV ionizer evaluation system. (See text for material characteristics.)



TABLE III

Some Physical Properties of the Experimental Ionizers

	Sample Material	
Physical Property	Porous Tungsten Philips Mod E	Porous Tungsten EOS 1-40 $\mu$
Density, percent	75	73.4
Pore dia., $\mu$	3.5	2.85
Pore count, No. /cm <sup>2</sup>	$2.3 \times 10^6$	$3.08 \times 10^6$
Nitrogen permeability, gm/cm-sec-Torr	$2.88 \times 10^{-7}$	$5.6 \times 10^{-7}$
Predicted Cs transmission coefficient based on nitrogen measurements	$3.24 \times 10^{-5}$	$7.7 \times 10^{-5}$
Observed Cs transmission coefficient	$(1.17 \pm .1 \times 10^{-4})$	$1.13 \pm .07 \times 10^{-4}$
	Sample Material	
	Rhenium (Sputter Coated On Porous Tungsten)	Iridium (Chemical Reduction On Porous Tungsten)
Nitrogen permeability of substrate	$1.45 \times 10^{-6}$	$7.75 \times 10^{-7}$
Nitrogen permeability of coated surface	$1.55 \times 10^{-6}$	$6.85 \times 10^{-7}$
Observed cesium trans- mission coefficient	$(1.24 \pm .1 \times 10^{-4})$	$2.15 \pm .08 \times 10^{-4}$

120° higher than the L-T value, the unit was operating in an unusual manner. After the unit was shut down, a significant leak was found in the internal cesium feed line. The leak was caused by a failure of the metal gasket. This gasket failure probably occurred when the feed line developed a crack.

The second sample evaluated was the EOS 1-40  $\mu$  material. The initial runs were made on the EOS material at 1.5 and 3 mA/cm<sup>2</sup> levels. The critical temperature was found to be about 150° above the L-T line. The ionizer was operated at higher beam currents over a total of about 10 hours. During this period, the critical temperature decreased to a value approximately 60° above the L-T line. Values obtained after stabilization are shown in Figs. 45, 46 and 47. The superimposed line in Fig. 45 represents the critical temperature as determined by the minimum neutral efflux. In Fig. 46, the neutral fraction is presented as a function of the temperature of the ionizer. It is significant that once the ionizer surface stabilized, the work function remained essentially constant at  $4.58 \pm .02$  eV over a range of beam currents from 5 to 20 mA/cm<sup>2</sup> and was reproducible. This is a clear indication of freedom from contamination in this vacuum system.

One result of the porous tungsten studies was a verification of the design and construction of the apparatus. A few minor changes were made. Of most significance is the fact that the critical temperature and the neutral fraction data obtained after the stabilization (clean-up) of the surface are in good agreement with the data obtained from multistrip ion engines operating in conventional vacuum systems. Thus, from the aspect of neutral fraction, the engine test environment adequately simulates the vacuum in space as represented by the UHV single strip tests.

### C. Coated Porous Ionizer Studies

The porous tungsten ionizer material described above exhibits a minimum neutral efflux about 60° above the L-T line and a work function of 4.58 eV. For engine operation under these conditions at

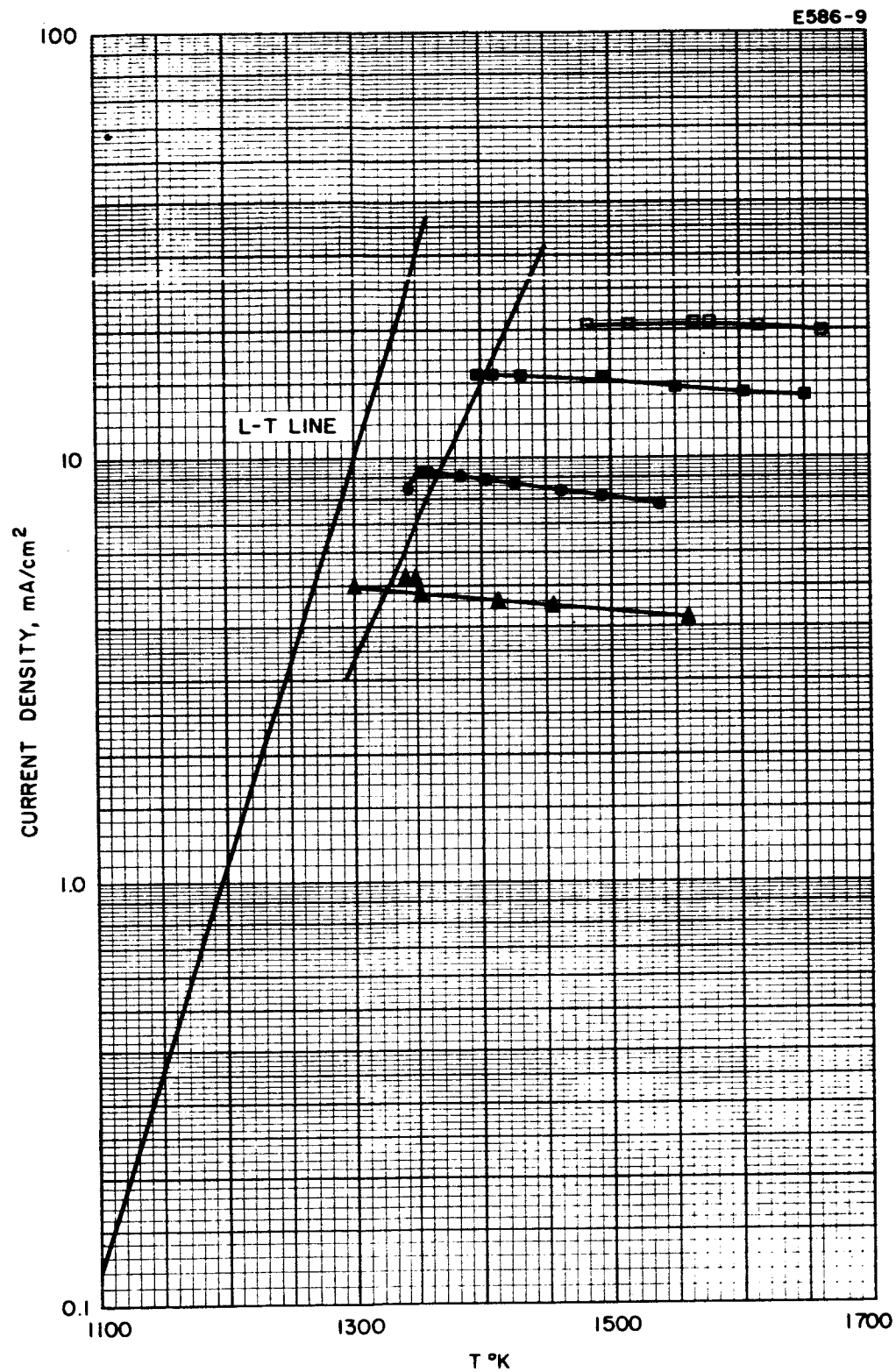


Fig. 45. Current density as a function of ionizer temperature for EOS 1 to 40  $\mu$  porous tungsten.

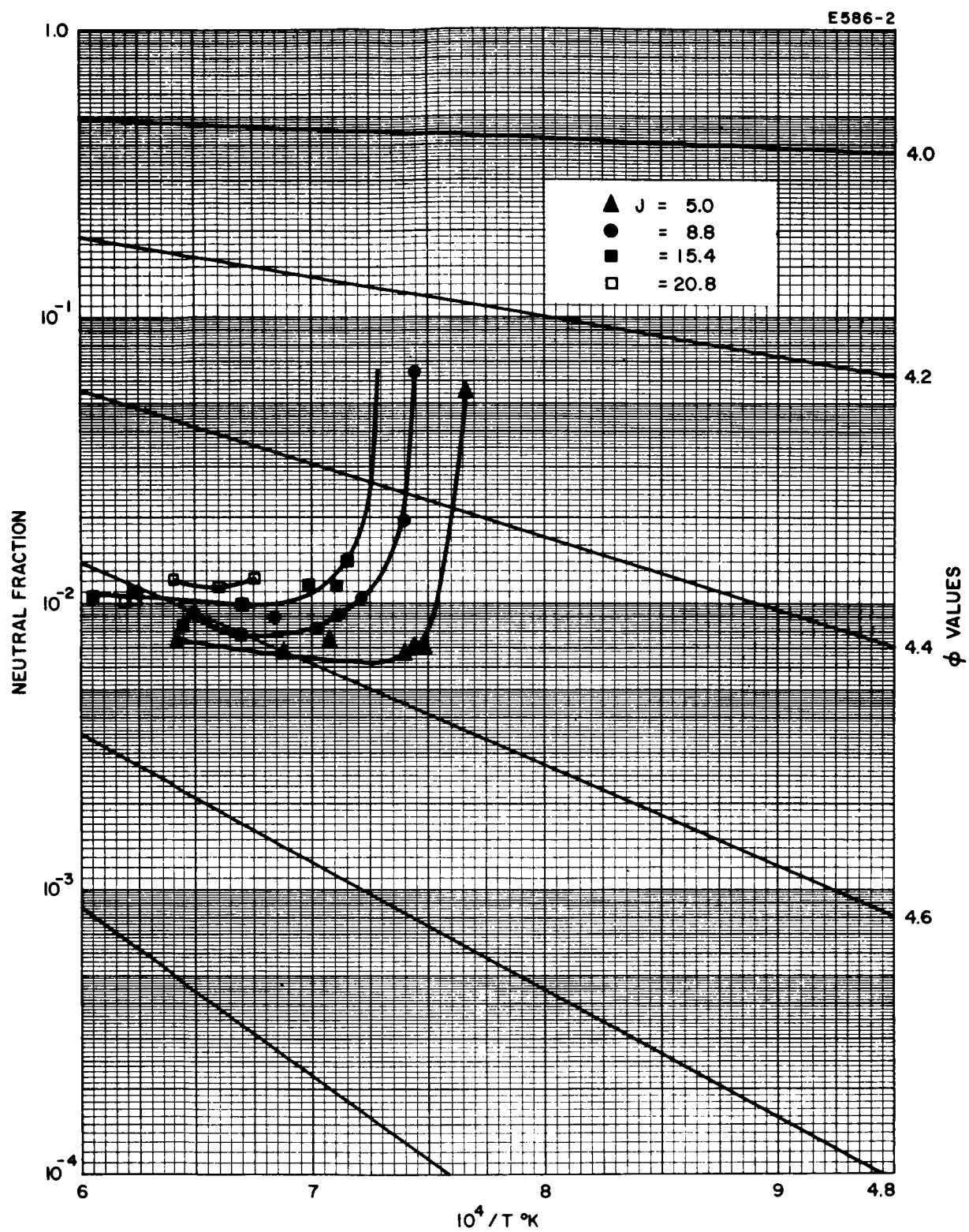


Fig. 46. Neutral efflux as a function of ionizer temperature for EOS 1 to 40  $\mu$  porous tungsten.

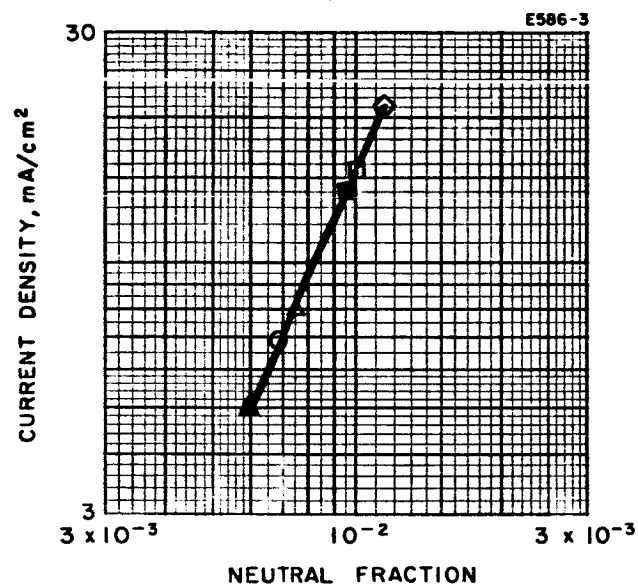


Fig. 47. Neutral fraction as a function of current density for EOS 1 to 40 porous tungsten.

20 mA/cm<sup>2</sup>, the neutral fraction would be 1.2%. Accel electrode lifetime, based on a charge exchange value computed from this neutral fraction is only 1300 hours. Therefore, it is necessary to develop an ionizer of higher work function so as to decrease the neutral efflux and attain an ultimate engine life greatly in excess of 10,000 hours. The most promising metals, iridium and rhenium, were selected as materials for coating tungsten ionizers.

The sample ionizers were prepared as follows. Porous tungsten ionizer assemblies (Mod E material in all but one case) were prepared in the usual manner. After the nitrogen flow check, the porous tungsten surface was coated either by chemical reduction of a metal salt or by vacuum sputtering the metal onto the surface. The vacuum sputtering was performed by Philips Metalonics. After being coated, the assemblies were rechecked for nitrogen transmission. In all cases, the coating resulted in little or negligible changes in the nitrogen flow rate. The remaining processes were similar to that previously described.

In general terms, the rhenium coated sample and the iridium coated sample exhibited similar behavior which was different from the porous tungsten behavior. Both coated samples appeared to be free of any surface contamination as evidenced by a lack of any "clean-up" behavior.

The rhenium coated ionizer had a 1.5  $\mu$  thick sputter-coated layer. During the preliminary heat up (no fields or cesium present) several dark crystals appeared to grow on the copper accel electrode. They disappeared with the formation of the ion beam. On removal of the gun, a few large crystals were found on the edge of the accel electrode. These are being analyzed. There were signs of flaking of the sputtered rhenium from the smooth EB weld area of the ionizer. A critical temperature run was made at 2.2 mA/cm<sup>2</sup>. The results are shown in Figs. 48 and 49. The critical temperature is 150° higher than the porous tungsten. A number of attempts were made to operate at higher levels but a strange pulsation occurred in the beam current. This was evidence of a feed line leak so the

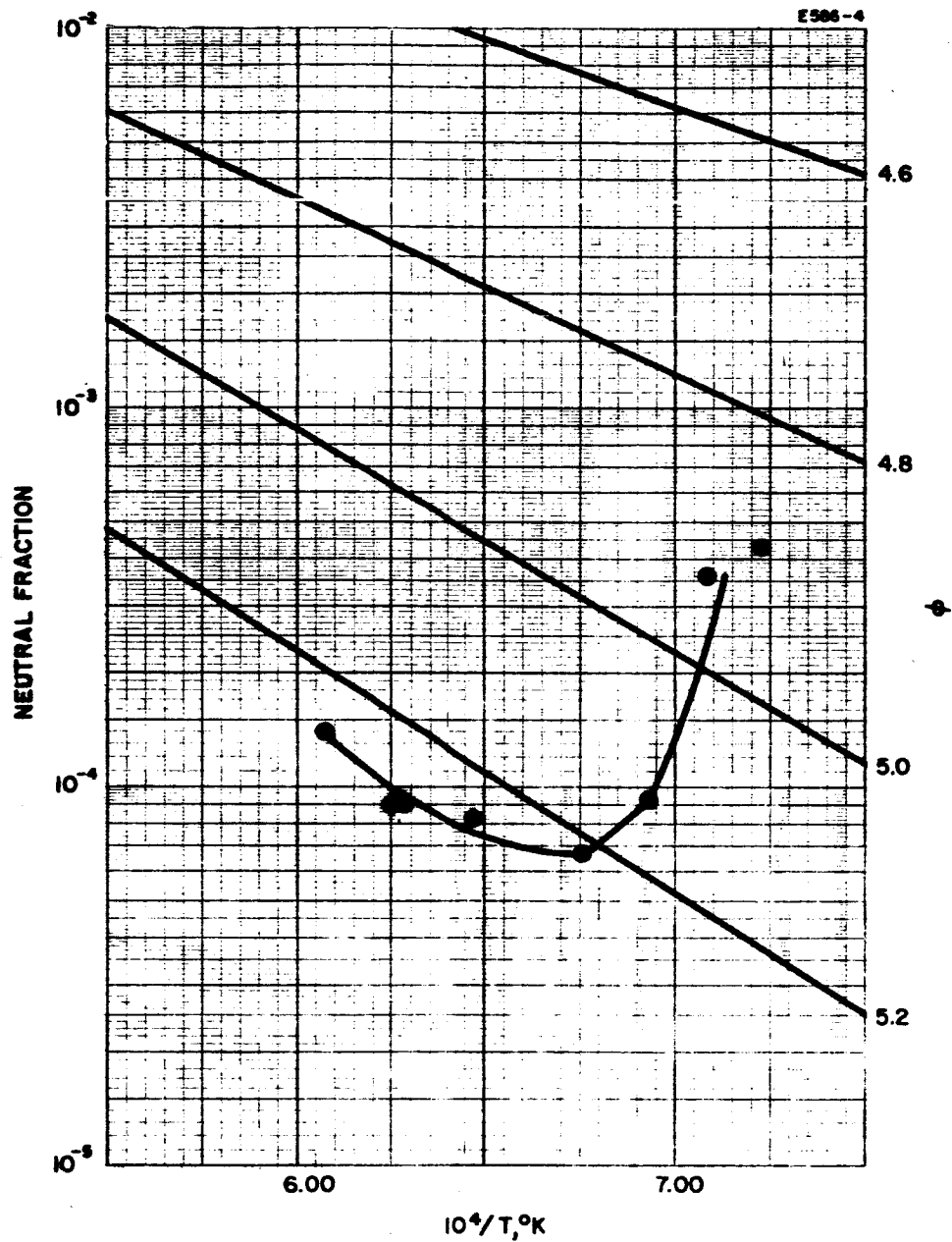


Fig. 48. Neutral fraction as a function of temperature of 1.5 μ thick rhenium sputter coated ionizer.

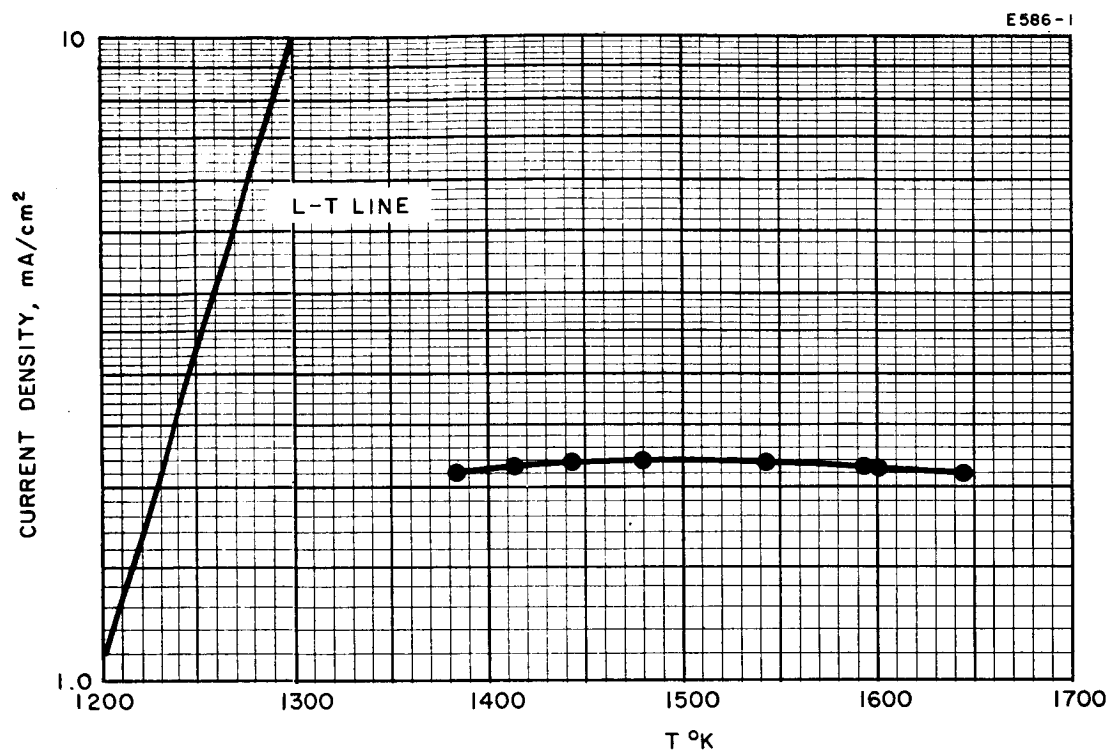


Fig. 49. Current density as a function of the temperature of the 1.5 thick rhenium sputter coated ionizer.



system was shut down. A fine crack was discovered in the EB weld of the manifold and feed line. This has been rewelded and this unit is to be rerun at a later time.

The last sample to be run in this report period was an ionizer with a 3  $\mu$  thick iridium coat. The iridium coat was formed by the chemical reduction of an iridium salt on the EOS 1 to 40  $\mu$  porous tungsten ionizer which had been previously studied. The ionizer was operated at beam levels of about 2.4 and 8 mA/cm<sup>2</sup> for a five-day period. The neutral fractions and critical temperatures exhibited reasonable reproducibility during this period. A composite plot of the critical temperatures is shown in Fig. 50. Typical neutral fraction versus temperature graphs are shown in Fig. 51. Attempts to obtain data at 12 mA/cm<sup>2</sup> and higher were not successful due to random arcing. This problem was finally identified as being caused by a charging up of the neutral detector shutter. The ceramic hinge rods which support the shutter also isolate it from ground potential. This problem is being corrected. A composite neutral fraction versus current density plot is presented in Fig. 52. This summarizes the results of all four experiments.

During the two test runs of coated ionizers, a 5 cm radius electrostatic scanning mass spectrometer was used to monitor the residual gas in the vacuum system. Based on the approximation that all the gases have the same ionization cross section, the total concentration of gases which contain oxygen and carbon was less than 10<sup>-9</sup> Torr throughout the run. In Table IV, there are shown typical spectra for the residual gas in the system. The data in the first column were taken during the thermal cycling of all the electrodes (before admission of cesium). The second set of data was taken during the operation of the ionizer. The major part of the gas in the system was hydrogen. Its presence is explained by the fact that most of the electrodes and heaters are hydrogen brazed or fired just prior to assembly.

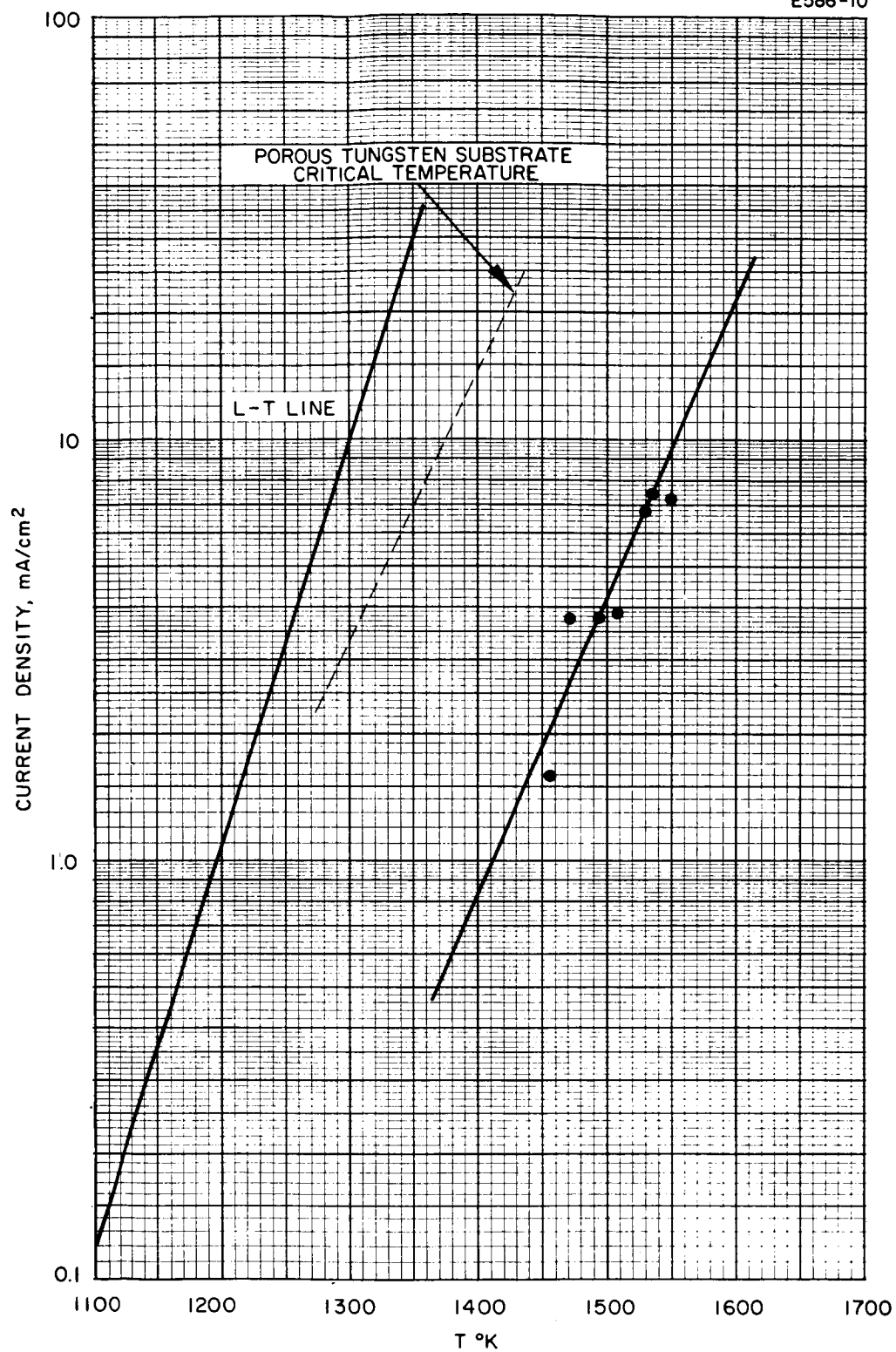


Fig. 50. Critical temperature as a function of the temperature of the 3  $\mu$  thick iridium chemically coated ionizer.

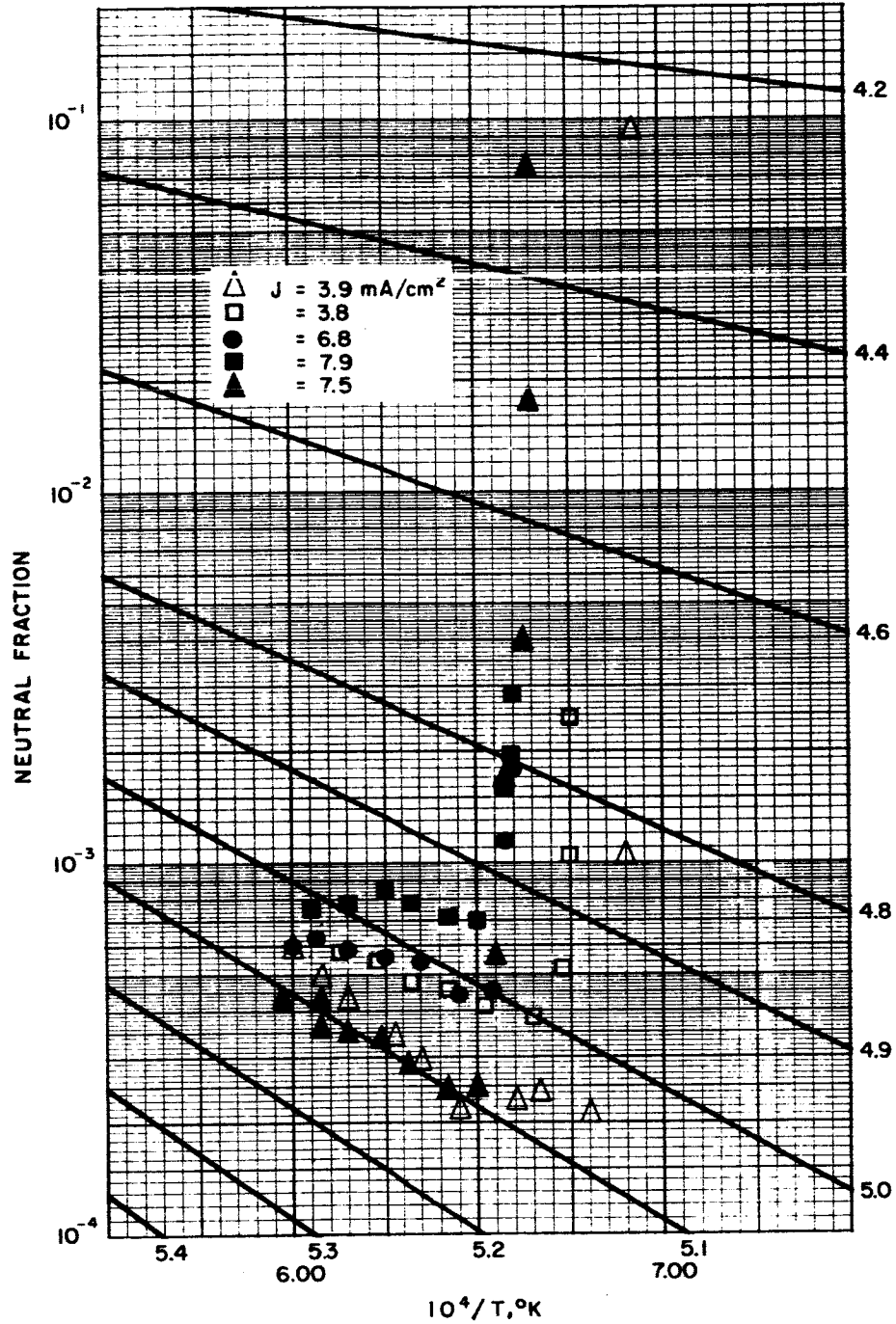


Fig. 51. Neutral fraction as a function of the temperature of the 3  $\mu$  thick iridium chemically coated ionizer.

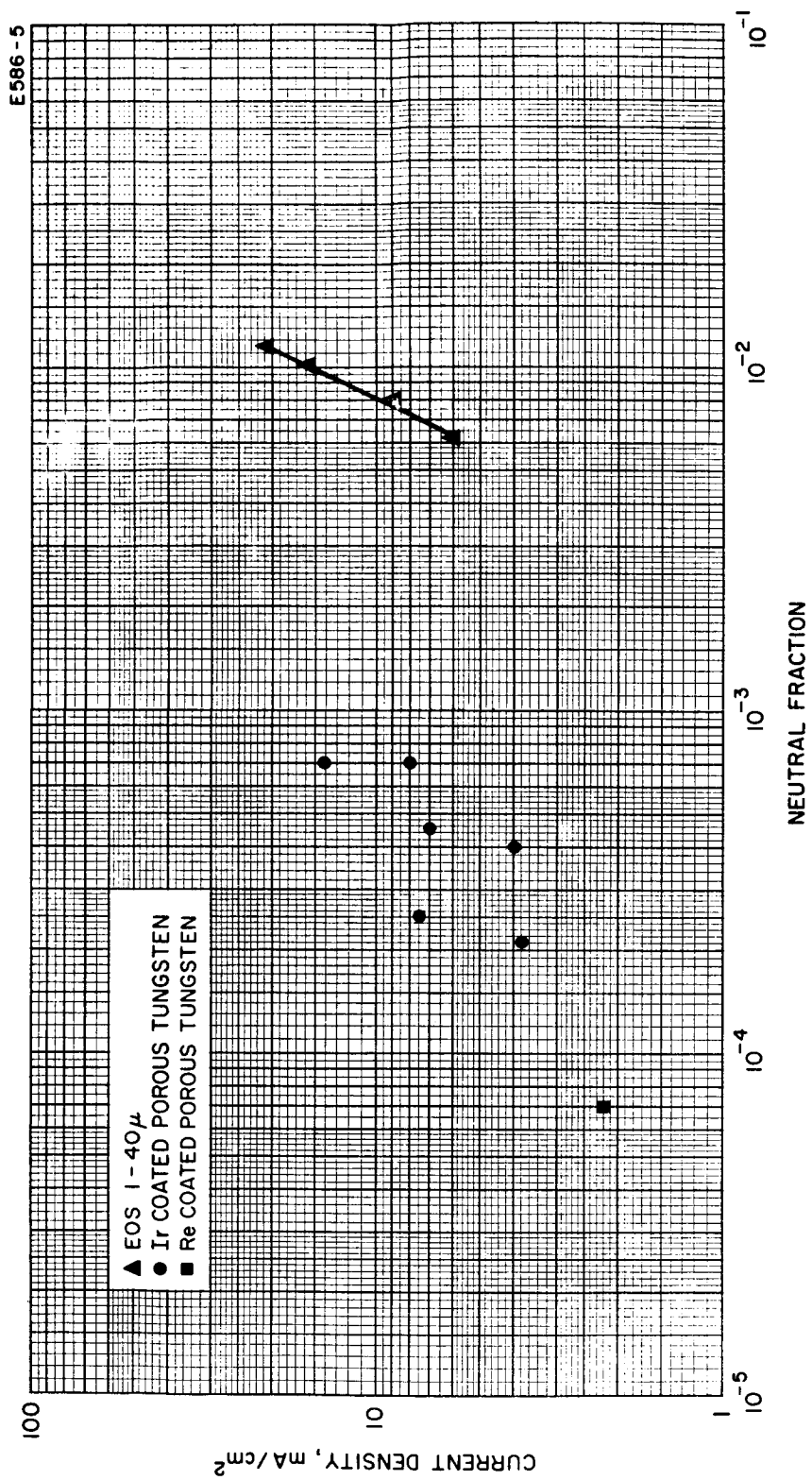


Fig. 52. Neutral fraction as a function of current density for 3 samples.

#### D. Future Work

During the next report period, additional samples of coated ionizers will be measured. Among the goals of this work is the determination of the surface characteristics, i.e., the degree to which different samples have the same operating characteristics as well as the repeatability of operation of a single sample. The long range objective is to determine what effect the method of coating the porous tungsten and the thickness of the coating have on the operation of these ionizers.

TABLE IV

Partial Pressure of Residual Gases Present in System

Ionic Species	AMU	Partial Pressure Observed During Outgassing of Components (after Completion of Chamber Bakeout), Torr	Partial Pressure Observed During Run, Torr
$\text{H}_2^+$	2	$1 \times 10^{-8}$	$2 \times 10^{-8}$
$\text{C}^+$	12	$<5 \times 10^{-12}$	$5.0 \times 10^{-11}$
$\text{CH}^+$	13	$<5 \times 10^{-12}$	$4 \times 10^{-12}$
$\text{N}^+, \text{CO}^{++}$	14	$3.2 \times 10^{-10}$	$8 \times 10^{-11}$
$\text{CH}_3^+$	15	$3 \times 10^{-11}$	$1.55 \times 10^{-11}$
$\text{O}^+, \text{CH}_4^+$	16	$6 \times 10^{-11}$	$4.3 \times 10^{-11}$
$\text{OH}^+$	17	$<5 \times 10^{-12}$	$8.5 \times 10^{-13}$
$\text{H}_2\text{O}^+$	18	$<5 \times 10^{-12}$	$3.5 \times 10^{-13}$
$\text{CO}^+\text{N}_2^+$	28	$2.3 \times 10^{-10}$	$6 \times 10^{-10}$
$\text{C}^{13}\text{O}^+$	29	$<5 \times 10^{-12}$	$7 \times 10^{-12}$
$\text{O}_2^+$	32	$<5 \times 10^{-12}$	$<10^{-13}$
$\text{A}_r^+$	40	$<5 \times 10^{-12}$	$1.5 \times 10^{-11}$
$\text{CO}_2^+$	44	$<5 \times 10^{-12}$	$<10^{-13}$
Total Pressure (Ion Gauge)		$1.0 \times 10^{-8}$	$2 \times 10^{-8}$

## VII. AUTOMATIC CONSOLE

### A. Introduction

The fabrication of the new operational life test console is nearing completion. The major components are complete and the remaining tasks include panel symbolization, intercabinet cabling, instrument calibration and checkout of completed units.

The completion of this console is of major importance in the engine development program because of the high power handling capacity and the degree of control which can be applied to the engine system. The capability of this console is difficult to summarize in terms of engine performance; however, as tabulated in previous reports, there are regulated supplies designed to operate an engine system plus data acquisition and diagnostic instrumentation. The maximum beam current supply is 3 amperes at 10,000 volts.

### B. Console Description

A series of photographs have been taken to indicate the status of the equipment. Figure 53 represents an operator's view of the front of the console. The overall length of the console is approximately 16 ft., with a height of 6 ft. and a depth of 3 ft.

A cabinet designation diagram is shown in Fig. 54. A general description of the equipment contained in each cabinet is provided below and can be correlated with Fig. 53. The following paragraphs describe the various sections of the console.

#### 1. Section A-1

A plus high voltage supply capable of 10 kV at 3 amps is provided from a 3 phase power line. Three single phase saturable reactors provide 90% control on each of three ranges. The step-up transformer has tapped secondary windings to provide 3.3 kV, 6.6 kV and 10 kV output voltages. A six phase rectifier and filter network provide low ripple output. A series regulator tube with full voltage and current capability provides a special type of current and voltage control.

M 4117



Fig. 53. Front view of life test console.



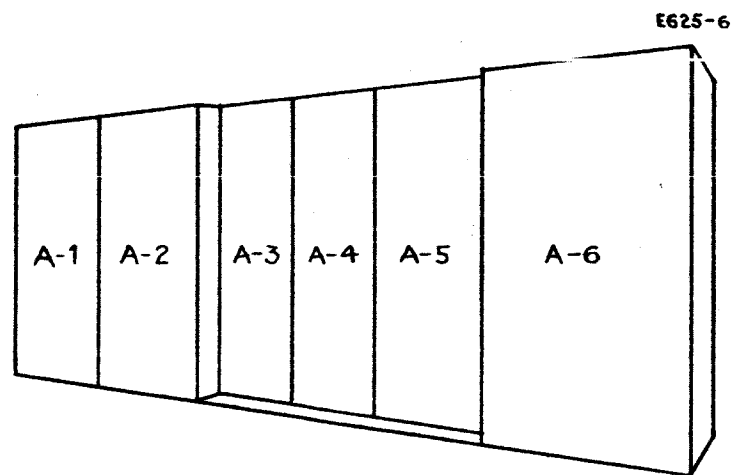


Fig. 54. Cabinet designation diagram of life test console.

Figure 55a and 55b show rear and side views respectively of the +10 kV power supply. Description of call-outs is as follows:

1. Three single phase saturable reactors
2. Two kilowatt H.V. isolation transformer (2)
3. Ten Henry filter choke
4. Screen supply for series regulator tube
5. Blower for series tube
6. Series tube
7. Filament transformer
8. H.V. rectifiers
9. Filter capacitor
10. Control mag-amp
11. Primary power bandpass filter
12. Breaker for isolation transformer
13. Breaker for H.V. supply

## 2. Section A-2

A double rack with the inner rack isolated for high voltage permits this section to contain standard operational amplifier, differential amplifiers, power supplies and magnetic amplifiers used to control engine system components referenced to the plus high voltage. Isolated front panel controls permit adjustment of operating points and selection of automatic or manual control of various parameters. Multiplex data acquisition is provided for the operator by direct reading meters and independently to the ground level recorders.

Figures 56a, 56b, and 56c show front panel, open front panel and rear views of the high voltage instrumentation and controller network assembly. Description of call-outs is as follows:

M 4120

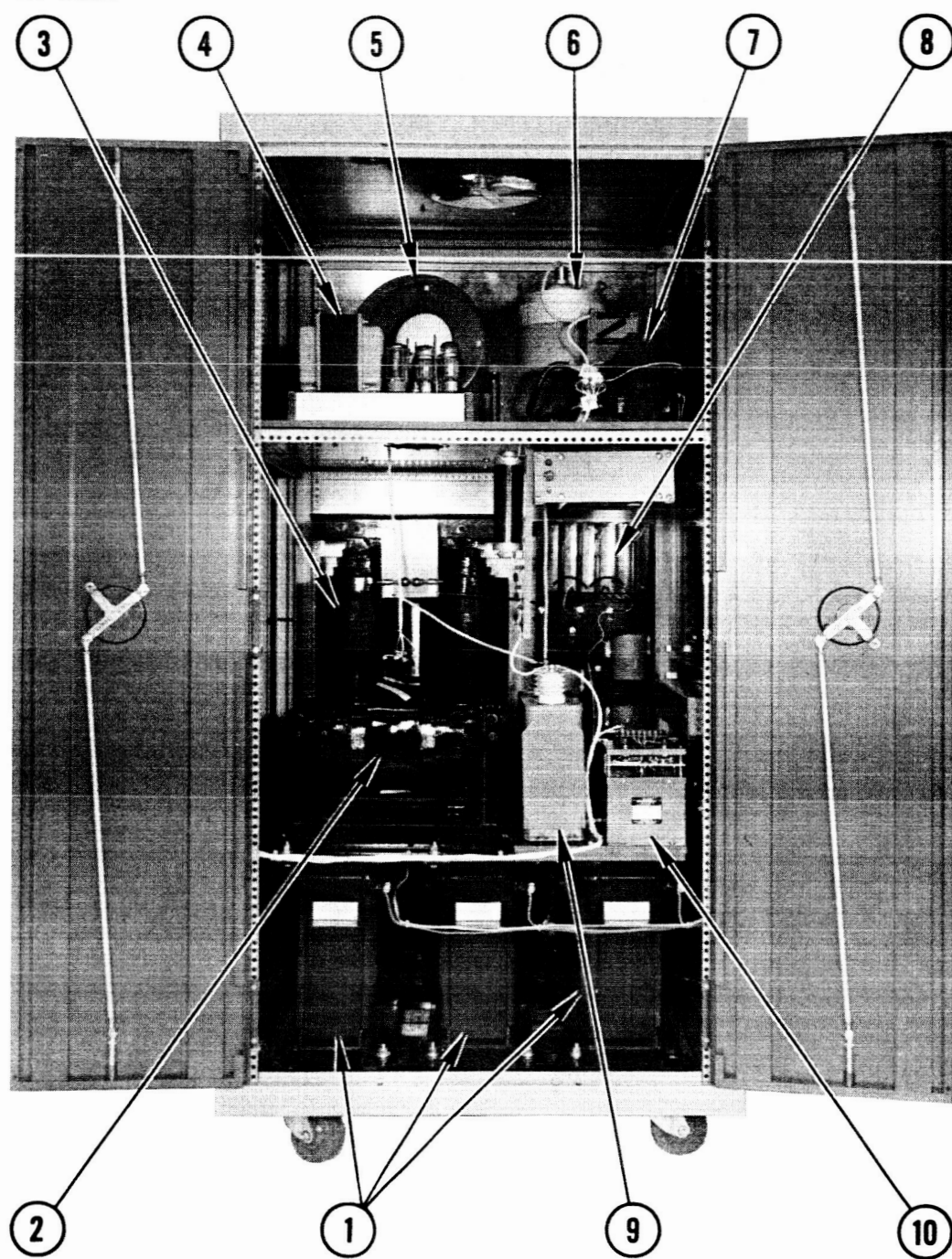


Fig. 55(a). +10 kV power supply (see text for callout identification).

M 4118

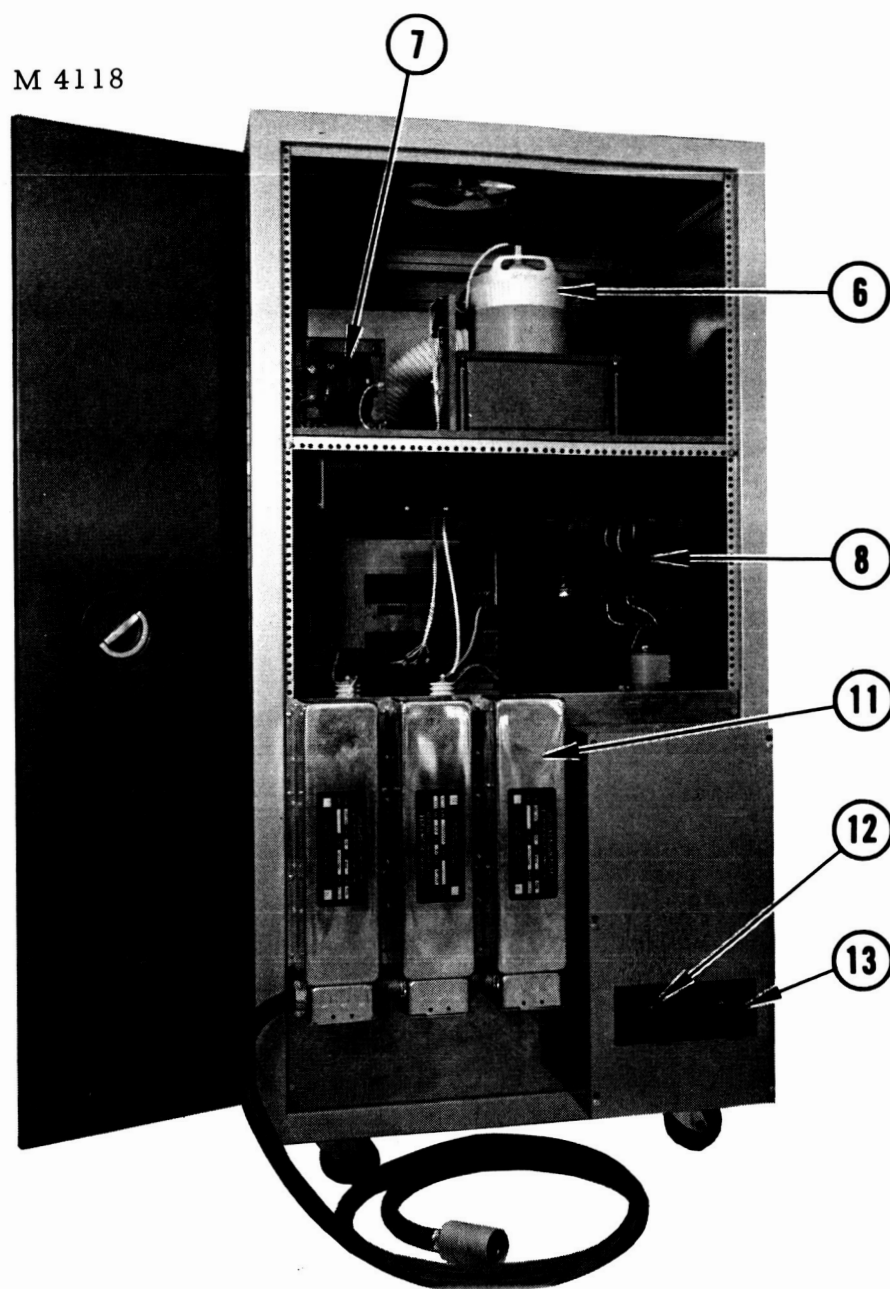


Fig. 55(b). +10 kV power supply (see text for callout identification).

M 4121

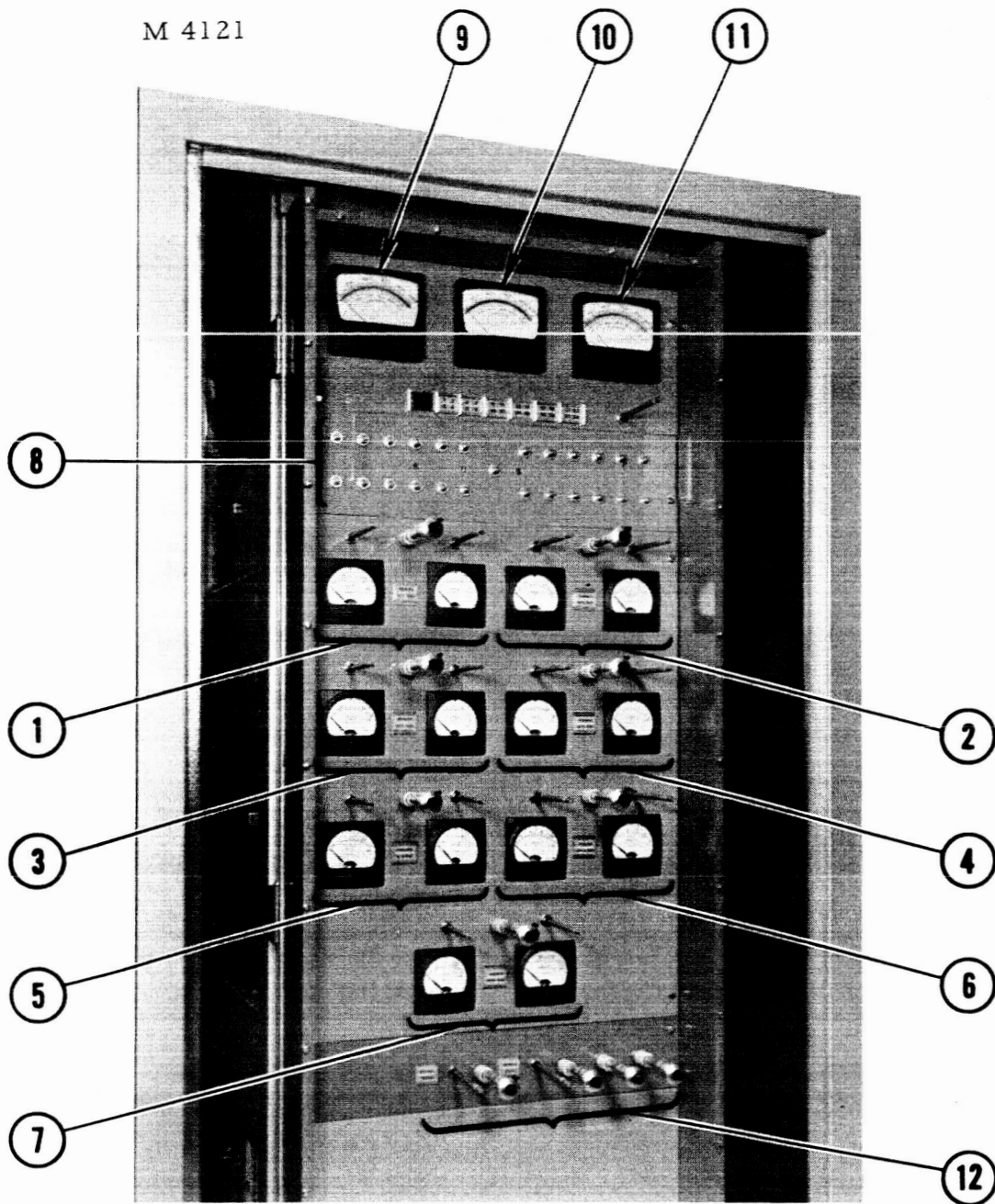


Fig. 56(a). HV instrumentation and controller network assembly  
(see text for callout identification).

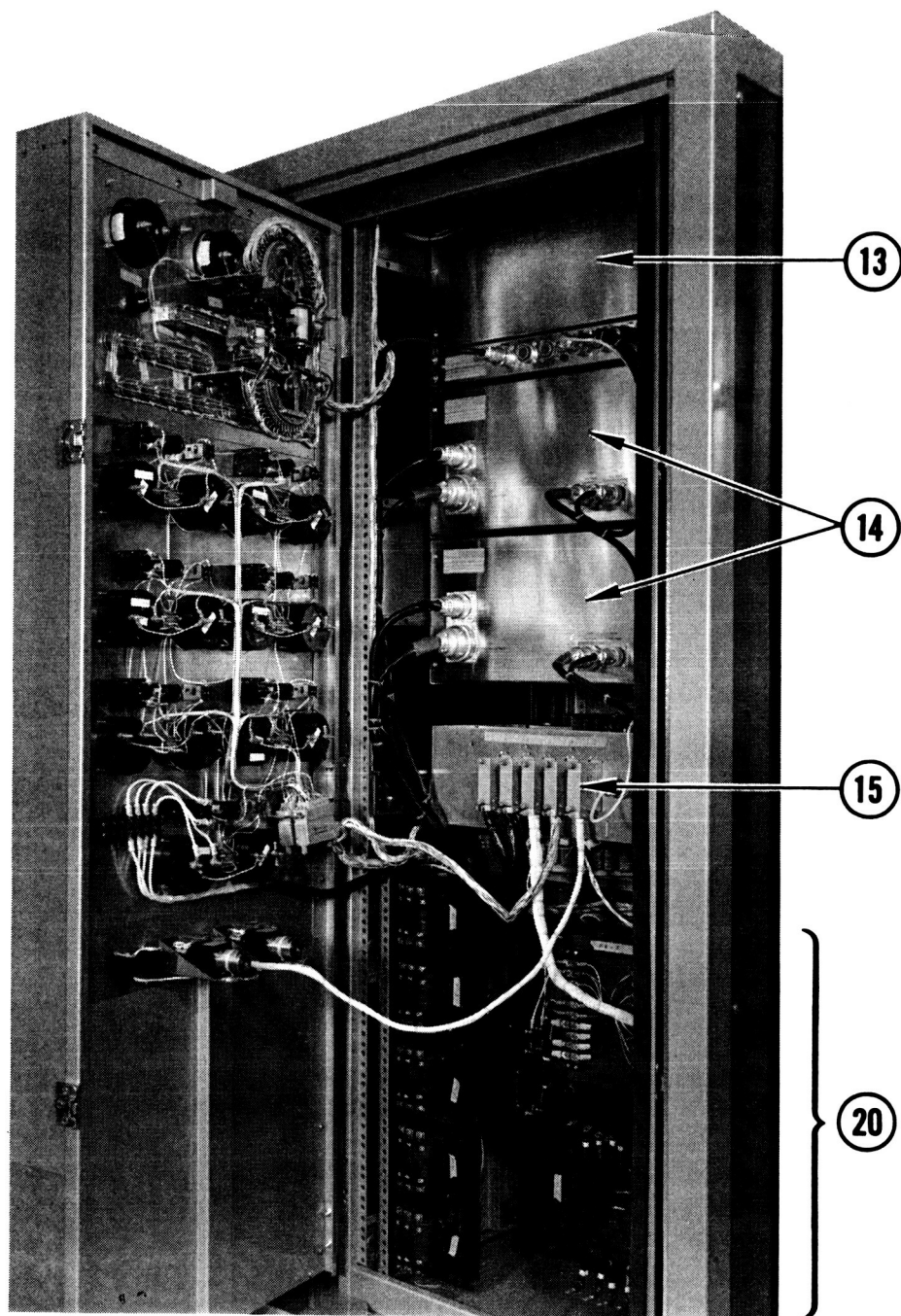


Fig. 56(b). HV instrumentation and controller network assembly (see text for callout identification).

M 4122

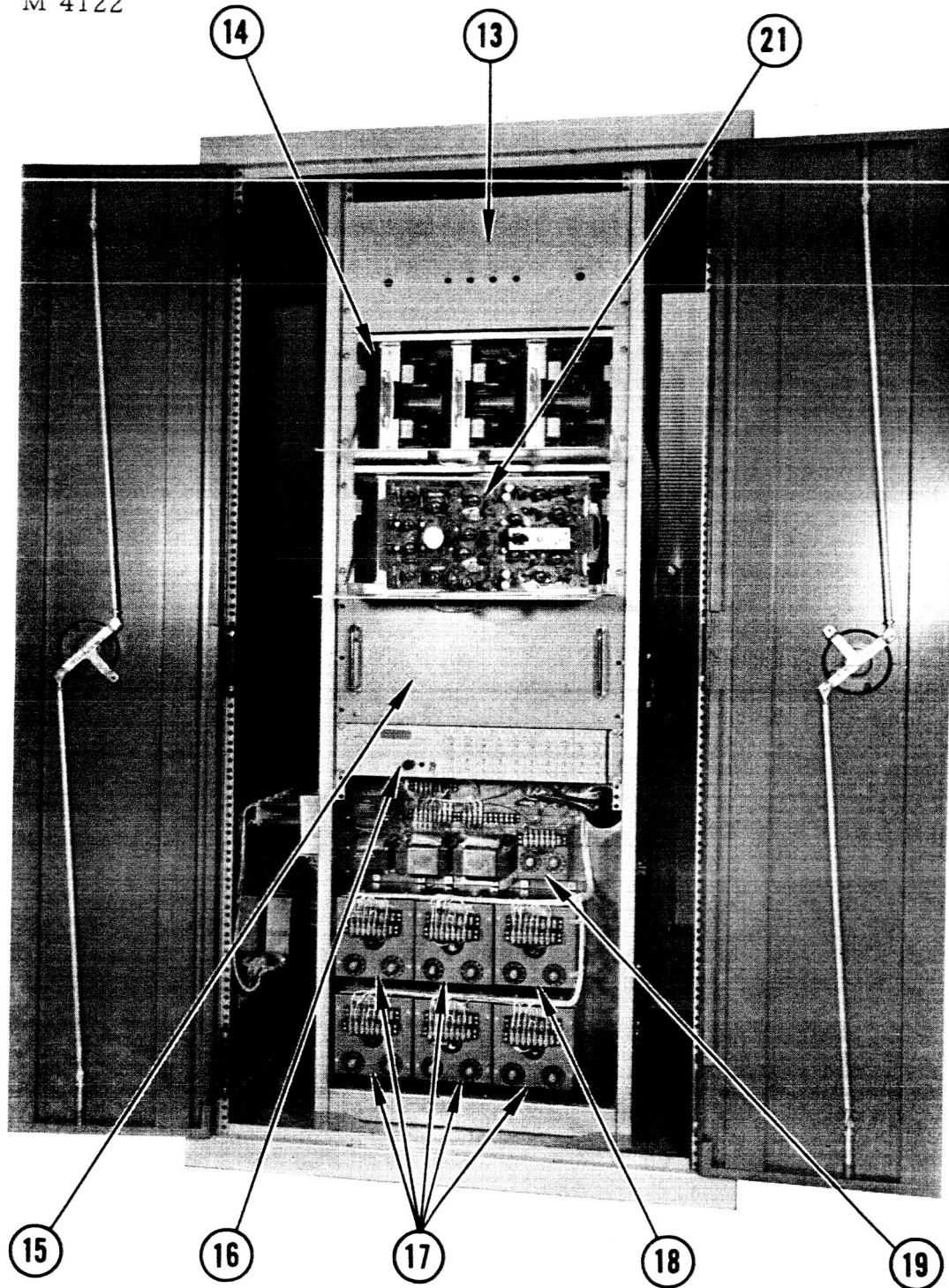


Fig. 56(c). HV instrumentation and controller network assembly (see text for callout identification).



1. No. 1 (300 watt) constant temperature heater
2. No. 2 (300 watt) constant temperature heater
3. No. 3 (300 watt) constant temperature heater
4. No. 4 (300 watt) constant temperature heater
5. No. 5 (300 watt) constant temperature heater
6. No. 6 (300 watt) constant temperature heater
7. No. 7 (2000 watt) constant temperature heater
8. Thermocouple type selectors (24)
9. Iron-Constantan direct readout
10. Chromel-alumel direct readout
11. W-5% Re/W-26% Re direct readout
12. Ionizer temperature interrogation controls
13.  $\pm 250$  V supply for operational amplifiers
14. Open racks of quad operational amplifiers (12)
15. Network box for operational amplifiers
16. Differential amplifiers (10)
17. Mag amps for items 1-6
18. Mag amp for feed valve supply
19. Mag amp control unit for item 7
20. Output transformer for heater supplies
21. Quad amplifier unit placed on open door of amplifier rack

### 3. Section A-3

This section is the first of three that provide ground level instrumentation and control. The primary 3-phase power of the entire console comes in through the base of A-3. All primary wiring is run in conduit and all breakoff junction boxes and controllers are shielded. Distribution is provided to A-1 and A-6 by boxes located on the rear of the pontoon bases of A-3 and A-5. Power for ground level circuits is distributed to the line filters mounted on the front of A-3. A breaker mounted in the same area provides protection of all control power for the entire console.



A Dymec DY 2013A digital data system is mounted in the upper panel area and provides 26 channels of digital readout. All data from A-2 plus ground level data is sequentially read and recorded by this scanner system.

4. Section A-4

This section includes the neutral partical detector readout and provides mounting space for equipment required by ground level instrumentation, primary power and for future expansion.

5. Section A-5

This is the primary operator control panel. Mounted directly above the desk top are the controls of heater start-up, engine control, interrogation of engine operating point and direct readout of voltage and current. A continuous plot of 12 engine parameters is provided by a Speedomax-W point plotter mounted in the top panel of A-5. Six cam-operated process control switches are included in the recorder to permit automatic shutdown or operator alarm for variables that are out of tolerance. Below the desk area is a manually controlled 1.2 kW heater supply for neutralizer power.

Figures 57a, 57b and 57c show front panel and rear views of the ground level instrumentation. Description of call-outs is as follows:

1. Breaker for control power
2. Line filters for ground level instrumentation
3. Dymec DY 2013A Data Acquisition System
4. Neutral detector power supply
5. Neutral detector micro-ammeter readout
6.  $\pm 250$  V power supply of operational amplifiers
7. Operational amplifiers (12)
8. 12-channel Speedomax point plotter
9. Engine system control panel

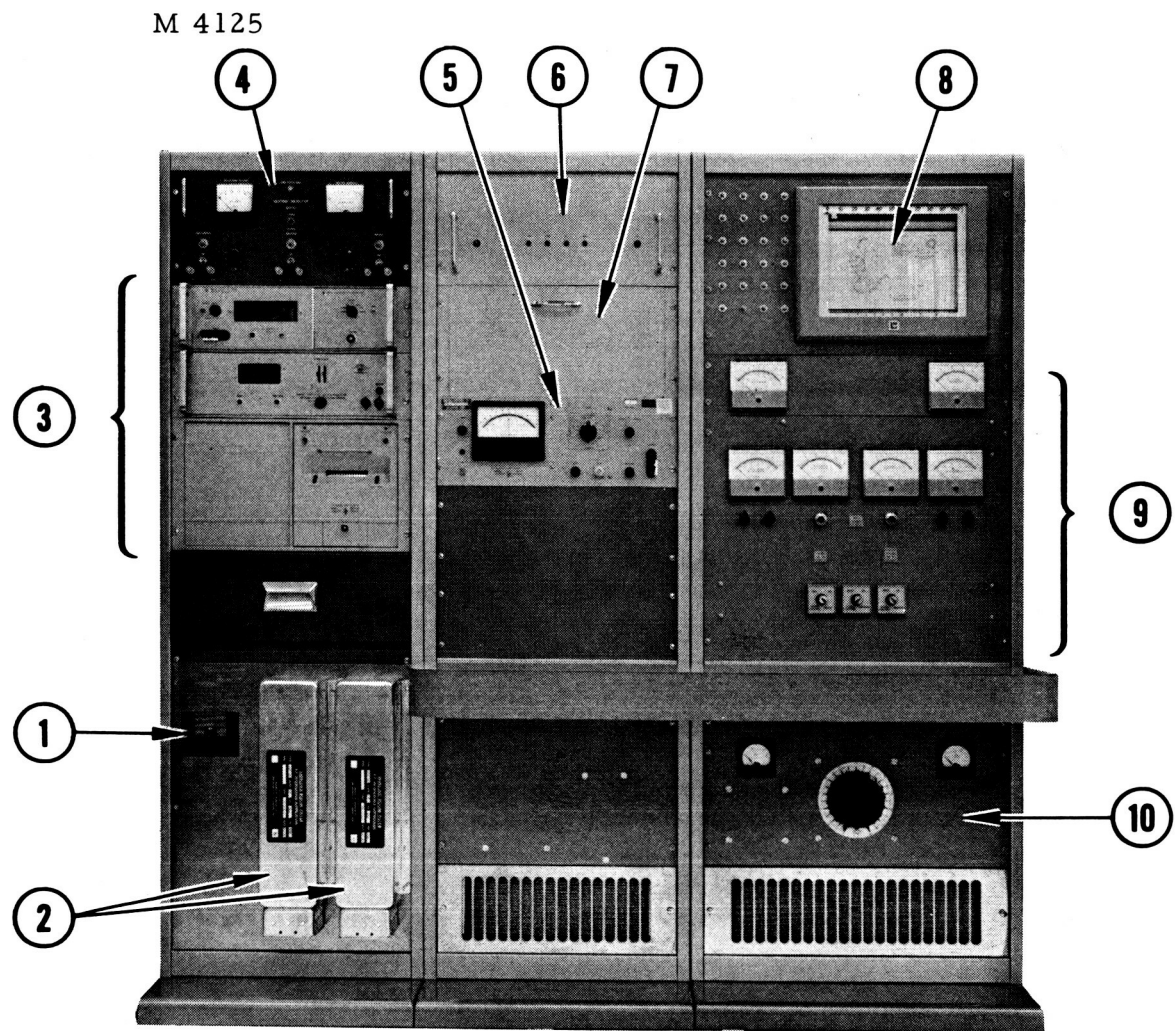


Fig. 57(a). Ground level instrumentation (see text for callout identification).

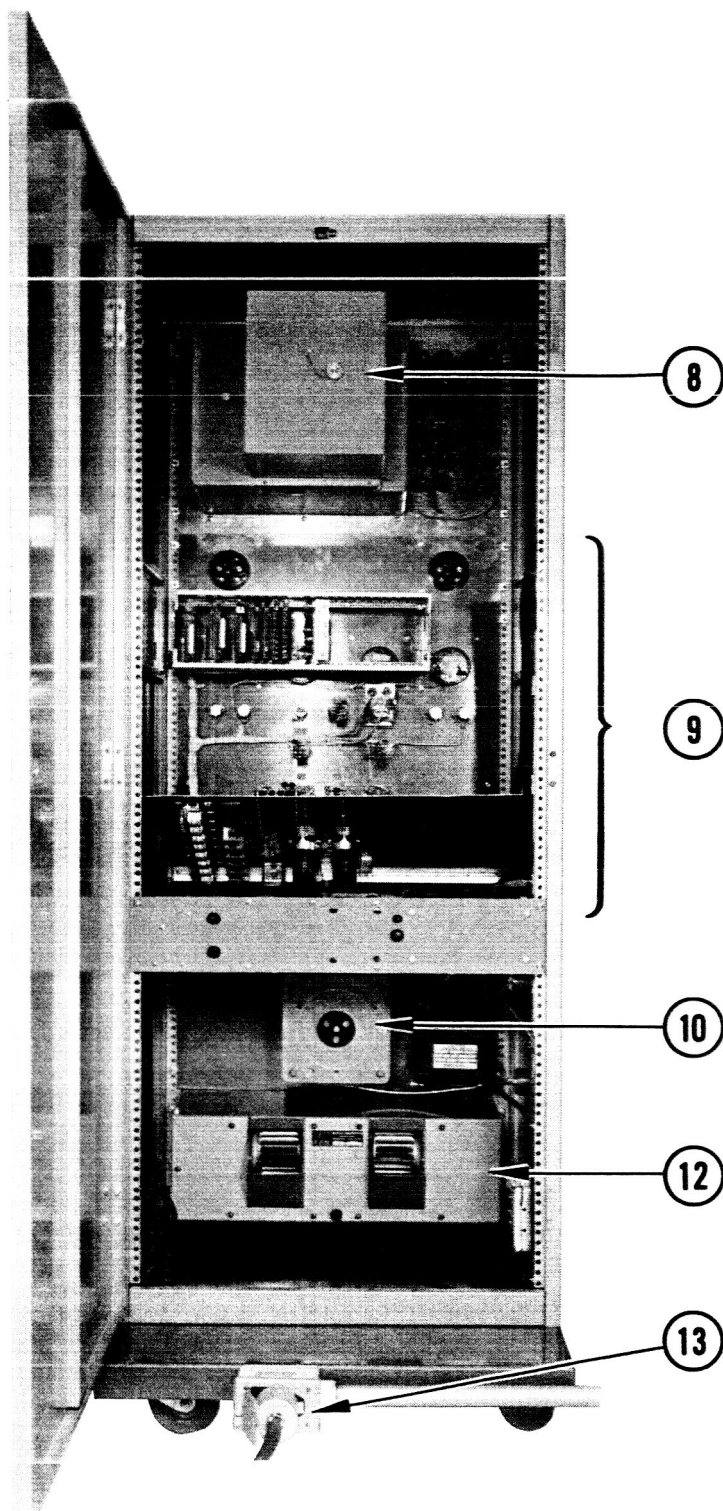


Fig. 57(b).  
Ground level instru-  
mentation (see text  
for callout identification).

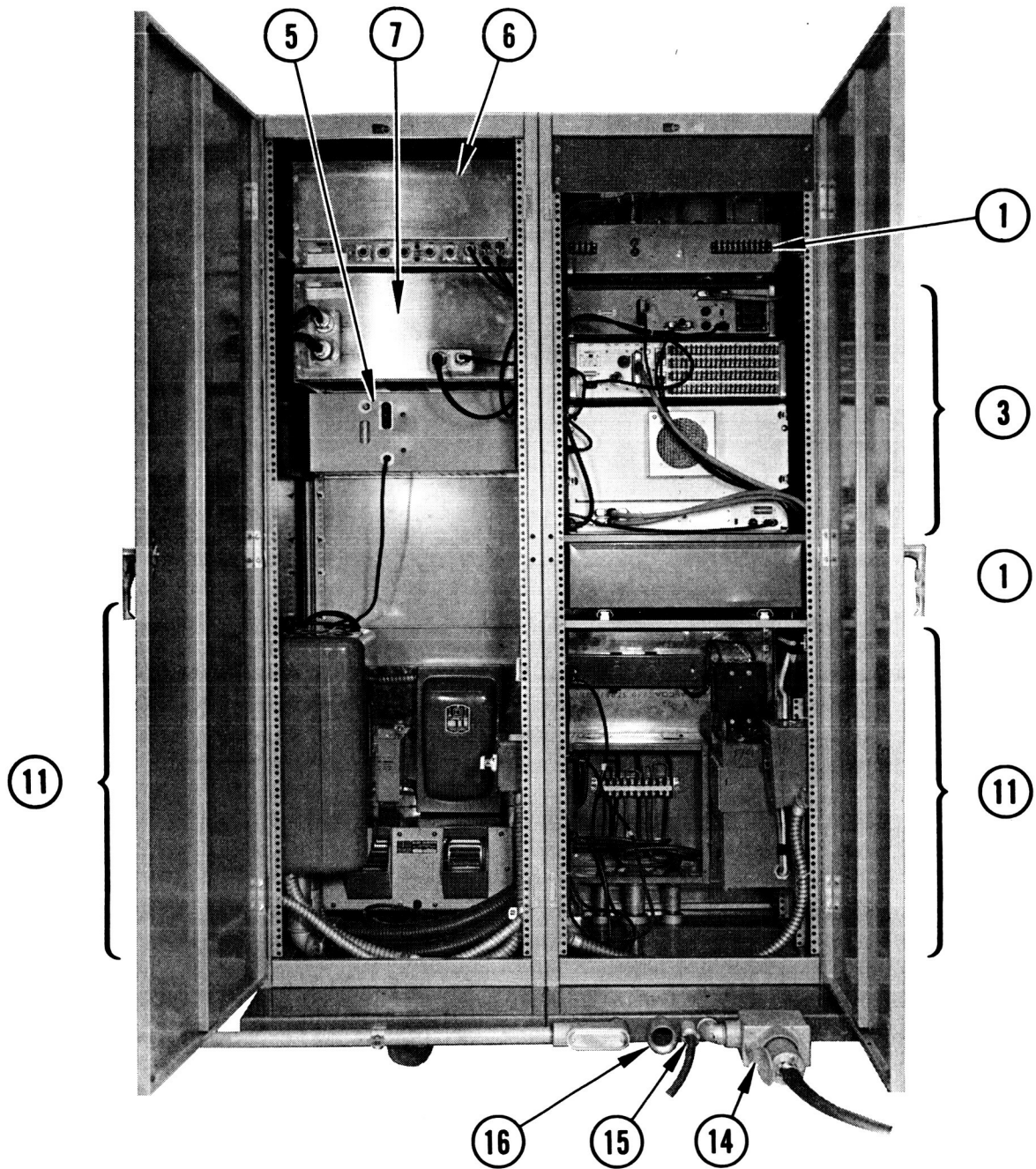


Fig. 57(c). Ground level instrumentation (see text for callout identification).

10. 1.2 kW low voltage neutralizer supply
11. Primary power distribution center
12. Blower
13. Outlet to -15 kV supply
14. Outlet to +10 kV supply
15. Vacuum interlock cable
16. Primary power

6. Section A-6

A minus high voltage supply capable of 15 kV at 0.25 amperes is provided from a 3-phase power line similar in design to the supply in Section A-1. Also provided for future use is a 5 kV, 0.25 amp supply referenced to the minus potential and a temperature or power regulator 2 kW heater supply.

The primary power provided to A-1 and A-6 is through band-pass filters. Three filters are provided on each cabinet to minimize power transients which may be caused by the engine system.

Figures 58a and 58b show open front and open rear views of the -15 kV power supply. Description of call-outs is as follows:

1. Three single phase saturable reactors
2. 2 kW isolation transformers (2 provided)
3. Mag-amp control for heaters at minus potential
4. Filter capacitor
5. Mag-amp control for H.V. supply
6. Step-up transformer and choke for diverter supply
7. Filter choke for -H.V. supply
8. Step-up transformer for - H.V. supply
9. Rectifier panel
10. Series regulator tube

C. Summary

The operational console presented in the preceding sections will significantly improve the engine evaluation programs. The closed loop control provided on all engine system parameters will permit

M 4119

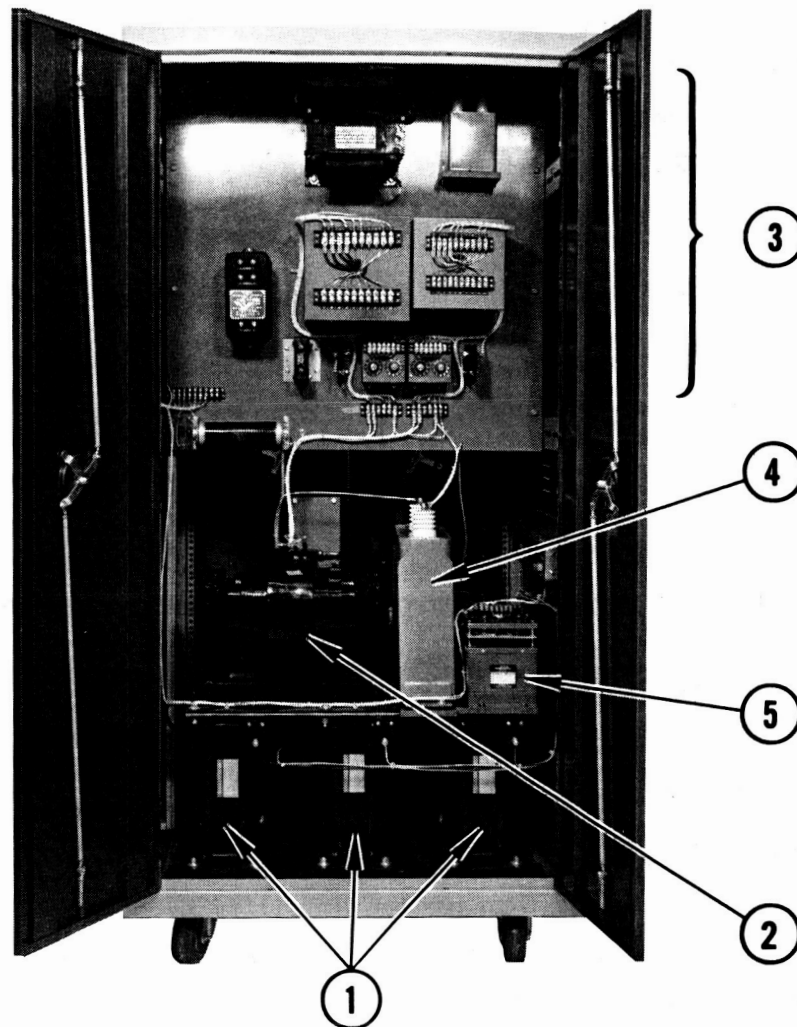


Fig. 58(a). -15 kV power supply (see text for callout identification).

M 4127

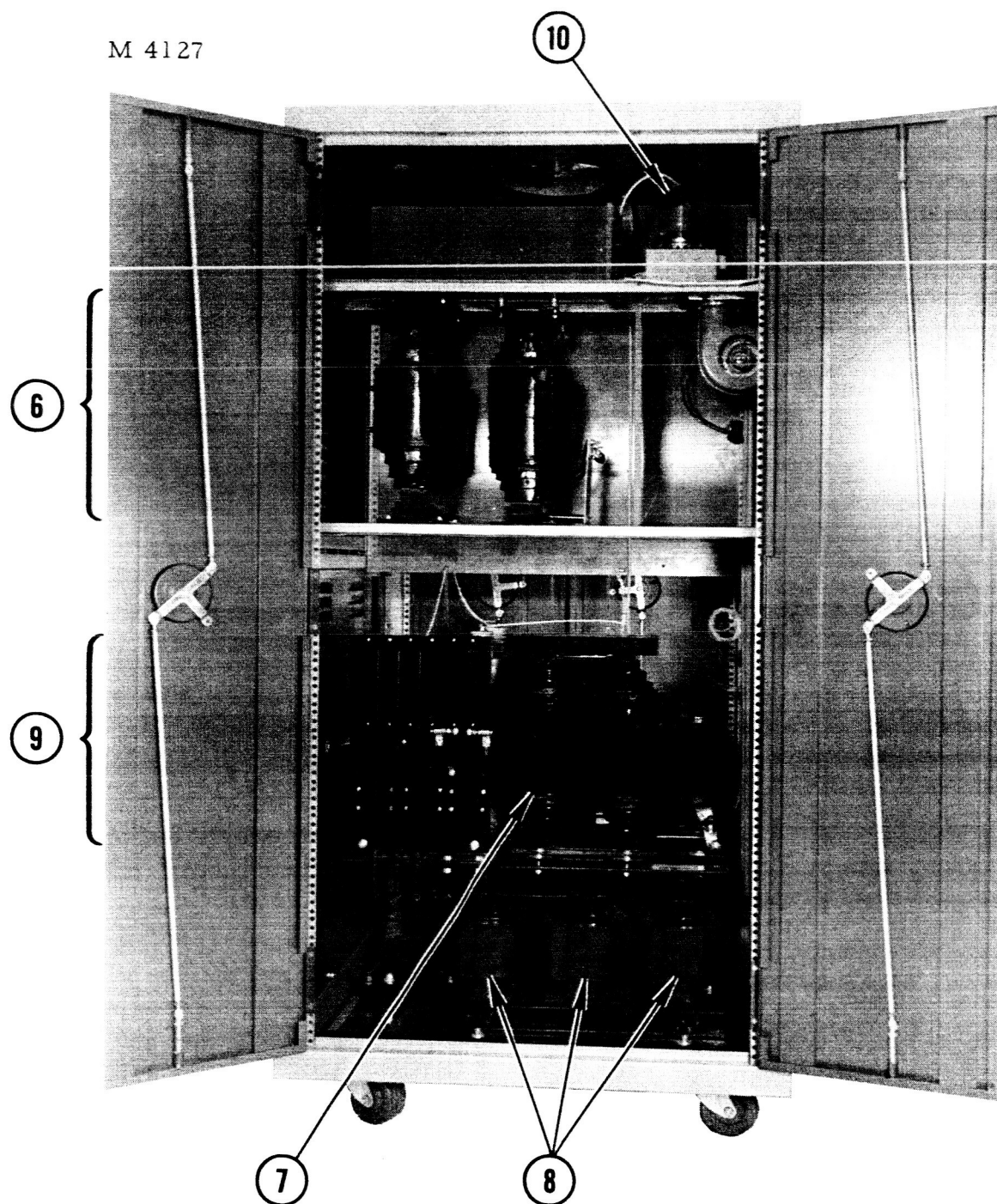


Fig. 58(b). -15 kV power supply (see text for callout identification).

precise cross correlation. Accuracy of measurement and control have been held to the highest practical levels.

New diagnostic instrumentation has been provided to permit periodic interrogation of engine perveance, operating point and ionizer critical temperature. Also included is a new type of voltage and current regulation for the plus and minus high voltage supplies. This type of regulation will provide good long term voltage regulation and inhibit instantaneous dumping of the stored energy in the filter network. A precisely controlled rate of change of beam current has been provided so that optimum power supply characteristics can be determined.

The completed console will be checked out on dummy loads and engine system components during the next reporting interval.



#### VIII. PLANS FOR NEXT QUARTER

1. Life test 13-strip engine
2. Evaluate additional coated ionizer samples